CHEMICAL REVIEWS

REVIEW

pubs.acs.org/CR

Fluorescent Chemosensors Based on Spiroring-Opening of Xanthenes and Related Derivatives

Xiaoqiang Chen,[†,‡] Tuhin Pradhan,[§] Fang Wang,[†] Jong Seung Kim,[*,§] and Juyoung Yoon[*,†]

[†]Departments of Chemistry and Nano Science and of Bioinspired Science (WCU), Ewha Womans University, Seoul 120-750, Korea

[‡]State Key Laboratory of Materials-Oriented Chemical Engineering, College of Chemistry and Chemical Engineering, Nanjing University of Technology, Nanjing 210009, China

[§]Department of Chemistry, Korea University, Seoul 136-701, Korea

CONTENTS

1. INTRODUCTION

The recognition and sensing of biologically and environmentally important species has emerged as a significant goal in the field of chemical sensors in recent years.[1−10] Several methods, such as high-performance liquid chromatography, mass spectrometry, atomic absorption spectroscopy, inductively coupled plasma atomic emission spectrometry, electrochemical sensing, etc., have been developed to analyze the targets concerned.[11−13] However, these methods suffer from extensive and time-consuming procedures that involve the use of sophisticated instrumentation. Fluorogenic methods in conjunction with suitable probes are preferable approaches for the measurement of these analytes because fluorimetry is rapidly performed, is nondestructive, is highly sensitive, is suitable for high-throughput screening applications, and can afford real information on the localization and quantity of the targets of interest.[9,10,14−18] To date, various fluorophores with different excitation and emission wavelengths have been employed as signal reporters of chemosensors, such as coumarin, pyrene, 1,8-naphthalimide, xanthenes, squaraine, cyanine, boron dipyrromethene difluoride (BODIPY), nitrobenzofurazan, etc.[1−10,19,20]

Among the fluorophores developed, xanthenes, including rhodamines and fluoresceins, are highly favorable because of their excellent photophysical properties, such as high extinction coefficients, excellent quantum yields, great photostability, and relatively long emission wavelengths. Rhodamine was first synthesized by Noelting and Dziewonsky in 1905[21] and has been widely used in many research fields, including the lasing medium in dye lasers and fluorescent markers in biological studies.[22,23] However, it was only in 1997 that the rhodamine B derivative and its ring-opening reaction received a great deal of attention from organic chemists.[24] Rhodamine spirolactam or spirolactone derivatives are nonfluorescent and colorless, whereas ring-opening of the corresponding spirolactam/lactone gives rise to strong fluorescence emission and a pink color (Figure 1). In general, rhodamine derivative displays a red color change and strong fluorescence in acidic solutions by activation of a carbonyl group in a spirolactone or spirolactam moiety. In a similar way, an appropriate ligand on a spirolactam ring can induce a color change as well as a fluorescence change upon addition of metal ions, even though this process is somewhat dependent on the solvent system. As another typical xanthene dye, fluorescein was first synthesized by von Bayer in 1871 with

Received: June 5, 2011
Published: October 31, 2011

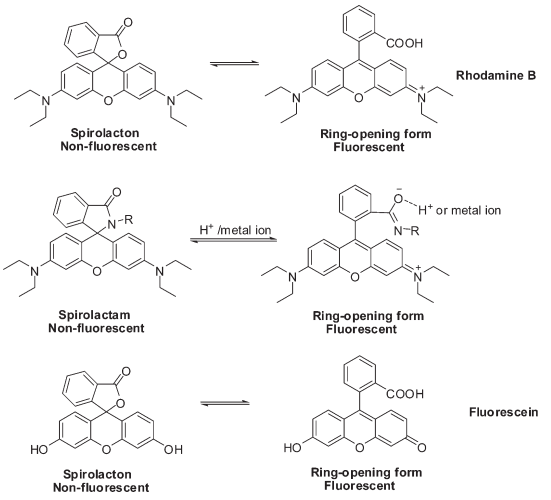

Figure 1. Ring-opening of spirocyclic xanthenes and related derivatives.

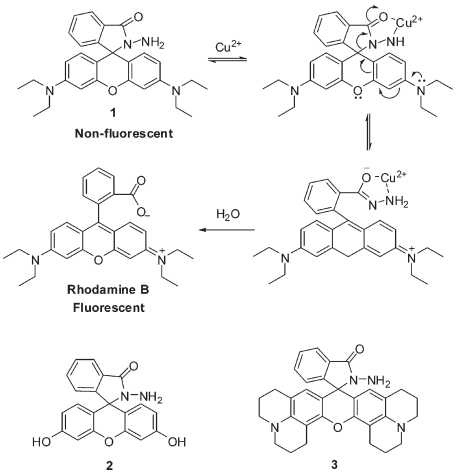

Figure 2. Cu^{2+}-assisted hydrolysis of Czarnik's rhodamine B hydrazide (**1**) and structures of **2** and **3**.

resorcinol and phthalic anhydride via Friedel–Crafts acylation/cyclodehydration.[25] Some of the advantageous features of the fluorescein fluorophores are good water solubility, visible excitation and emission (an absorption maximum at 494 nm and emission maximum of 521 nm in water), and maximum brightness at physiological pH.[26] Similarly, fluorescein derivates are nonfluorescent when they exist in the lactone form, and the ring-opened form can induce color changes and fluorescence enhancements (Figure 1).

Spirocyclic derivatives of rhodamine and fluorescein dyes are useful sensing platforms because the ring-opening process leads to a turn-on fluorescence change. Since the first rhodamine-based fluorescent chemosensor for Cu(II) was reported by Anthony W. Czarnik in 1997, a large number of papers involving fluorescent chemosensors based on spiroring-opening processes have been published. The analytic objects have included various metal ions (Cu^{2+}, Hg^{2+}, Fe^{3+}, Zn^{2+}, Cr^{3+}, Ag^{+}, Au^{+}, Pb^{2+}, Pd^{2+}, and Pt^{2+}), anions (cyanide and pyrophosphate), reactive oxygen species, and thiols and involved various pH values, temperatures, etc. This review introduces different xanthene derivatives according to their analytes with mechanistic schemes. In addition, we explain successful applications of these probes for bioimaging and environmental assay and incorporation into polymers, nanoparticles, and microfluidic chips. This review covers mostly the work published from 1997 to February 2011.

2. DETECTION OF METAL IONS BY SPIRORING-OPENING OF XANTHENES AND RELATED DERIVATIVES

2.1. Sensors for Detecting Cu^{2+}

Various transition-metal ions are crucial for the life of organisms.[27] Among these is the copper ion, which plays a critical role as a catalytic cofactor for a variety of metalloenzymes, including superoxide dismutase, cytochrome *c* oxidase, and tyrosinase. However, under overloading conditions, copper exhibits toxicity, in that it causes neurodegenerative diseases (e.g., Alzheimer's and Wilson's diseases), probably by its involvement in the production of reactive oxygen species.[28,29] Owing to its biological importance, using optical techniques to monitor the trafficking and location of Cu^{2+} in living cells has attracted much attention and resulted in fruitful work in recent years.[30] In 1997, Czarnik's group reported a pioneering work for sensing Cu^{2+} utilizing a rhodamine B derivative ring-opening reaction.[24] In their study, rhodamine B hydrazide (**1**) was used as a fluorescent chemodosimeter for Cu^{2+}. As shown in Figure 2, Czarnik's rhodamine B hydrazide can recognize Cu^{2+} selectively, and Cu^{2+}-promoted hydrolysis can provide fluorescent rhodamine B as a product. They demonstrated that this system can detect 10 nM Cu^{2+} within 2 min at pH 7. This work resulted in a great deal of attention being given to the application of the ring-opening processes of rhodamine B derivatives to fluorescent chemosensors.

Ma and co-workers reported fluorescein hydrazide (**2**; Figure 2) as a highly selective and sensitive fluorescence probe for Cu^{2+}.[31] In 0.01 M Tris–Cl buffer (pH 7.2), the probe displayed a highly selective fluorescence-on response (λ_{em} = 516 nm) to Cu^{2+} only. As the mechanism of Czarnik's rhodamine hydrazide reaction, the hydrazide group of **2** recognizes and binds Cu^{2+}, and the subsequent complexation of Cu^{2+} promotes hydrolytic cleavage of the amide bond, causing the release of a fluorophore (fluorescein) and thereby the recovery of fluorescence. A calibration curve was linear over the concentration range of 0.1–10 μM Cu^{2+}, and the detection limit for Cu^{2+} was 64 nM.

A new chemodosimeter based on the spirolactam form of rhodamine 101 hydrazide (**3**) has been synthesized (Figure 2).[32] This chemodosimeter exhibited an irreversible colorimetric and fluorogenic response toward Cu^{2+} in CH_3CN–Tris–HCl (0.02 M; pH 7.2; 3:7, v/v) via a mechanism similar to that of Czarnik's hydrazide reaction. However, the dominating fluorescence maximum was red-shifted to 600 nm. Interestingly, the authors performed density functional theory (DFT) calculations and suggested that in the Cu^{2+} ion promoted ring-opening reaction, the carbonyl O atom and amine N atom in the hydrazide moiety become electron-rich centers and exhibit a higher affinity for the Cu^{2+} ion.

Tong's group reported the first example of the hydrazone derivative of rhodamine, salicylaldehyde rhodamine B hydrazone (**4**), which displayed selective Cu^{2+}-amplified absorbance and fluorescence emission above 500 nm in a neutral buffered medium.[33] Upon addition of Cu^{2+}, the spirolactam ring of **4** was opened and a 1:1 metal–ligand complex was formed (Figure 3). Furthermore, the sensitivity of **4** for Cu^{2+} can be lower than 25 nM in 50% (v/v) buffered H_2O–CH_3CN when using the absorption spectrum method. Even in neutral buffered aqueous solutions, the fluorescence sensing of Cu^{2+} at lower micromolar levels was successful.

dx.doi.org/10.1021/cr200201z |*Chem. Rev.* 2012, 112, 1910–1956

Yin's group reported a rhodamine-based derivative, **5**, capable of detecting both Cu^{2+} and VO^{2+} ions using two different modes (Figure 3).[34] **5** exhibited different selectivities at micromolar levels for Cu^{2+} in UV−vis spectroscopy and at nanomolar levels for VO^{2+} in fluorescence spectroscopy. This is, to the best of our knowledge, the first reported example of a dual-detecting rhodamine derivative capable of detecting both Cu^{2+} and VO^{2+}. **5** displayed Cu^{2+}-selective chromogenic behavior and turned from colorless to purple red, which allowed naked eye detection of Cu^{2+} in aqueous 50% CH_3OH solution (methanol:HEPES = 1:1, v/v; pH 7.0). The "off−on" type of fluorescence changes of the spirolactam moiety could be used to conveniently detect VO^{2+}. In addition, **5**−M^{2+} (M = Cu or VO) complexes were further applied as chemosensors to sense PPi anions.

A rhodamine derivative, **6** (Figure 3), was used to detect Cu^{2+} in an aqueous medium [50% (v/v) water−ethanol and 10 mM acetate neutral buffer (pH 7.0)].[35] Under optimized conditions, the quantification of Cu^{2+} by **6** using an absorptiometric method was satisfactory in the linear working range 0.05−5.00 μM, with a detection limit of 10 nM for Cu^{2+} and good tolerance of other metal ions.

Tong's group also reported a salicylaldehyde fluorescein hydrazone, **7** (Figure 3), as a Cu^{2+}-selective sensor in 50% water−ethanol (10 mM Tris−HCl) solution.[36] The association constants of **7** with Cu^{2+} at pH 5.0 and 8.0 were calculated as K_a = 8.6 × 10^3 and 7.8 × 10^4 M^{-1}, respectively. Besides, the absorbance at 502 nm and pH 8.0 was nearly 6 times larger than that at 420 nm and pH 5.0, which was attributed to the difference in molecular absorptivity of protonated and deprotonated states of the ring-opened **7**−Cu^{2+} complex. Molecular logic gates were also proposed, which integrated a Cu^{2+}-driven YES logic gate as well as an INHIBIT logic gate, with pH and Cu^{2+} as its chemical inputs based on encoding binary digits of logical conventions.

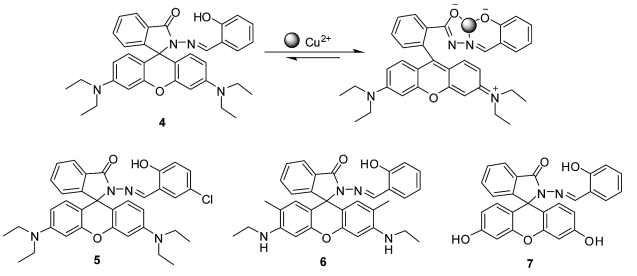

Figure 3. Proposed binding mode of **4** with Cu^{2+} and structures of **5**−**7**.

A rhodamine−pyrene derivative, **8**, has been synthesized as a ratiometric and off−on sensor for the detection of Cu^{2+} in CH_3CN−HEPES buffer (0.02 M; pH 7.4; 4:6, v/v) by Yoon's group.[37] When Cu^{2+} was added to the solution, a significant decrease in the fluorescence intensity at 424 nm and a new fluorescence emission band centered at 575 nm were observed with a clear isoemissive point at 558 nm, which was attributed to the Cu^{2+}-induced ring-opening of the spirolactam moiety (Figure 4). Upon addition of up to 7 equiv of Cu^{2+}, the absorbance at 424 nm decreased sharply, while those at 356 and 557 nm increased significantly, which induced a color change from primrose yellow to pink. The nonlinear fitting of the titration curve and the data of Job's plot from absorption spectra assumed a 1:1 stoichiometry for the **8**−Cu^{2+} complex with an association constant of 2.5 × 10^4 M^{-1}.

Kim and co-workers reported the design and synthesis of a new rhodamine-based derivative, **9**, bearing an *N*-butyl-1,8-naphthalimide group (Figure 4). **9** displayed selective colorimetric and fluorescence "turn-on" changes at 550 nm via a rhodamine ring-opening approach toward Cu^{2+} among other metal ions examined in CH_3CN−HEPES buffer (0.02 M; pH 7.4; 5:5, v/v).[38] It was reported that **9** forms a 2:2 complex with Cu^{2+} as shown in Figure 4. On the other hand, probe **9** also showed a remarkable ratiometric fluorescence enhancement toward Zn^{2+} with a 100 nm red shift via a typical intramolecular charge transfer (ICT) response in a 2:1 (**9**:Zn^{2+}) binding mode. As expected, the naphthalimide moiety served successfully as a source of these ratiometric changes. Moreover, another ratiometric fluorescence signal output for Cu^{2+} was observed when the Zn^{2+} in the **9**−Zn^{2+} complex was displaced with Cu^{2+}. These results demonstrated that **9** could act as a dual-mode Cu^{2+}-selective sensor via two mechanisms: the rhodamine ring-opening mechanism and ratiometric displacement from the **9**−Zn^{2+} complex.

Rhodamine B hydrazide oxalamide (**10**) was reported by Tong's group (Figure 5).[39] The probe showed a high selectivity and sensitivity to Cu^{2+} by forming a 1:1 complex in CH_3CN, and the chelating is reversible. The limit of detection for Cu^{2+} in CH_3CN was found to be 3.7 × 10^{-8} M. It was also found that Cu^{2+} could catalyze the hydrolysis of the probe in 50% (v/v) buffered (10 mM Tris−HCl, pH 7.0) water−CH_3CN, giving a highly fluorescent product, and the fluorescence detection of

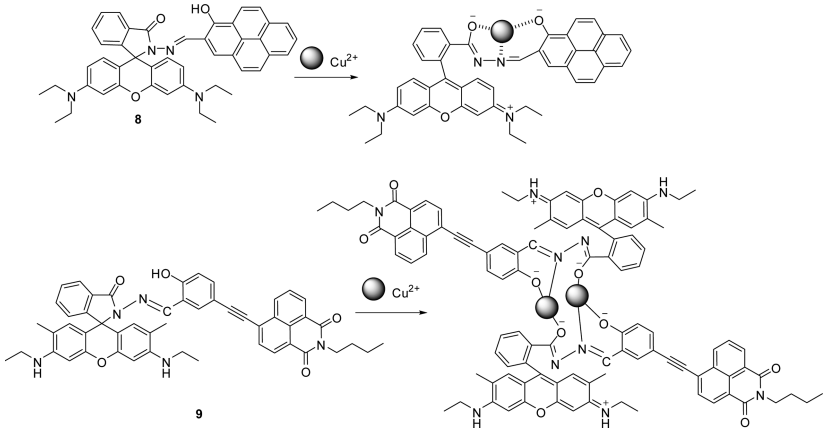

Figure 4. Proposed binding modes of **8** and **9** with Cu^{2+}.

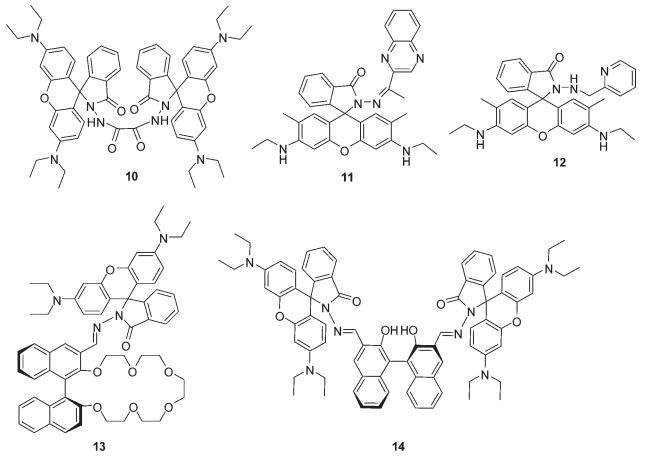

Figure 5. Structures of **10**−**14**.

copper ions in this neutral buffered medium with a detection limit of 6.4×10^{-7} M was developed.

Tang and co-workers reported a rhodamine derivative as a reversible fluorescent chemosensor, **11** (Figure 5), for Cu^{2+} in an aqueous solution (20 mM phosphate-buffered saline (PBS), pH 7.4),[40] in which rhodamine 6G was utilized as a fluorophore and 2-acetyl-(1,4)-benzodiazine, a Cu^{2+}-selective ligand, as the ion acceptor. Its crystal structure was also presented to explain the binding mode. There was a good linear correlation between the relative fluorescence intensity and the Cu^{2+} concentration in the range from 5.0×10^{-7} to 1.0×10^{-6} M, and the dissociation constant (K_d) of the probe with Cu^{2+} was found to be 0.1 μM. The off−on-type fluorescence change upon addition of Cu^{2+} was also applied in bioimaging.

Zhang's group reported a rhodamine spirolactam derivative, **12** (Figure 5), for the fluorescence detection of Cu^{2+} in aqueous solution buffered (Tris−HCl, pH 7.1) water−ethanol (8:2, v/v).[41] **12** exhibits a highly sensitive turn-on fluorescent response toward Cu^{2+} in aqueous solution with an 80-fold fluorescence intensity enhancement upon addition of 10 equiv of Cu^{2+}. With the experimental conditions optimized, the probe exhibits a dynamic response range for Cu^{2+} from 8.0×10^{-7} to 1.0×10^{-5} M, with a detection limit of 3.0×10^{-7} M. The response of the chemosensor for Cu^{2+} is instantaneous and reversible. The proposed chemosensor has been used for direct measurement of the Cu^{2+} content in river water samples and imaging of Cu^{2+} in living cells.

New rhodamine derivatives bearing a binaphthyl group were synthesized as selective fluorescent and colorimetric sensors **13** and **14** (Figure 5) for Cu^{2+} by Yoon and co-workers.[42] Highly selective off−on-type fluorescence changes were observed upon addition of Cu^{2+} among various metal ions in CH_3CN−HEPES buffer. Probe **13** displayed a 380-fold increase in its emission upon addition of 8.0 equiv of Cu^{2+}, and the value of log K for the binding of **13** and Cu^{2+} was calculated as 4.93. For sensor **13**, one carbonyl oxygen as well as crown ether oxygens can provide a nice binding pocket for Cu^{2+}. On the other hand, from the fluorescence titrations in CH_3CN−HEPES buffer, the values of log $K_{1:1}$ and log $K_{1:2}$ for the binding of **14** and Cu^{2+} were determined as 4.19 and 4.83, respectively. The chemosensing of **14** with Cu^{2+} was further applied to the microfluidic system.

The first example of boronic acid linked fluorescent and colorimetric chemosensors for copper ions was reported by Yoon, Shin, and co-workers.[43] The monoboronic acid conjugated rhodamine

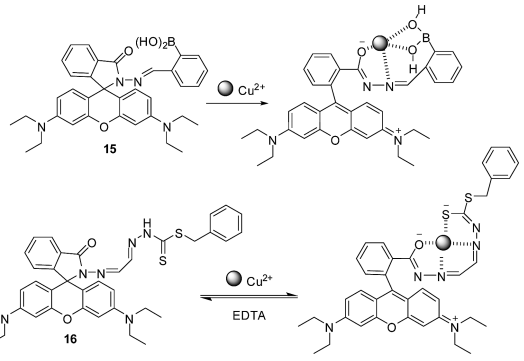

Figure 6. Proposed binding mechanisms of **15** and **16** with Cu^{2+}.

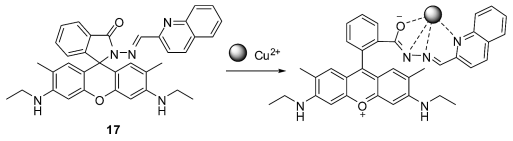

Figure 7. Proposed binding mechanism of **17** and Cu^{2+}.

probe **15** displayed a highly selective fluorescence enhancement with Cu^{2+} among various metal ions in 20 mM HEPES (0.5% CH_3CN) at pH 7.4. Upon addition of Cu^{2+} to this solution, a pink color developed and the resulting species exhibited strong orange fluorescence. The absorption (λ_{max} = 556 nm) and emission (λ_{max} = 572 nm) changes are associated with Cu^{2+}-induced spirolactam ring-opening that forms the Cu^{2+}−**15** complex (Figure 6). The association constant of **15** with Cu^{2+} was determined to be 2.8×10^3 M^{-1} on the basis of the results of a fluorescence titration experiment. Furthermore, practical use of the monoboronic acid conjugated rhodamine probe is demonstrated by its application to the detection of copper ions in mammalian cells and organisms.

Chen's group reported a rhodamine derivative, **16** (Figure 6), as a selective fluorescent and colorimetric sensor for Cu^{2+} in 20% (v/v) water−methanol solution (0.02 M HEPES, pH 6.0).[44] A pH titration experiment revealed that the absorbance of a **16**−copper complex displayed a plateau in the pH range from 4.0 to 8.0, and the maximum absorbance toward the Cu^{2+} was obtained below pH 6.0. As shown in Figure 6, addition of EDTA to the solution containing **16** and Cu^{2+} significantly diminished the absorbance. The association constant was determined from the slope to be 1.7×10^5 M^{-1}, and the detection limit was reported as 3 nM.

Most recently, Zeng's group reported a rhodamine-based derivate, **17** (Figure 7), bearing the quinaldine unit as the fluorescent sensor for Cu^{2+}.[45] In water−CH_3CN (1:1, v/v) solution, compound **17** is colorless and weakly fluorescent. Upon binding with Cu^{2+}, the solution turned from colorless to pink and fluorescence enhancement occurred over a comparatively wide pH range, indicating formation of the ring-opened amide form from the spirolactam form of **17**. The association constant for Cu^{2+} was estimated to be 4.03×10^3 M^{-1} by fluorescence titration experiments, and Job's plot revealed a 1:1 stoichiometry for the binding between **17** and Cu^{2+}.

A tripodal rhodamine fluorescent chemosensor, **18** (Figure 8), has also been developed by Zeng's group,[46] which exhibited prominent absorption and fluorescence enhancement upon Cu^{2+}

dx.doi.org/10.1021/cr200201z |*Chem. Rev.* 2012, 112, 1910–1956

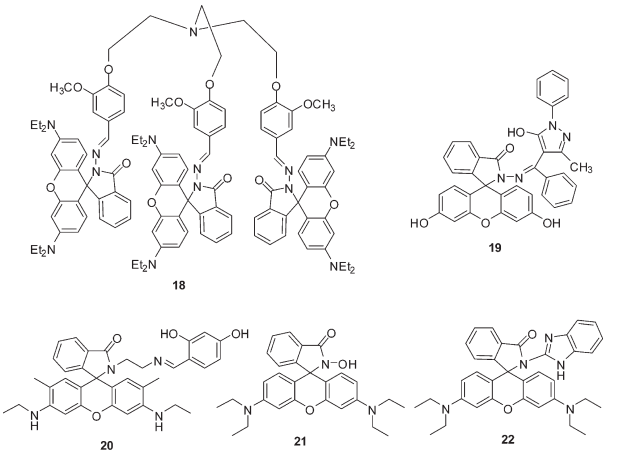

Figure 8. Structures of **18**−**22**.

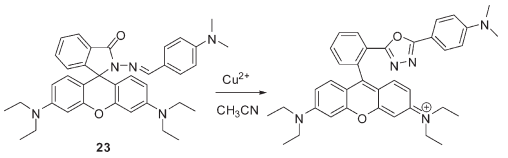

Figure 9. Proposed reaction mechanism of **23** with Cu^{2+}.

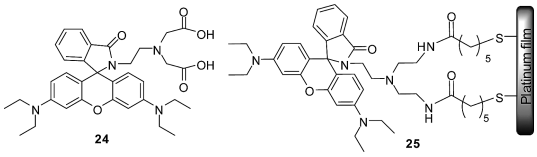

Figure 10. Structure of rhodamine diacetic acid derivative **24** and the thiol-functionalized rhodamine-based chemodosimeter **25**.

addition in ethanol−water (8:1, v/v; Tris−HCl buffer, pH 6.8). The association constant for a Cu^{2+}−**18** complex was estimated to be 5.8×10^4 M^{-1} from the fluorescence measurements and 5.9×10^4 M^{-1} from the UV−vis measurements with a 1:1 binding stoichiometry. The results of IR and ^1H NMR experiments showed that **18**−Cu^{2+} and **18**−Hg^{2+} bind through different reaction mechanisms and showed evidence for a synergistic effect between Hg^{2+} and the **18**−Cu^{2+} complex. Compound **18** and the **18**−Cu^{2+} complex were reported as off−on fluorescent chemosensors for Cu^{2+} and Hg^{2+}, respectively.

Yang and co-workers synthesized a fluorescein derivative, **19** (Figure 8), through the reaction of fluorescein hydrazide and 1-phenyl-3-methyl-4-benzoyl-5-pyrazolone.[47] Addition of Cu^{2+} to an aqueous solution (DMSO:H_2O = 4:6, v/v) of **19** resulted in an obvious color change (from colorless to deep yellow) and UV−vis absorption spectral changes. The association constant of **19** with Cu^{2+} was calculated as 3.3×10^4 M^{-1}.

Zeng's group reported 4-[[(*E*)-*N*-(rhodamine 6G lactam)-ethylenediamineimino]methyl]benzene-1,3-diol (**20**; Figure 8), which showed a reversible, selective, and sensitive fluorescence enhancement response to Cu^{2+} in HEPES buffer (20 mM, pH 7.0) containing 50% (v/v) CH_3CN.[48] Upon the increasing addition of Cu^{2+}, a new absorption band centered at 528 nm and a new emissive peak at 545 nm appeared. Using sensor **20**, a subcellular distribution of Cu^{2+} in SPC-A-1 (lung cancer) cells can be observed by laser scanning confocal microscopy.

Rhodamine B hydroxylamide (**21**; Figure 8) was characterized as a highly selective and sensitive fluorescence probe for Cu^{2+} by Ma's group.[49] In Tris−HCl buffer (25 mM, pH 6.0) containing 60% (v/v) acetonitrile, the probe exhibited specific absorbance-on and fluorescence-on responses to Cu^{2+} only, and the probe was demonstrated to directly analyze trace amounts of Cu^{2+} in biological fluids such as human serum. The reaction mechanism proposed was that the hydroxylamide group of **21** binds Cu^{2+}, and the subsequent complexation of Cu^{2+} displayed a high catalytic activity for the hydrolytic cleavage of the amide bond, causing the release of rhodamine B. The fluorescence intensity was proportional to the concentration of Cu^{2+} in the range of 1−20 μM with a detection limit of 33 nM.

Tang, Nandhakumar, and co-workers reported a new and simple rhodamine-based colorimetric chemosensor, **22** (Figure 8), by incorporating rhodamine B and benzimidazole, which displayed high selectivity and sensitivity toward Cu^{2+} in a CH_3CN−water solution (HEPES buffer, pH 7.0) and showed no significant response to the other metal ions evaluated.[50] The Cu^{2+} recognition process of **22** was not significantly influenced by other coexisting metal ions. The interaction of **22** and Cu^{2+} was shown to be reversible with a 1:1 binding stoichiometry, and the detection limit was found to be 2.8×10^{-7} M.

A new rhodamine derivative, rhodamine B 4-(*N*,*N*-dimethylamino)benzaldehyde hydrazone (**23**), was designed for ratiometric sensing of Cu^{2+} selectively in CH_3CN.[51] The addition of Cu^{2+} to the solution of **23** caused a simultaneous enhancement of absorbance at 560 nm and a fluorescence red shift from 515 to 585 nm, indicating that the spirolactam ring was opened by Cu^{2+} as expected (Figure 9). The optical changes were attributed to the Cu^{2+}-induced oxidation of **23**, resulting in ring-opening of the rhodamine moiety.

Shiraishi et al. reported a rhodamine diacetic acid derivative, **24** (Figure 10), which shows strong green fluorescence in CH_3CN with Cu^{2+} while showing very weak orange fluorescence with other metal ions.[52] Without cations, **24** shows a very weak fluorescence at 575 nm; however, Cu^{2+} addition creates a remarkably enhanced (49-fold) and blue-shifted (45 nm) green fluorescence at 530 nm. Hg^{2+} also induced an emission enhancement, but the enhancement was very small (2.8-fold) and the emission appears at 570−580 nm (orange fluorescence), which is similar to that obtained using rhodamine-based probes that have already been reported.

Kim and co-workers have successfully demonstrated that a thiol-functionalized rhodamine-based chemodosimeter on platinum films, **25**, can be utilized as a molecular switch for the fluorescence sensing of Cu^{2+} (Figure 10).[53] These films displayed sensitivity (the detection limit was approximately 10^{-5} M) for Cu^{2+} and selectivity, clearly shown by experiments in the presence of a 10^{-2} M concentration of other metal ions. In addition, the colorimetric response (colorless to pink) of **25** could be detected by the naked eye as platinum films display an optical transparency (transmittance of ca. 0.70) in the visible spectral region.

The excitation energy of one fluorophore (donor) can be transferred by a radiationless process to its neighboring fluorophore (acceptor) if their energy level difference corresponds to a quantum of excitation energy. As a result, the electron of the acceptor was excited to a higher energy level, leading to the emission of the acceptor fluorophore. This fluorescence resonance energy

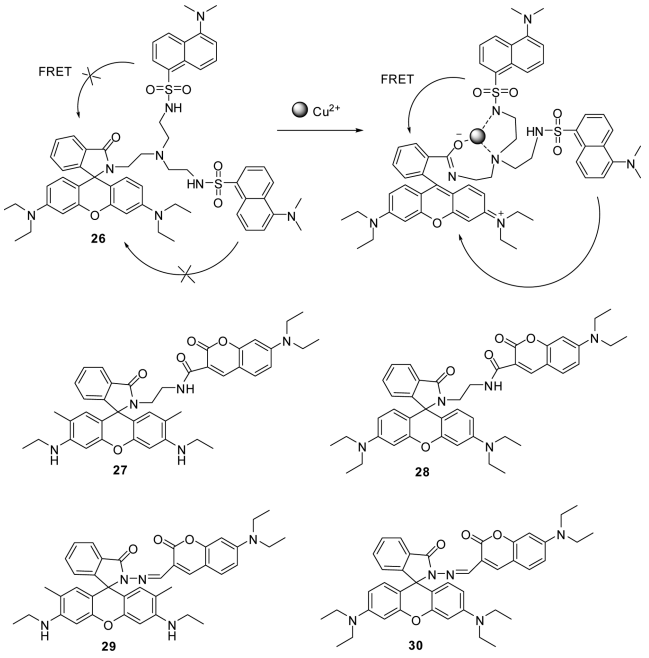

Figure 11. Cu^{2+}-induced FRET mechanism for **26** and structures of **27**−**30**.

transfer (FRET) off−on sensing system has two distinct advantages: one is the large shift between donor excitation and acceptor emission, which rules out any influence of excitation backscattering effects on fluorescence detection; the other is the presence of two well-separated emission bands with comparable intensities, which ensures accuracy in determining their intensities and ratios. Kim et al. reported a rhodamine−dansyl (energy acceptor−energy donor) fluorophore, **26**, which implements the FRET system in Cu^{2+} ion recognition (Figure 11).[54] Upon irradiation at 420 nm, a strong emission at ∼507 nm was observed, which was attributed to the fluorescence emitted from the dansyl energy donor unit. When Cu^{2+} was added, **26** showed an emission band at ∼580 nm, which is in the appropriate region for an energy acceptor. The binding of the Cu^{2+} ion induced opening of the spirolactam ring in molecule **26**, inducing a shift of the absorption spectrum of rhodamine. Subsequently, increased overlap between the emission of the energy donor (dansyl) and the absorption of the energy acceptor (rhodamine) greatly enhances the intramolecular FRET, producing an emission from the energy acceptor unit in molecule **26** (Figure 11). In addition, DFT calculations provided further structural evidence for the switching on of the FRET upon addition of Cu^{2+}.

A system based on the FRET mechanism, comprising a coumarin donor and a rhodamine acceptor, was developed for the selective and quantitative detection of metal ions by Duan's group.[55] Fluorescent chemosensors **27** and **28** (Figure 11), linked by 1,2-diethylamine, exhibited significant fluorescence enhancement and excellent selectivity toward Cu^{2+} in CH_3CN. Due to the larger spectral overlap between the acceptor and donor of **27** than that of **28**, the FRET efficiency of **27** (90%) is higher than that of **28** (33%). Fluorescent probes **29** and **30** (Figure 11), linked by hydrazide, functioned as ratiometric receptors for Cu^{2+} chromogentically and fluorogentically in CH_3CN-H_2O (9:1, v/v). Furthermore, the characteristic rhodamine-based fluorescence response of **30** (excitation at 550 nm)

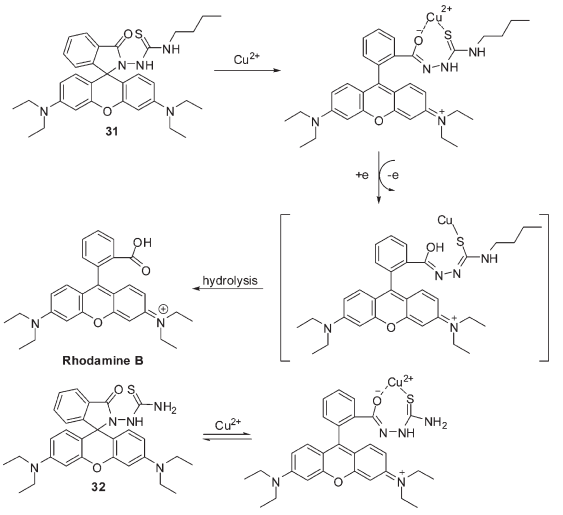

Figure 12. Proposed binding and reaction mechanisms of **31** and **32** with Cu^{2+}.

exhibited high selectivity for Hg^{2+}. In addition, the titration experiments at 495 nm revealed a 2:1 stoichiometry for **30** and Cu^{2+} with an association constant of $(6.50 \pm 0.20) \times 10^{10}$ M^{-2}. On the other hand, the titration experiments at 560 nm assumed a 1:1 stoichiometry for **30** and Hg^{2+} with an association constant of 1.89×10^5 M^{-1}.

Huang's and Li's groups reported a rhodamine B derivative, **31**, containing a highly electron-rich S atom as a fluorescence turn-on chemodosimeter for Cu^{2+} in an aqueous medium.[56] The reaction mechanism involves Cu^{2+}-promoted ring-opening and then a redox process followed by hydrolysis reactions (Figure 12), which may be attributed to the highly electron-rich S atom in **31**. This chemodosimeter displayed very high sensitivity (detection limit ≤10 ppb), a rapid response time (≤1 min), and high selectivity for Cu^{2+} over other transition-metal ions. In addition, confocal and two-photon fluorescence microscopy were used to prove the utility of **31** in monitoring Cu^{2+} within living cells and mapping its subcellular distribution.

Yang's group developed a rhodamine-based chemosensor, **32**, for the detection of copper ions.[57] As a free probe, **32** is colorless and nonfluorescent in CH_3CN-H_2O (30:70, v/v) solution. Upon addition of Cu^{2+}, the ring-opening process of the spirolactam resulted in dramatic increases in both the fluorescence and absorbance intensities (Figure 12). The fluorescence and absorbance signals are linearly proportional to the concentration of Cu^{2+} in the ranges of 0.2−4.0 and 0.5−10 μM, respectively. A 1:1 stoichiometry for the binding mode of **32** and Cu^{2+} is supported by Job's plot, and the association constant of **32** binding with Cu^{2+} is evaluated to be 2.67×10^5 M^{-1}. Except for Hg^{2+}, other metal ions, such as Ag^+, Cd^{2+}, Cr^{3+}, Cu^{2+}, Mg^{2+}, Mn^{2+}, Ni^{2+}, Pb^{2+}, and Zn^{2+}, do not interfere with the Cu^{2+} assay under the present conditions.

A new and simple rhodamine B based chemodosimeter, **33**, for Cu^{2+} has been developed by Hu, Lu, and co-workers.[58] An efficient Cu^{2+}-selective turn-on fluorescence and chromogenic change was observed in 50% (v/v) H_2O-CH_3CN buffered by 10 mM HEPES solution. A linear increase in the fluorescence intensity could be observed with increasing Cu^{2+} concentration over the range of 1−14 μM with a detection limit of 10 nM. The Cu^{2+}-complexed adduct as well as the hydrolyzed product were confirmed by mass spectrometry (Figure 13).

dx.doi.org/10.1021/cr200201z |*Chem. Rev.* 2012, 112, 1910–1956

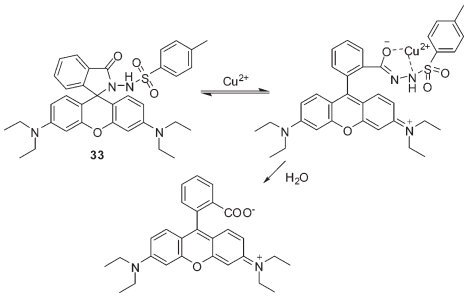

Figure 13. Proposed reaction mechanism of **33** with Cu^{2+}.

The Fenton reaction, discovered in 1894, demonstrated that some metals (Fe^{2+}, Cu^{2+}) can be powerful catalysts to generate highly reactive hydroxyl radicals ($^{\bullet}OH$).[59−61] Xie's group recently reported a new approach for highly sensitive naked eye and fluorescence turn-on detection of Cu^{2+} using a Cu^{2+}-catalyzed Fenton reaction promoted ring-opening of triazole-linked fluorescein lactones.[62] As illustrated in Figure 14, under aerobic conditions, ascorbate ($AscH^-$) is not only involved in the reduction of Cu^{2+} (a), but also reacts with O_2 to produce H_2O_2 (b). Hydroxide and $^{\bullet}OH$ were then produced in the next Fenton reaction (c). The increase in pH from the increasing levels of hydroxide ions promoted the ring-opening of **34** (d), resulting in fluorescence enhancement (λ_{max} = 517 nm) and color change (from colorless to light yellow). The naked eye detection limit of this protocol was as low as 200 nM.

Qin et al. prepared an optical film for the detection of Cu(II) ions by incorporating **35**, *N*,*N*,*N*′,*N*′-tetracyclohexyl-3-thiaglutaric diamide (as a copper ionophore), and sodium tetrakis[3,5-bis(trifluoromethyl)phenyl]borate (as a cation exchanger) into a poly(vinyl chloride)−bis(2-ethylhexyl) sebacate membrane.[63] In buffered aqueous solutions at pH 5.5, the sensing system is strongly fluorescent due to the presence of protons in the film, which induce a ring-opened form of **35-I** (Figure 15). With the addition of Cu(II), a metal ion−proton exchange process results in proton release from the film and the formation of nonfluorescent spirolactam. A nanomolar detection limit level was determined by monitoring the fluorescence quenching of the film. Furthermore, when BODIPY fluorophore was introduced into the system, the FRET process went from the excited BODIPY fluorophore to the rhodamine moiety, leading to a ratiometric fluorescence change.

2.2. Sensors for Detecting Hg^{2+}/CH_3Hg^+

Mercury is one of the most prevalent toxic metals in the environment and gains access to the body orally or dermally. The U.S. EPA (Environmental Protection Agency) standard for the maximum allowable level of inorganic Hg in drinking water is 2 ppb.[64] Due to the high toxicity of mercury, considerable attention has been devoted to the development of new fluorescent chemosensors with sufficient selectivity for the detection of mercury and mercuric salts.[3] Rhodamine B hydrazide (**1**) has been used as a fluorescent chemodosimeter for Cu^{2+}, while Chang et al. have explored its application in the detection of Hg^{2+} by switching the testing medium (Figure 16).[65] In an acetate-buffered aqueous 10% methanol solution at pH 5, the fluorescence intensity of **1** increased rapidly upon addition of Hg^{2+} ions due to the hydrolysis of the lactam ring of the hydrazide, while an intense absorption band centered at 556 nm appeared. By monitoring the fluorescence intensity at 578 nm, the reaction

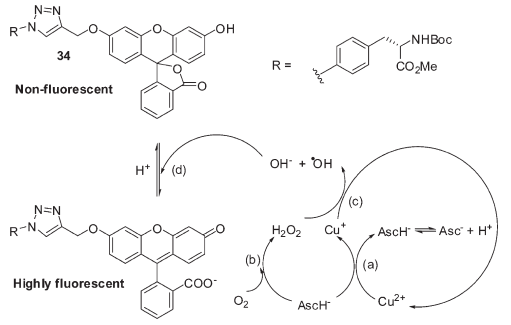

Figure 14. Proposed mechanism for detection of Cu^{2+} based on the Fenton reaction.

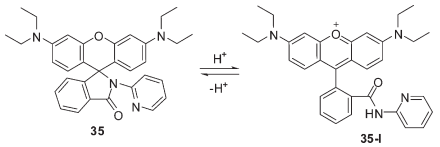

Figure 15. Reversible ring-opening process of probe **35** induced by H^+.

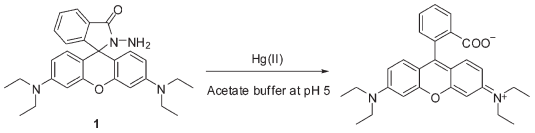

Figure 16. Hydrolysis of **1** upon addition of Hg^{2+} in acetate buffer (pH 5).

between **1** (5 μM) and 10 equiv of Hg^{2+} is complete within 10 min. A linear increase in the fluorescence intensity with the concentration of Hg^{2+} ranging from 0 to 2.0×10^{-5} M was observed, and the detection limit was calculated to be 0.2 μM. The fluorescence responses were observed only with the addition of Hg^{2+}, exhibiting the selectivity of **1** toward Hg^{2+} under the present conditions.

Das et al. reported a rhodamine-based chemosensor, **36**, for the detection of Hg^{2+} and Cu^{2+} (Figure 17).[66] In water−methanol (1:1, v/v) solution at pH 7.0, both Hg^{2+} and Cu^{2+} induced color changes with new absorption peaks appearing at 534 nm for Hg^{2+} and 528 nm for Cu^{2+}. A 90-fold enhancement in fluorescence intensity at 554 nm was observed with the addition of only 8 equiv of Hg^{2+}, while no fluorescence change was found in the presence of Cu^{2+}; this was attributed to the quenching effect of paramagnetic copper ions. In contrast, other metal ions did not induce any significant color and fluorescence changes under identical conditions. Absorption titrations revealed that **36** can bind Cu^{2+} and Hg^{2+} to form the corresponding complexes Cu^{2+}−**36** and Hg^{2+}−$(\mathbf{36})_2$, with association constants of $(1.68 \pm 0.012) \times 10^5$ M^{-1} and $(8.0 \pm 0.1) \times 10^5$ M^{-2}, respectively. The fluorescence and color of the solution containing **36** and Hg^{2+} fade upon addition of KI, indicating the reversibility of the chemosensor for Hg^{2+}. Furthermore, using an optical microscope, **36** can be used to detect Hg^{2+} absorbed on the cell surface of *Pseudomonas putida*, in that the color of bacterial cells treated with Hg^{2+} changed to pink after treatment with **36**.

Yoon et al. reported two rhodamine hydrazone derivatives, **37** and **38** (Figure 18), bearing thiol and carboxylic acid groups,

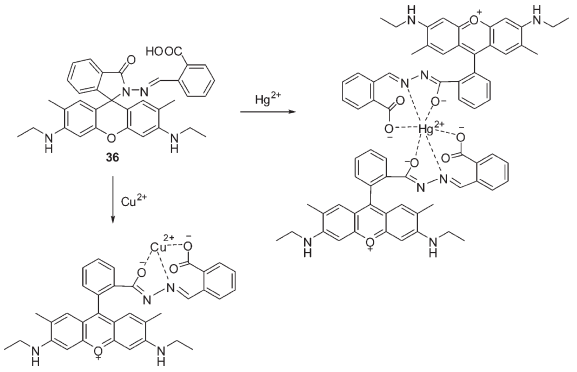

Figure 17. Binding mechanisms of **36** with Hg^{2+} and Cu^{2+}.

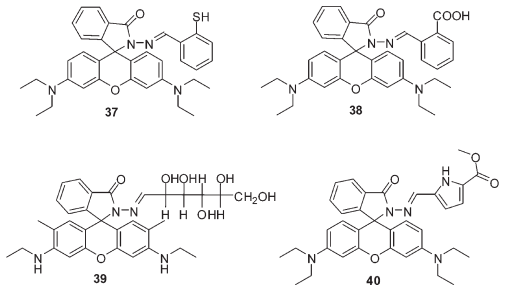

Figure 18. Structures of **37**−**40**.

respectively, as selective fluorescent and colorimetric chemosensors for Hg^{2+}.[67] The ring-opening process of spirolactam leads to a large fluorescence enhancement and colorimetric change upon addition of Hg^{2+}. In CH_3CN-H_2O (1:99, v/v) solution, the addition of 100 equiv of Hg^{2+} induces enhancements in the fluorescence intensities at the maximum emission wavelengths of **37** and **38** of approximately 10-fold and 50-fold, respectively. By monitoring the fluorescence of a microchannel containing **37**/**38** with Hg^{2+}, a plot of the fluorescence intensities of both chemosensors versus the log concentration of Hg^{2+} exhibited a linear response in the range from 1 nM to 1 μM, and the detection limits were 1 nM for **37** and 4.2 nM for **38**. Addition of excess KI to a mixture of chemosensor **37** or **38** with Hg^{2+} showed a decrease in fluorescence, which indicated that the interaction of chemosensor **37** or **38** with Hg^{2+} is chemically reversible. Furthermore, Job's plot methods demonstrated a 2:1 stoichiometry for the binding of **37** and Hg^{2+} and a 1:1 stoichiometry for the binding of **38** and Hg^{2+}. Both chemosensors also enable the visualization of Hg^{2+} accumulated in the nematode *Caenorhabditis elegans* previously exposed to nanomolar concentrations of Hg^{2+}.

Duan and Li's groups presented a Hg^{2+}-selective sensor, **39** (Figure 18), by the combination of rhodamine and a sugar group.[68] In neutral aqueous solution, free sensor **39** displayed a weak emission band at about 550 nm when excited at 500 nm. Upon addition of Hg^{2+}, typical absorption and emission spectra of ring-opened rhodamine appeared. The 1:1 stoichiometry for binding between **39** and Hg^{2+} was evaluated by the Job's plot method, and the association constant was calculated to be $(5.4 \pm 0.1) \times 10^5\ M^{-1}$. The addition of NaI or Na_2S to a solution containing **39**−Hg^{2+} quenched fluorescence, indicating the reversible binding mode between **39** and Hg^{2+}. Probe **39** also showed good selectivity for Hg^{2+} because no significant changes

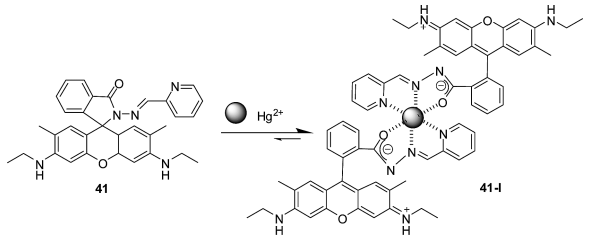

Figure 19. Proposed binding mode of **41** with Hg^{2+}.

in absorption and emission spectra were observed in the presence of other metal ions. The limit of 1 ppb for the detection of Hg^{2+} suggested that **39** can be applied to monitor Hg^{2+} levels in drinking water. When HeLa cells were supplemented with 10 μM $Hg(NO_3)_2$ and then incubated with **39**, a significant fluorescence increase was observed in the perinuclear region of the cytosol.

On the basis of the concept of a "single sensor for multiple analytes", Tang and Nandhakumar et al. developed a novel rhodamine B derivate, **40** (Figure 18),[69] which enables the detection of both Cu^{2+} and Hg^{2+} by colorimetric and fluorescence methods, respectively. In MeOH−H_2O (3:1, v/v) solution buffered at pH 7.4 (HEPES, 10 mM), free **40** was colorless and weakly fluorescent when excited at 530 nm. Upon addition of 2.0 equiv of Cu^{2+}, a new strong absorption band centered at 556 nm was observed. However, the solution was still weakly fluorescent, indicating that the fluorescence of the rhodamine spirolactam ring-opened form was quenched by Cu^{2+} due to its paramagnetic nature. In contrast, addition of Hg^{2+} induced a remarkable fluorescence enhancement, while no absorption response was observed. Using Benesi−Hildebrand plots based on a 1:1 binding mode, the binding constants were estimated to be $2.44 \times 10^5\ M^{-1}$ for **40**−Cu^{2+} and $3.4 \times 10^2\ M^{-1}$ for **40**−Hg^{2+}.

Duan et al. reported a simple and easy-to-prepare rhodamine-based probe, **41**, which contains a carbohydrazone unit for detection of Hg^{2+} (Figure 19). The structures of both **41** and complex **41-I** were fully characterized using an X-ray method.[70] This first X-ray crystal structure with metal ions clearly showed the ring-opened structure of the rhodamine derivative with Hg^{2+}. This probe, **41**, showed Hg^{2+}-selective fluorescence enhancement, and the detection limit was evaluated to be as low as 2 ppb in a DMF aqueous (50:50, v/v) solution.

By introducing a ferrocene moiety to the rhodamine 6G chromophore, Duan et al. prepared a Hg^{2+}-selective sensor **42** (Figure 20) with a detection limit of 1 ppb by fluorescence means.[71] In water, Hg^{2+} can cause great color and fluorescence enhancement of **42**, and the characteristic color change from colorless to pink showed that **42** can be used for "naked eye" detection of Hg^{2+} in water. Due to the existence of the ferrocene moiety, the binding between **42** and Hg^{2+} also causes a significant shift of the redox potential of the ferrocene/ferrocenium couple. Via an electrochemical method, Hg^{2+} can be quantified at the parts per million level. Job's plot and electrospray-ionization mass spectrometry (ESI-MS) demonstrated the formation of the complex **42**−Hg^{2+}, and the association constant was evaluated to be $(1.16 \pm 0.04) \times 10^6\ M^{-1}$. Compared with **42**, **43** (Figure 20) bearing two fluorescently active rhodamine groups showed inferior affinity to Hg^{2+} with an association constant of $(2.8 \pm 0.2) \times 10^5\ M^{-1}$ on the basis of a 2:2 stoichiometry. In addition, the binding between Hg^{2+} and **43** cannot induce a significant potential shift of the ferrocene/ferrocenium redox couple.

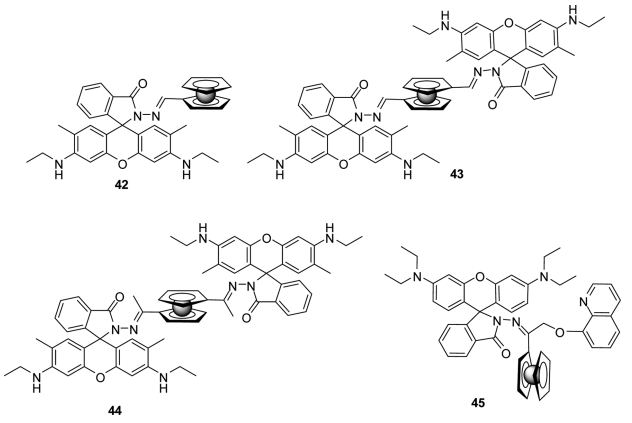

Figure 20. Structures of **42**−**45**.

Duan et al. reported a conformationally flexible chemosensor, **44** (Figure 20), by incorporating two rhodamine fluorophores and a ferrocene group for the detection of Hg^{2+}.[72] In aqueous solution, upon addition of Hg^{2+}, an obvious color change from colorless to pink and an enhancement in the fluorescence intensity were observed due to the binding between **44** and Hg^{2+}. The stability constant of **44** binding with Hg^{2+} was calculated to be 3.2×10^4 M^{-1}. The 1:1 stoichiometry of **44**−Hg^{2+} was supported by the titration experiment and ESI-MS spectra. Furthermore, sensor **44** can detect the parts per billion level of Hg^{2+}, indicating high sensitivity toward Hg^{2+}.

Huang, Li, and co-workers recently reported a multisignaling optical−electrochemical sensor, **45** (Figure 20), for Hg^{2+} based on a rhodamine dye bearing both an 8-hydroxyquinoline moiety and a ferrocenyl group.[73] Upon addition of Hg^{2+} in ethanol−HEPES buffer (1:1, v/v; pH 7.2) containing sensor **45**, a selective fluorescence enhancement was observed, accompanied by a colorimetric change (colorless to pink) and a clear evolution of the oxidation peak ($E_{1/2}$) versus decamethylferrocene (from 0.40 to 0.15 V). By laser scanning confocal microscopy, a significant increase in the fluorescence from the intracellular area was observed in staining Caov-3 ovarian carcinoma cells with a solution of **45** after treatment with Hg^{2+}.

Peng et al. reported a rhodamine-based chemodosimeter, **46**, via a mechanism of Hg^{2+}-promoted hydrolysis (Figure 21).[74] In ethanol−water (1:1, v/v; pH 7.0) solution, free **46** exhibited no obvious fluorescence and absorption because it mostly exists in the spirocyclic form. Upon addition of Hg^{2+}, the intensity of fluorescence emission was significantly enhanced by over 370-fold at 579 nm, accompanied by a new absorption band centered at 554 nm. The fluorescence intensity of **46** was proportional to the amount of Hg^{2+} added at the parts per billion level, and the detection limit was evaluated to be 0.91 ppb using 5 μM sensor. The ESI-mass spectra provided evidence for the following mechanism: upon addition of Hg^{2+}, a complex, **46**−Hg^{2+}, forms in the first equilibrium, resulting in ring-opening, and then the complex is further hydrolyzed to fluorescent rhodamine B in the presence of water. The fluorescence response of **46** to Hg^{2+} does not interfere with sulfur compounds such as cysteine and glutathione, and the sensor could be used for Hg^{2+} imaging in living cells.

Shiraishi et al. designed sensor **47** using a rhodamine platform in conjunction with a cyclen moiety (Figure 22).[75] In CH_3CN, free probe **47** is colorless and nonfluorescent due to it existing in

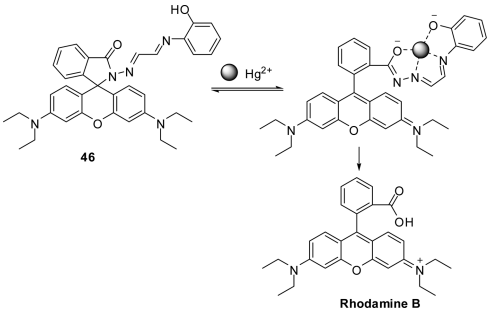

Figure 21. Proposed binding mode of **46** with Hg^{2+}.

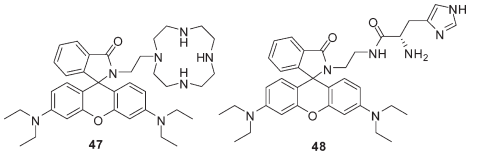

Figure 22. Structures of **47** and **48**.

the spirocyclic form. With the addition of 10 equiv of Hg^{2+}, a 1700-fold fluorescence enhancement at 580 nm and a new absorption band at 450−600 nm were observed. The fluorescence increase became saturated after addition of Hg^{2+} for 1 min. The good selectivity of **47** for Hg^{2+} was confirmed because no fluorescence enhancement was observed with the addition of other metals. The color and fluorescence disappeared when triethylenetetramine was added to the solution containing **47** and Hg^{2+}, indicating the reversible coordination of **47** and Hg^{2+}. ESI-MS analysis, absorption, and IR titrations showed that **47** can bind with two mercury ions to form a 1:2 complex, where one Hg^{2+} is anchored by the cyclen moiety and the second Hg^{2+} binds with the carbonyl oxygen, leading to the spiroring-opened form of the rhodamine moiety.

Yoon's group reported a rhodamine-based sensor, **48** (Figure 22), bearing a histidine unit for the detection of Hg^{2+}.[76] Two carbonyl oxygens as well as the imidazole nitrogen in probe **48** provide a nice binding pocket for Hg^{2+}. In EtOH−HEPES buffer (9:1, v/v; pH 7.4), the addition of 100 equiv of Hg^{2+} induced an increase in fluorescence of over 100-fold due to the spirolactam ring-opening. In contrast, no response was observed when other metal ions were added. From the fluorescence titrations, the association constant of **48** with Hg^{2+} was calculated to be 2.0×10^3 M^{-1}. The binding between **48** and Hg^{2+} is reversible because the addition of 1,10-diaza-4,7,14,17-tetrathiacyclooctadecane can lead to the disappearance of fluorescence. Using confocal laser scanning microscopy, HeLa cells treated with sensor **48** for 1 h showed a fluorescence enhancement after incubation with $HgCl_2$ for 20 min.

Kim's group and Bharadwaj's group developed a cryptand−rhodamine conjugated chemodosimeter, **49**, for the detection of Hg^{2+}.[77] The geometric arrangement of aliphatic N atoms in the cryptand core in **49** provides good binding sites for Hg^{2+} (Figure 23). In 20% EtOH−H_2O medium, addition of Hg^{2+} results in prominent changes in both the absorption and emission spectra of **49**, while other ions are silent. The UV−vis titration revealed a 1:3 stoichiometry for the **49**−Hg^{2+} complex with an association constant of around 7×10^{11} M^{-3}. Further sensitivity assays showed that **49** can detect a parts per billion

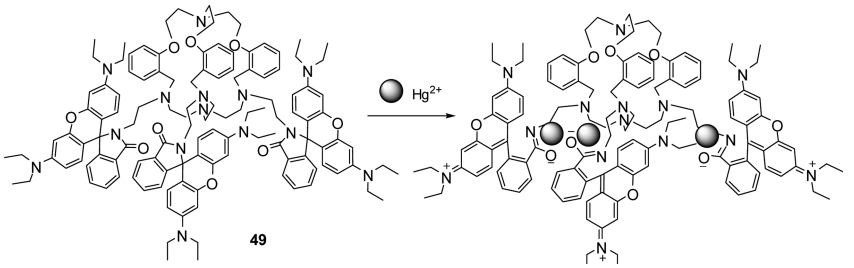

Figure 23. Proposed binding mode of **49** with Hg^{2+}.

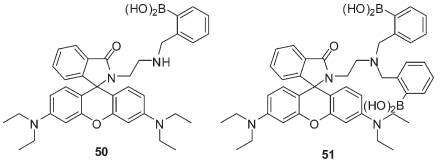

Figure 24. Structures of **50** and **51**.

level of Hg^{2+} in 1% EtOH−H_2O solution. The HEK 293 cells incubated with **49** initially displayed a very weak fluorescence image, but the cellular fluorescence immediately increased upon addition of Hg^{2+}, indicating that this sensor is useful to map Hg^{2+} in living cells.

Rhodamine derivatives **50** and **51** (Figure 24) bearing mono- and bis(boronic acid) groups were also presented as selective fluorescent and colorimetric sensors for Hg^{2+}.[78] In CH_3CN−HEPES buffer (pH 7.4; 10 mM; 9:1, v/v), two sensors displayed selective off−on-type fluorescence enhancements and distinct color changes with Hg^{2+}. The 1:1 stoichiometries for the binding mode of two sensors with Hg^{2+} were confirmed by Job's plot, and the association constants of **50** and **51** with Hg^{2+} were calculated as 3.3×10^3 and 2.1×10^4 M^{-1}, respectively. Bisboronic probe **51** displayed binding with Hg^{2+} as high as 9-fold tighter than that of the monoboronic probe **50**; this can be attributed to the additional boronic acid moiety of **51**.

Yoon et al. reported rhodamine derivatives **52** and **53** with urea groups.[79] The dimeric system **53** showed a highly selective fluorescence enhancement and colorimetric change upon addition of Hg^{2+} in acetonitrile, which were attributed to the ring-opening process of the spirolactam (Figure 25). In contrast, compound **52** showed poorer selectivity toward Hg^{2+}. From the fluorescence titrations, the association constants of **52** and **53** with Hg^{2+} were observed to be 2.9×10^4 and 3.2×10^5 M^{-1}, respectively.

Kim et al. reported new rhodamine-based tris(2-aminoethyl)-amine (tren)/diethylenetriamine (**54**/**55**) with tosyl groups.[80] Because Hg^{2+} could be trapped by tren or diethylenetriamine, the addition of Hg^{2+} ions to the CH_3CN solutions of molecule **54** or **55** produced both a visual color change and enhanced fluorescence intensity (Figure 26). In addition, the increased fluorescence intensity of complex **54**−Hg^{2+} is 6 times greater than that of complex **55**−Hg^{2+}. It should be noted that, compared to molecule **55**, tosylated ethyleneamine from the tren in molecule **54** can also bind Hg^{2+} ions, inducing ring-opening of the spirolactam of molecule **54** more effectively. In terms of practical applicability, the conditions of Hg^{2+} detection were optimized in 90% CH_3CN aqueous solution with a pH spanning 3−6.

Kumer reported a terphenyl derivative, **56**, bearing double rhodamine fluorophores as a selective fluorescent and colorimetric sensor for Hg^{2+} ions.[81] In THF solution, the addition of Hg^{2+} induced a 2500-fold enhancement in the fluorescence intensity of **56** at 576 nm when excited at 550 nm, suggesting the formation of

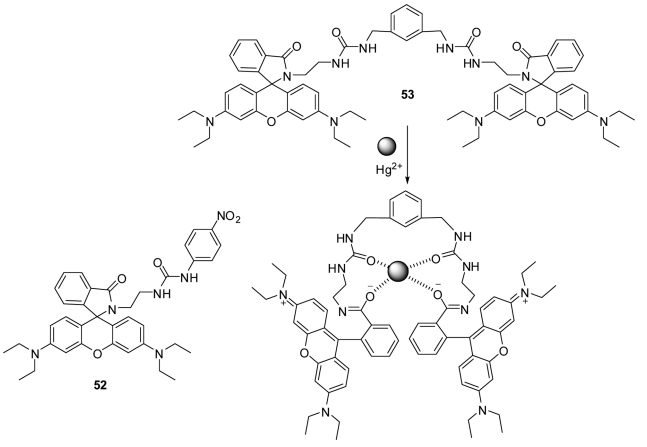

Figure 25. Structures of rhodamine B urea derivatives **52** and **53** and a proposed binding mode of **53** with Hg^{2+}.

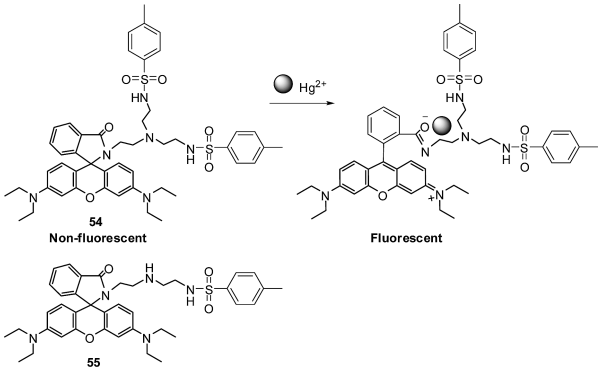

Figure 26. Proposed binding mode of **54** with Hg^{2+} and structure of **55**.

ring-opened rhodamine (Figure 27). The 1:2 binding stoichiometry between **56** and Hg^{2+} ions was confirmed by the Job's plot method, and the binding constant was found to be $(4.8 \pm 0.5) \times 10^8$ M^{-2} from the Hg^{2+} titration curves. The detection limit of **56** as a fluorescent sensor for the detection of Hg^{2+} was evaluated to be 5×10^{-7} M.

Guo et al. reported a reversible, selective, and sensitive fluorescent sensor, **57**, based on a rhodamine fluorophore and the 8-hydroxyquinoline group (Figure 28).[82] In CH_3CN−water solution (95:5, v/v; pH 7.2), upon addition of 7 equiv of Hg^{2+}, **57** showed a >1200-fold enhancement in the fluorescence intensity at 586 nm, accompanied by a new absorption peak appearing at around 560 nm. A 1:1 binding mode was supported by the Job's plot method, and the association constant for Hg^{2+} was estimated to be 2.18×10^6 M^{-1}. By fluorescence titration with 1 μM

dx.doi.org/10.1021/cr200201z |*Chem. Rev.* 2012, 112, 1910–1956

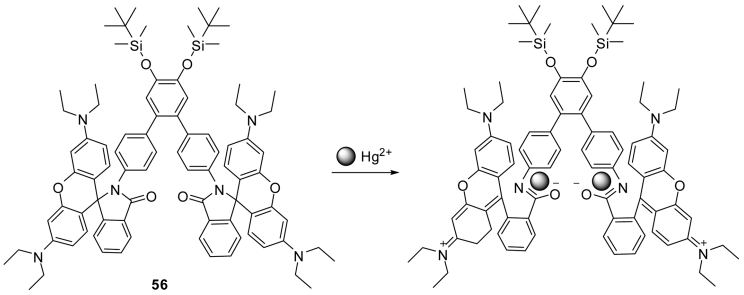

Figure 27. Proposed binding mode of **56** with Hg^{2+}.

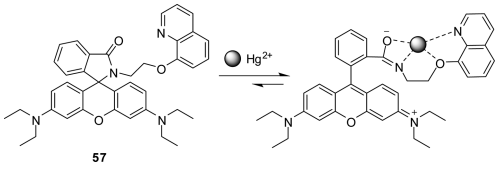

Figure 28. Proposed binding mode of **57** with Hg^{2+}.

sensor **57**, the detection limit for Hg^{2+} was measured to be 1.14 ppb with a signal-to-noise ratio (S/N) of 3. Only Hg^{2+} resulted in significant changes in the spectra, confirming the remarkable selectivity toward Hg^{2+} under the present conditions. The addition of iodide anions caused the color and fluorescence of **57**−Hg^{2+} to fade, indicating the reversibility of sensor **57**. After HeLa cells were incubated with **57** and then treated with Hg^{2+}, a significant increase in fluorescence intensity was observed using fluorescence microscopy.

Qian et al. developed a rhodamine-based sensor, **58** (Figure 29), bearing ionophore NS_2 with a high affinity for Hg^{2+}.[83] In CH_3CN−HEPES (15:85, v/v; pH 6.98) solution containing sensor **58**, treatment with 2 equiv of Hg^{2+} induced a significant color change (from colorless to purple) and a 400-fold fluorescence enhancement of the sensor. The 1:1 stoichiometry of the binding between **58** and Hg^{2+} was confirmed by the Job's plot method, and the binding constant was calculated to be $(1.18 \pm 0.13) \times 10^6\ M^{-1}$. The addition of EDTA led to both the color and fluorescence fading, indicating the reversibility of the binding between **58** and Hg^{2+}. Under the same conditions, sensor **58** is highly specific toward Hg^{2+} because there is no significant variation in fluorescence intensity in the presence of other metal ions.

Ma et al. and Xu et al. independently reported the rhodamine B thiolactone **59** as a highly selective and sensitive sensor for Hg^{2+} in 20 mM phosphate buffer (pH 7) and 10 mM acetate buffer (pH 4).[84,85] Under these conditions, **59** displayed a selective fluorescence enhancement as well as colorimetric change only with Hg^{2+} among the various metal ions examined. Even though Xu et al. reported that this ring-opening process was reversible under their experimental conditions, Ma et al. reported that the introduction of KI to the system can reverse the color reaction only in the presence of less than 0.5 equiv of Hg^{2+}. On the basis of the ESI-MS data, Ma et al. further proposed, as shown in Figure 30, that complex **59-I** is relatively stable in the solution; however, complex **59-II** can be further degraded to rhodamine B.

Yoon et al. used X-ray crystallography to explicitly prove the geometry of the bound Hg^{2+}-ring-opened rhodamine 6G complex formed from the Hg^{2+} ion induced spirothiolactone ring-opened system.[86] With respect to fluorescence enhancement after metal ion binding, compound **60** (Figure 30) showed a very high selectivity toward Hg(II) ions over other metal ions in CH_3CN−HEPES buffer

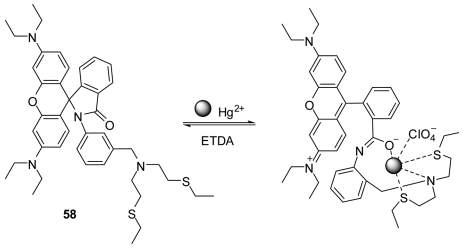

Figure 29. Proposed binding mode of **58** with Hg^{2+}.

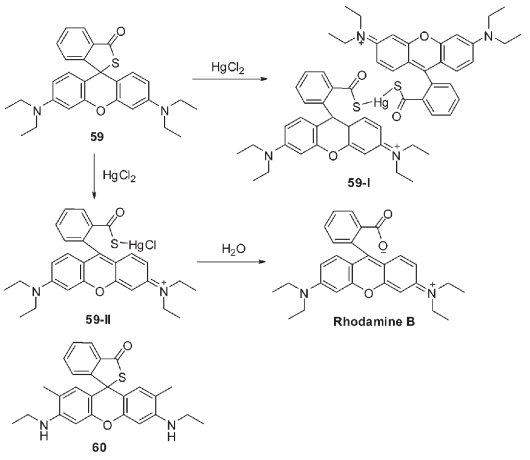

Figure 30. Proposed binding mode of **59** with Hg^{2+} and structure of **60**.

(0.01 M; pH 7.4; 1:99, v/v). This behavior is similar to that of **59**. An enhancement of up to a 200-fold off−on-type fluorescence for **60** was observed after addition of Hg^{2+}. Evidence for a 2:1 binding mode (**60**:Hg^{2+}) was provided by ESI-MS, Job's plot, and X-ray crystal structure data. The spirothiolactone ring-opened structure, as well as the coordination of the two sulfur atoms to Hg^{2+}, was clearly confirmed. Since the nature of probe **60** is based on a reversible coordination event, it really can be considered as a chemosensor.

Duan et al. reported a series of rhodamine derivatives, **61**, **62**, and **63** (Figure 31), by combination of a spirothiolactone chromophore and assorted carboxaldehydes.[87] In DMF−H_2O (1:1, v/v) solution containing **61**, upon addition of Hg^{2+}, both the fluorescence intensity at 585 nm and absorption peak at 565 nm were significantly enhanced, owing to the formation of the ring-opened rhodamine. Furthermore, the 1:1 stoichiometry for the **61**−Hg^{2+} complexation was determined with an association constant of $(1.82 \pm 0.04) \times 10^5\ M^{-1}$. Compared to **61**, **62** and **63** showed better water solubility. In DMF−H_2O (0.5%, v/v)

dx.doi.org/10.1021/cr200201z |*Chem. Rev.* 2012, 112, 1910–1956

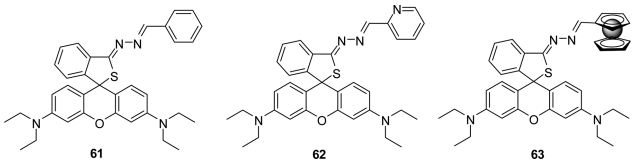

Figure 31. Structures of **61**−**63**.

solution containing 100 nM **62** or **63**, the fluorescence intensities were proportional to the concentration of Hg^{2+} at the parts per billion level. **62** and **63** bind Hg^{2+} with 1:2 and 1:1 stoichiometries, respectively. The association constants were calculated to be $7.6 \times 10^9\ M^{-2}$ for Hg^{2+}−(**62**)$_2$ and $3.33 \times 10^6\ M^{-1}$ for Hg^{2+}−**63**. All three sensors showed selective responses in fluorescence spectra with the addition of Hg^{2+}. High sensitivity and selectivity were attributed to the following factors: the suitable coordination conformation of the receptor, the large radius of Hg^{2+}, the strong affinity between sulfur and Hg^{2+}, and the electronic or spatial effects of aromatic or ferrocenyl groups.

On the basis of the strong affinity between Hg^{2+} and sulfur, Duan et al. designed three rhodamine derivatives, **64**, **65**, and **66** (Figure 32), bearing thiophene groups for the detection of Hg^{2+}.[88] In CH_3CN-H_2O (7:3, v/v) solution, free **64** mostly exists as the spirolactam form, only exhibiting weak fluorescence at 550 nm and faint absorption bands at 525 nm. Upon addition of Hg^{2+}, both fluorescence and absorption showed significant enhancement, suggesting the formation of the ring-opened amide form of sensor **64**. The fluorescence titration assays using 1 μM **64** exhibited the detection of Hg^{2+} was at the parts per billion level. A 1:2 stoichiometry for Hg^{2+}−(**64**)$_2$ complexation was supported by Job's plot, and the association constant was evaluated to be $8.18 \times 10^7\ M^{-2}$. In the same medium, **65** showed obvious responses to Fe^{2+}, Cu^{2+}, Pb^{2+}, Ag^+, and Hg^{2+}, indicating poorer selectivity toward Hg^{2+} compared with that of **64**. The titration assays demonstrated that **65** binds Hg^{2+} with a 2:1 stoichiometry and an association constant of ca. $1.58 \times 10^{13}\ M^{-2}$. Compared to **64** and **65**, sensor **66**, which contains two rhodamine carbohydrazone units, exhibited the best selectivity toward Hg^{2+}. A 1:1 stoichiometry for the complexation of **66**−Hg^{2+} with an association constant of ca. $4.8 \times 10^6\ M^{-1}$ was demonstrated through titration experiments. In CH_3CN-H_2O (7:3, v/v) solution, low-concentration fluorescence titration showed that **66** (1 μM) can detect Hg^{2+} at the parts per billion level.

Lin et al. presented a rhodamine-based probe, **67**, composed of a sulfur atom and an alkyne moiety for the irreversible detection of Hg^{2+} (Figure 33).[89] Thiol and alkyne moieties were sited on the probe due to the thiophilic and π-philic natures of Hg^{2+}. In PBS buffer (25 mM, pH 7.2, containing 20% DMF as a cosolvent), treatment with Hg^{2+} induced probe **67** to undergo a transformation from colorless to bright yellow, as well as a dramatic enhancement (140-fold) in fluorescence. The spectral changes of probe **67** were attributed to the formation of compounds **67-I** and **67-II** upon addition of Hg^{2+}. A linear fluorescence response to the concentration of Hg^{2+} ranging from 5×10^{-8} to 4×10^{-6} M was observed, and the detection limit was evaluated to be 39 nM. pH effect studies imply that the probe can detect Hg^{2+} in the pH 6.0−7.4 range. Both the S atom and alkyne of probe **67** played indispensable roles because the control compounds lacking S atoms or alkyne moieties show no response to Hg^{2+}. After human Tca-8113 cells were treated with probe **67** and then were incubated with Hg^{2+}, a large fluorescence

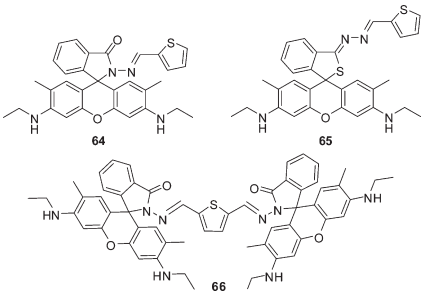

Figure 32. Structures of **64**−**66**.

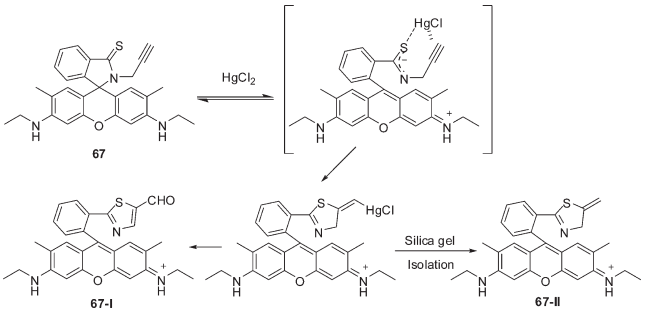

Figure 33. Proposed reaction mechanism of **67** with Hg^{2+}.

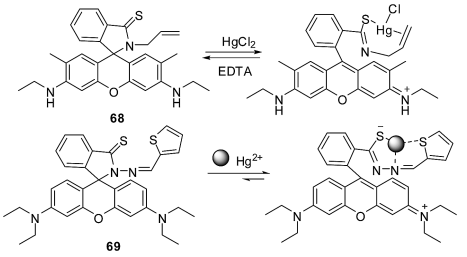

Figure 34. Proposed binding modes of **68** and **69** with Hg^{2+}.

enhancement was observed, indicating that probe **67** was cell membrane permeable and able to sense Hg^{2+} in living cells.

On the basis of a receptor composed of a thiol atom and an alkene moiety, a similar sensor, **68**, for the detection of Hg^{2+} was developed by Lin's group.[90] Due to the thiophilic and π-philic natures of mercury ions, the receptor bearing a S atom and the alkene unit provided a suitable binding pocket for Hg^{2+}. In PBS buffer (25 mM, pH 7.0, containing 2.5% CH_3CN as a cosolvent), the addition of Hg^{2+} can induce a 1000-fold enhancement in emission intensity at 561 nm, as well as the formation of a new absorption peak at around 534 nm (Figure 34). The stoichiometry of binding between **68** and Hg^{2+} and the dissociation constant were determined to be 1:1 and 2.5×10^{-5} M, respectively. The detection limit of 2.75×10^{-8} M showed the high sensitivity of **68** toward Hg^{2+}. Compared to **67**, only the coordination, instead of further reaction, induced the transformation of the rhodamine dye from the spirocyclic form to the opened-ring form, and **68** showed its reversibility in the presence of EDTA.

Yao et al. designed a Hg^{2+}-selective sensor, **69**, containing a thiospirolactone rhodamine chromophore and a thiophene moiety (Figure 34).[91] In ethanol−HEPES (50 mM; pH 7.0; 50:50, v/v) solution, upon addition of Hg^{2+}, **69** showed a

dx.doi.org/10.1021/cr200201z |*Chem. Rev.* 2012, 112, 1910–1956

442-fold enhancement in fluorescence intensity at 593 nm. Only Ag^+ and Cu^{2+} exhibited optical response, with 15-fold and 39-fold enhancements, respectively. The two sulfur atoms of **69** provided the high affinity toward Hg^{2+} with a 1:1 binding mode, and the association constant of $1.86 \times 10^6\ M^{-1}$ was found by the Job's plot method. The enhancement in fluorescence intensity was proportional to the concentration of Hg^{2+} ranging from 0.5×10^{-8} to 3.14×10^{-8} M, and a detection limit of 1.72×10^{-9} M was evaluated.

Zheng, Xu, and co-workers utilized a rhodamine B thiohydrazide as a fluorescent chemosensor for Hg^{2+}.[92] This sensor, **70** (Figure 35), exhibits reversible chromo- and fluorogenic changes for Hg^{2+} in aqueous solution at pH 3.4 in a highly selective and sensitive manner. This result was attributed to the coordination of Hg^{2+} at the N and S binding sites in **70** (1:2 stoichiometry) to open its spirolactam ring.

By conjugating the rhodamine unit with the coumarin fluorophore, Zhang and co-workers reported a fluorescent probe, **71** (Figure 35), for the detection of Hg^{2+}.[93] In Tris−HCl buffer (pH 7.24) solution containing 50% ethanol as a cosolvent, probe **71** exhibited high sensitivity and selectivity toward Hg^{2+}, and excess Hg^{2+} induced an approximately 24-fold increase in emission intensity as well as a new absorption peak at 565 nm. The linear relationship between the fluorescence emission intensity and the concentration of Hg^{2+} ranging from 8.0×10^{-8} to 1.0×10^{-5} M was also observed. By the Job's plot method, the 1:1 stoichiometry of **71**−Hg^{2+} complexation was confirmed, and the association constant for Hg^{2+} was estimated to be $1.18 \times 10^6\ M^{-1}$. The addition of EDTA led to the fading of the fluorescence and color, indicating reversible binding between **71** and Hg^{2+}. Furthermore, **71** was successfully applied to the detection of Hg^{2+} in both tap and river water samples.

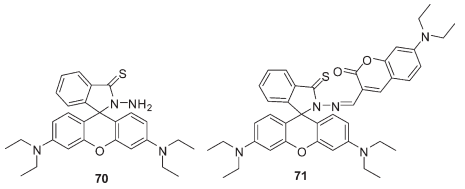

Figure 35. Structures of **70** and **71**.

Kim et al. reported a Hg^{2+}-selective probe by employing rhodamine and pyrene excimers.[94] In CH_3CN solution, the fluorescence of sensor **72** is weak due to the spirocyclic form of the rhodamine fluorophore and the photoinduced electron transfer (PET) effect from the nitrogen atom of the tren part to the excited state of the pyrene moieties. Upon addition of Hg^{2+}, sensor **72** show a new absorption band at 554 nm, as well as enhancement of the emission at 574 nm with excitation at 520 nm; this was attributed to the generation of ring-opened rhodamine. When excited at 340 nm, the fluorescence intensities of both the pyrenyl monomer and the excimer increase, mainly due to the metal ion induced chelation-enhanced fluorescence (CHEF) caused by the Hg^{2+}-bound tren nitrogen to the pyrene arms (Figure 36). Both the spirolactam carboxyl group in the rhodamine and tren part are involved in the Hg^{2+} binding to induce the ring-opening of **72**. The association constant of sensor **72** and Hg^{2+} was calculated to be $2.4 \times 10^3\ M^{-1}$.

Tae et al. developed a novel system using a rhodamine 6G derivative which works as a highly selective and sensitive chemodosimeter for Hg^{2+} in aqueous solution.[95] The system, which utilizes an irreversible Hg^{2+}-promoted oxadiazole-forming reaction involving rhodamine derivative **73**, is monitored by changes in colorimetric and fluorescence intensities that occur instantaneously at room temperature in a 1:1 stoichiometric manner to the amount of Hg^{2+} present (Figure 37). After addition of Hg^{2+} (1.0 equiv) to a solution of **73** in water−methanol (4:1, v/v), a 26-fold fluorescence enhancement was produced with a concomitant 4 nm red shift in the wavelength of the maximum emission, from 553 to 557 nm. Metal ion selectivity experiments indicated that the emission from **73** was unaffected by any of the following species: Cu^{2+}, Pb^{2+}, Cd^{2+}, Ni^{2+}, Co^{2+}, Fe^{2+}, Mn^{2+}, Mg^{2+}, Ca^{2+}, Ba^{2+}, Li^+, K^+, Na^+, Rh^{3+}, and Cr^{2+}. Although the addition of Ag^+ or Zn^{2+} caused small enhancements in fluorescence, the presence of these metal ions did not interfere with the Hg^{2+}-induced fluorescence response. The selectivity of this system for Hg^{2+} over other metal ions is remarkably high, and its sensitivity is less than 2 ppb in aqueous solutions. The color change was visible with the naked eye at a probe concentration of 10.0 μM.

Shin et al. further applied this system to a biological study.[96,97] They demonstrated that this system can be used as a real-time method for monitoring the concentration of mercury ions in living cells, particularly in vertebrate organisms. The real-time

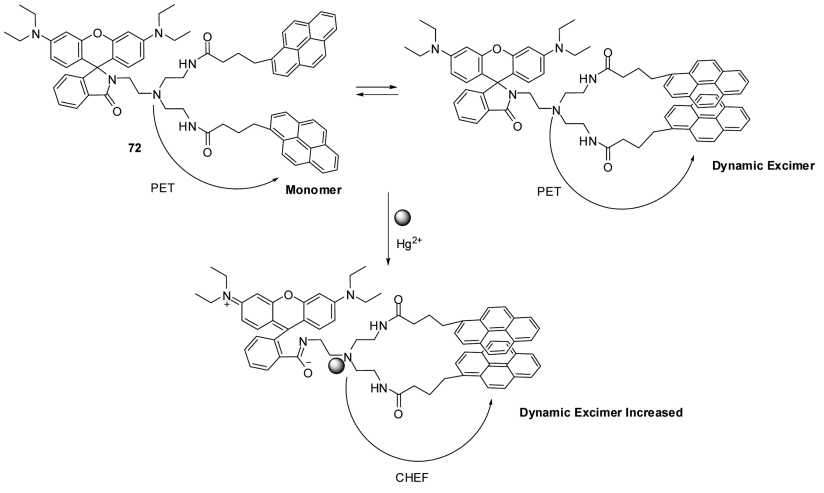

Figure 36. Proposed binding mode of **72** with Hg^{2+}.

dx.doi.org/10.1021/cr200201z |*Chem. Rev.* 2012, 112, 1910–1956

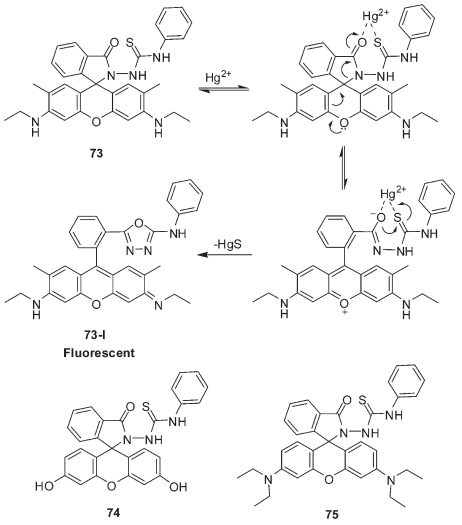

Figure 37. Hg^{2+}-promoted oxadiazole-forming reaction of rhodamine derivative **73** and structures of **74** and **75**.

monitoring of mercury ion uptake by cells and zebrafish using sensor **73** shows that saturation of mercury ion uptake occurs within 20−30 min in cells and organisms. The accumulation of mercury ions is readily detected by using **73** in zebrafish tissue and organs, such as brain, heart, liver, and gall bladder, suggesting that **73** is able to reach all of these organs. Most recently, in conjunction with a portable fiber-optic spectrofluorimeter, Gil et al. demonstrated that **73** is capable of measuring mercury levels in fish and water samples with a very low detection limit and high selectivity toward Hg^{2+}.[98]

On the basis of a framework structurally similar to that of **73**, probes **74** and **75** (Figure 37) were synthesized as chemodosimeters for Hg^{2+}.[99] In methanol−water (30:70, v/v) solution, titrations of **74** with Hg^{2+} revealed a stoichiometric 1:1 reaction via an irreversible spirolactam ring-opening process induced by Hg^{2+}, following strong fluorescence with an emission band centered at about 540 nm. Probe **74** was also remarkably selective and sensitive for Hg^{2+} over other metal ions. A linear fluorescence response depending on the concentration of Hg^{2+} in the range of 0−1.0 μM was observed. The detection limit of 1.0 μM **74** for Hg^{2+} was calculated to be 8.5×10^{-10} M. **74** requires a relatively longer response time (15−20 min) than **73** (<1 min), making it less appropriate for commercial use. Probe **75** has not been studied in detail in this work due to its poor stability and sensitivity compared to **74**. However, in later work reported by the Snee group, by coupling a CdSe/ZnS nanocrystal (NC) with probe **75**, a ratiometric sensing system for the detection of Hg^{2+} was developed.[100] Upon addition of Hg^{2+}, the subsequent desulfurization reaction induced the formation of a ring-opened rhodamine moiety that becomes an efficient energy transfer acceptor to the CdSe/ZnS NC donor, resulting in emission of the NC being decreased and fluorescence of the rhodamine being produced. Usually, Hg^{2+} is capable of quenching the emission of the CdSe/ZnS nanocrystal. However, the desulfurization reaction between probe **75** and mercuric ions produced HgS, as a highly water-insoluble mineral, which has no effect on the NC in aqueous solution. Furthermore, the detection limit of this system was calculated to be 79 ± 2 ppb.

A cyclometalated platinum(II)-containing rhodamine probe, **76**, was synthesized and investigated for Hg^{2+} detection.[101] The

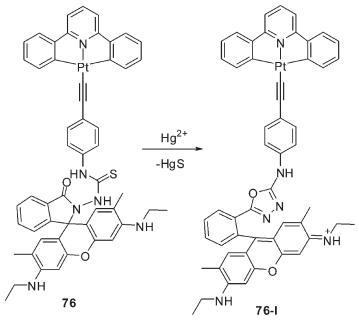

Figure 38. Hg^{2+}-promoted oxadiazole-forming reaction of rhodamine derivative **76**.

cyclometalated platinum moiety was introduced herein owing to its properties of nonlinear absorption and two-photon-induced luminescence. In CH_3CN−HEPES buffer (20 mM; pH 7.0; 50:50, v/v), a highly selective color change of **76**, from light yellow to pink, is observed only in the presence of Hg^{2+} ions due to the formation of the 1,3,4-oxadiazole ring in **76-I** (Figure 38). A remarkable turn-on and selective 20-fold fluorescence enhancement of **76** upon binding with Hg^{2+} over the other tested metal ions was observed. Furthermore, using two-photon microscopy, the water-soluble probe **76** was successfully applied in visualizing the site of Hg^{2+} accumulation, as well as estimating the levels of trace amounts of mercury ions in live HeLa cells.

Kim et al. synthesized molecular probe **77**,[102] *N*-(rhodamine 6G lactam)-*N*′-(phenylthiourea)ethylenediamine. This is potentially a selective probe for the detection of Hg^{2+} in aqueous solution. Compound **77** differs from **73** in the spacer used between the (rhodamine 6G)lactam and the phenylthiourea group. As a consequence of using this spacer, instead of forming the 1,2,3-oxadiazole with **73**, the addition of Hg^{2+} to a solution of **77** induced the N atom of the spirolactam to attack the C atom of the thiourea. This leads to ring-opening of the spirolactam of the rhodamine, followed by removal of HgS and the intramolecular guanylation (Figure 39). A background mixture of Fe^{2+}, Co^{2+}, Ni^{2+}, Cu^{2+}, Zn^{2+}, Pb^{2+}, Cd^{2+}, Ca^{2+}, Mg^{2+}, K^+, and Na^+ had no effect on the emission/absorption of **77** and did not interfere with the Hg^{2+}-induced fluorescence/absorption response. This indicated that the spirolactam ring-opening, followed by the cyclic guanylation, was very selective for Hg^{2+} over the other competitive metal ions tested. Introduction of Hg^{2+} also caused an emission color change from blue to yellow, visible with the eye when 10.0 μM solutions of **77** and **77**-Hg^{2+} were excited with 365 nm light from a hand-held UV lamp. For the absorption, a new band centered at 532 nm appeared with increasing intensity, inducing a definite color change from colorless to pink upon introduction of Hg^{2+} to a 10.0 μM solution of **77**.

A chemodosimeter based on the dual rhodamine urea derivative, **78** (Figure 39), was prepared and studied for use in the detection of Hg^{2+} in living cells.[103] A ca. 10-fold fluorescence enhancement of **78** occurred at 550 nm, with the solution changing from colorless to pink following the addition of Hg^{2+}. The detection limit for Hg^{2+} in methanol was below 2.0 ppb when 10^{-7} M **78** was employed. The addition of Hg^{2+} to a solution of **78** most likely caused spirolactam ring-opening, followed by the guanylation of thiourea. Favorable spectroscopic properties prompted the authors to further investigate fluorescence imaging of Hg^{2+} in living cells. HeLa cells were first incubated with 10.0 μM **78** for 30 min at 37 °C and then treated

dx.doi.org/10.1021/cr200201z |*Chem. Rev.* 2012, 112, 1910–1956

with 100 μM Hg^{2+} for 30 min at 37 °C. Confocal laser scanning microscopy experiments showed that the higher the concentration of Hg^{2+}, the stronger the fluorescence of the treated cells.

Li's group designed a fluorescent probe, **79**, bearing both BODIPY and rhodamine moieties for the detection of Hg^{2+} and Ba^{2+}.[104] In acetonitrile solution, probe **79** shows an absorption band centered at 499 nm, which is ascribed to absorbance of the BODIPY moiety. With excitation at 490 nm, the fluorescence intensity at 505 nm is very weak due to the efficient PET effect from the oxygen atoms in the oxa-crown-6 loop to the excited BODIPY fluorophore. The PET effect was canceled upon addition of 20 equiv of Ba^{2+}, resulting in a 15-fold enhancement in fluorescence intensity at 505 nm. When Hg^{2+} was added to a solution containing **79**, the spirolactam form of rhodamine transferred to the ring-opened state, accompanied by an absorption band centered at 558 nm and a strong emission peak at 585 nm (excitation at 490 nm). This fluorescence enhancement at long wavelengths was attributed to the FRET effect from excited BODIPY to the ring-opening of the rhodamine moiety. When both Hg^{2+} and Ba^{2+} were added to the sensing system, the emission at 505 nm was efficiently quenched and the emission at 585 nm was stronger (Figure 40). Other metal ions, such as Co^{2+}, Mg^{2+}, Ni^{2+}, Cs^{+}, Cd^{2+}, Ag^{+}, Al^{3+}, Pb^{2+}, Cu^{2+}, and Zn^{2+}, have lower fluorescence responses to probe **79**, indicating good selectivity of the probe toward Ba^{2+} and Hg^{2+}. Using the Job's plot method, the stoichiometry for the binding between **79** and Ba^{2+} or Hg^{2+} was determined to be 1:1, and the association constants were calculated to be 1.15×10^5 M^{-1} for **79**−Hg^{2+} and 1.68×10^5 M^{-1} for **79**−Ba^{2+}. Using Ba^{2+} and Hg^{2+} as input signals while using emission bands at 505 and 585 nm as output signals, the presenting system was constructed as an INHIBIT logic gate.

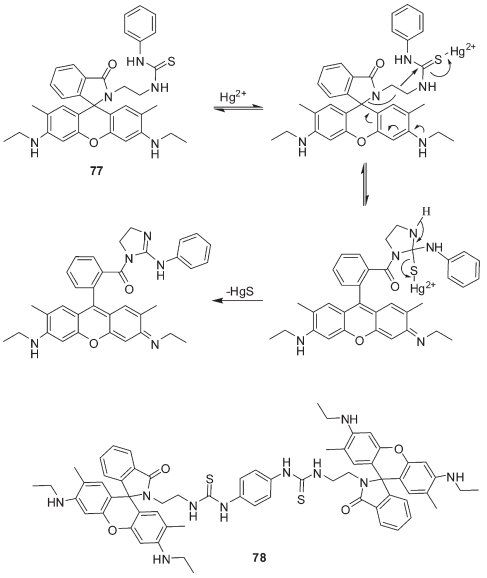

Figure 39. Hg^{2+}-promoted intramolecular guanylation of rhodamine derivative **77** and structure of **78**.

Vicens and Kim et al. reported a novel calix[4]arene rhodamine based chemosensor, **80** (Figure 41), for the detection of Hg^{2+} and Al^{3+}.[105] Fluorescence changes were observed in the case of complexation with only the two different metal ions. The addition of Hg^{2+} to a CH_3CN solution of molecule **80** resulted in significantly enhanced fluorescence intensity at 575 nm via the FRET effect from the pyrenyl excimer to the ring-opened rhodamine moiety with excitation at 343 nm. As a reference, compound **81** (Figure 41) showed a small change in the rhodamine emission (λ_{em} = 575 nm) due to the absence of the two pyrenyl groups (energy donors). On the other hand, complexation of Al^{3+} resulted in an obviously different fluorescence change. The addition of Al^{3+} induced strong emission of the pyrenyl excimer but weak rhodamine emission, suggesting that Al^{3+} prefers the formation of a pyrenyl excimer but not ring-opening of the spirolactam of the rhodamine. This can be rationalized by two different binding structures of molecule **80**: tren spirolactam and tren diamide units. In the presence of Hg^{2+},

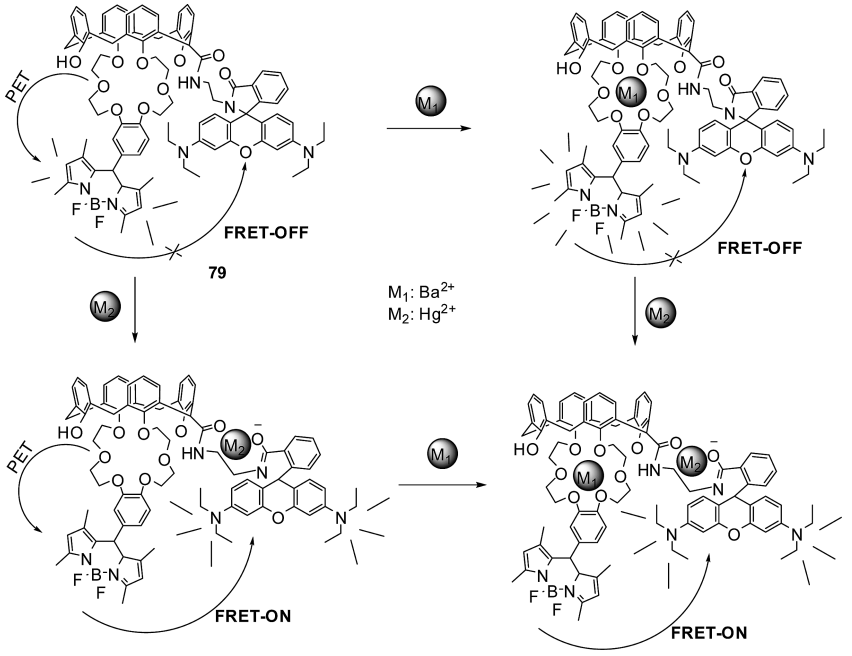

Figure 40. Proposed binding modes of **79** with Hg^{2+} and Ba^{2+}.

dx.doi.org/10.1021/cr200201z |*Chem. Rev.* 2012, 112, 1910–1956

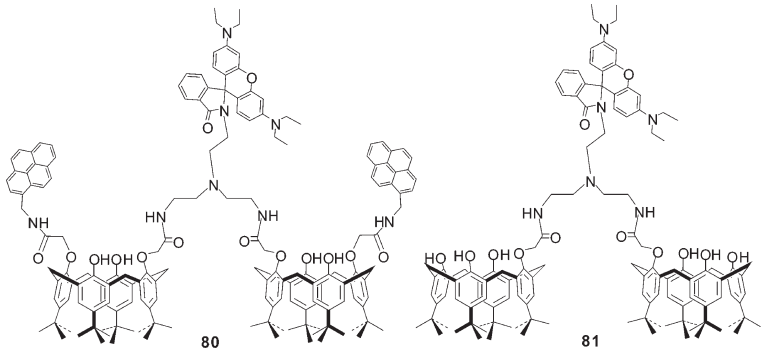

Figure 41. Structures of **80** and **81**.

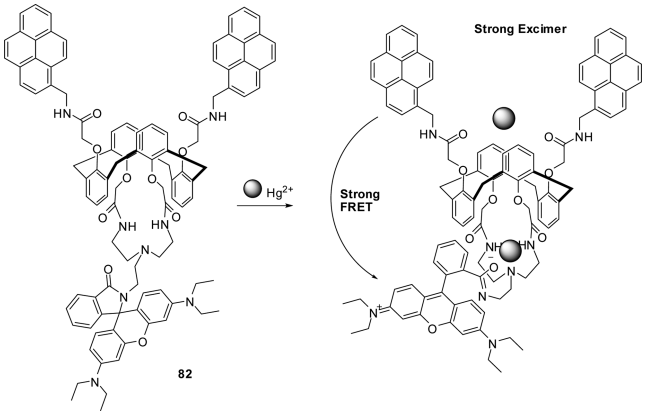

Figure 42. Proposed binding mode of **82** with Hg^{2+}.

the metal ion interacts with the tren spirolactam unit and induces ring-opening of the rhodamine to produce FRET-ON. On the other hand, Al^{3+} prefers to coordinate with the tren diamide unit, leading to enhanced pyrenyl excimer emission. However, this process does not open the spirolactam unit of the rhodamine moiety, which means that energy transfer cannot take place.

A calix[4]arene derivative locked in the 1,3-alternate conformation, **82**, bearing two pyrene and rhodamine fluorophores was synthesized as a selective sensor for the Hg^{2+} ion.[106] In $CHCl_3$–CH_3CN (50:50, v/v), upon addition of Hg^{2+}, **82** showed a new absorption band centered at 559 nm, as well as the increased emission of the ring-opened rhodamine at 576 nm that was observed with a concomitantly declining pyrenyl excimer emission at 470 nm with an isosbestic point centered at 550 nm. This ratiometric fluorescence change indicated that an energy transfer from the pyrene excimer to rhodamine was triggered by Hg^{2+} ions (Figure 42). Although Pb^{2+} also induced a similar fluorescence increase, the intensity was lower than that seen for Hg^{2+}. Furthermore, the ratiometric sensor shows a 5.0 μM detection limit for Hg^{2+}, and a 1:2 complexation between **82** and Hg^{2+} was evaluated by the Job's plot method.

On the basis of a FRET mechanism, Zeng and co-workers designed a ratiometric sensor, **83** (Figure 43), bearing a β-cyclodextrin (β-CD) moiety for detecting mercury ions.[107] In this sensing platform, the β-CD rim not only serves as a bridge for linking the energy acceptor and the donor dye owing to the strong affinity between its hydrophobic cavity and the adamantyl group in water, but also improves the water solubility of the sensing system. Upon addition of Hg^{2+}, a desulfurization process occurred,

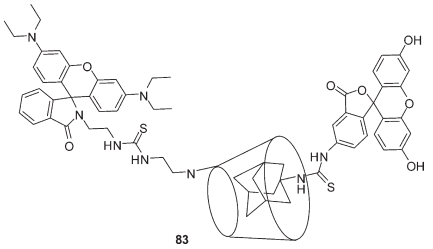

Figure 43. Structure of probe **83**.

accompanied by a transformation of the rhodamine moiety from the spirolactam to the ring-opened form. When excited at 495 nm, the donor emission at 518 nm decreased, and a new emission band with a maximum at 586 nm appeared. The emission lifetime of the donor shortening from 3.58 to 0.38 ns provided further evidence for the FRET mechanism. By monitoring the ratio of the emission intensities at 586 and 518 nm, the detection limit was determined to be 10 nM. The binding constant of this system with mercury ions was evaluated to be $5.3 \times 10^7\ M^{-1}$. After treatment with Hg^{2+}, both HeLa and L929 cells stained with **83** underwent a fluorescence change from green to red, indicating that the FRET sensing system was applicable in live cells.

Xiao et al. reported a ratiometric fluorescent sensor, **84**, for detecting Hg^{2+} based on a BODIPY–rhodamine FRET off–on system.[108] In ethanol–water (80:20, v/v) at pH 7.0, probe **84** showed an absorption peak at 501 nm and an emission peak at 514 nm when it was excited at 488 nm, which correspond to the absorption and emission of the BODIPY fluorophore. Upon addition of Hg^{2+}, a new absorption peak at 560 nm appeared due to the formation of open spirocyclic rhodamine (Figure 44). With the excitation of BODIPY at 488 nm, an increase in fluorescence from the rhodamine fluorophore (emission at 589 nm) and a decrease in fluorescence from BODIPY (emission at 514 nm) were observed upon addition of Hg^{2+}, indicating a Hg^{2+}-switched FRET process between excited BODIPY and rhodamine. Furthermore, the Förster energy transfer efficiency was calculated to be 99%. The ratio of the emission intensities at 589 and 514 nm plateaus when 1 equiv of Hg^{2+} is added to the solution containing **84**, revealing a 1:1 stoichiometry of **84** for Hg^{2+}. A pH titration on fluorescence showed good stability of **84** in the pH range of 4–10, and fluorescence image experiments demonstrated that **84** can provide ratiometric detection of intracellular Hg^{2+} ions. Using a similar strategy, Xiao and Qian et al. constructed other FRET sensors, **85** and **86**, by a BODIPY

dx.doi.org/10.1021/cr200201z |*Chem. Rev.* 2012, 112, 1910–1956

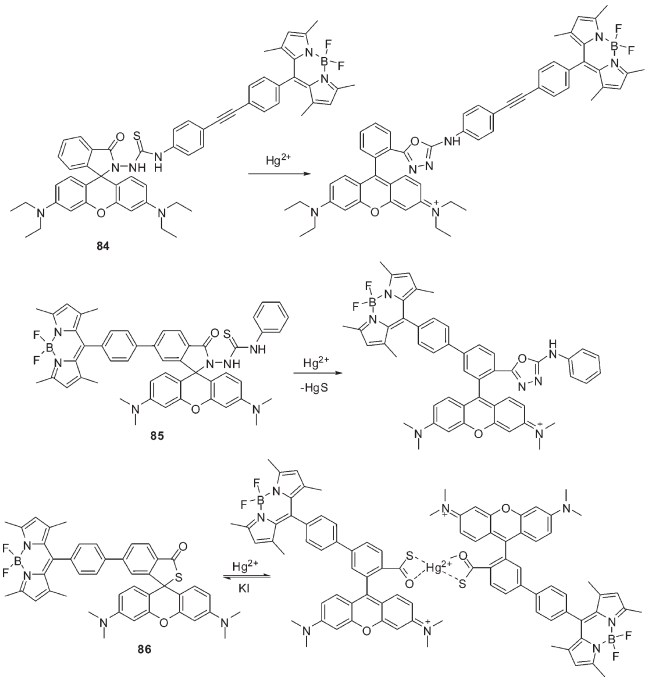

Figure 44. Proposed reaction or binding mechanisms of **84**, **85**, and **86** with Hg^{2+}.

donor coupled with a tetramethylrhodamine (TMR) acceptor (Figure 44).[109] As in **84**, the rigid biphenyl group as the spacer between the donor and acceptor was used to ensure the high efficiency of FRET. In ethanol/water (80:20, v/v) at pH 7.2, upon addition of Hg^{2+}, two sensors showed similar fluorescence responses: the emission intensity at 510 nm attributed to the BODIPY fluorophore decreased, and the emission signal at 584 nm from the rhodamine moiety gradually increased. In the chemical mechanisms of the ring-opening processes, **85** utilizes an irreversible Hg^{2+}-promoted oxadiazole-forming reaction while **86** undergoes a metal-coordination-induced reaction owing to the high thiophilicity of Hg^{2+}. **85** also exhibited a much higher sensitivity than **86** for the detection of Hg^{2+}, in that the detection limit of **85** is at the parts per billion scale while that of **86** is at the parts per milion level. Further imaging experiments using HeLa cells showed both sensors were applicable to monitor Hg^{2+} in living samples, and **85** displayed higher sensitivity and a faster response.

Das et al. developed a ratiometric sensor, **87**, based on the FRET mechanism by using a rhodamine 6G fluorophore and a dansyl moiety (Figure 45).[110] In the absence of Hg^{2+} or Cu^{2+}, free **87** showed only the characteristic absorption and emission bands of the dansyl moiety. In CH_3CN-H_2O (1:1, v/v) solution, upon addition of Hg^{2+} or Cu^{2+}, sensor **87** displayed a new absorption band centered at 530 nm as well as a distinct color change. The association constants of **87** binding with Hg^{2+} and Cu^{2+} were evaluated to be $(3.9 \pm 0.1) \times 10^4$ and $(6.8 \pm 0.2) \times 10^3\ M^{-1}$, respectively, and both the stoichiometries of **87**$-Hg^{2+}$ and **87**$-Cu^{2+}$ were calculated to be 1:1 by the Job's plot method. Reversible binding modes between **87** and Hg^{2+}/Cu^{2+} were confirmed because the addition of EDTA can lead to the regeneration of the spirolactam structure of **87**. Due to the FRET effect between the rhodamine 6G fluorophore and a dansyl moiety, the emission spectra of **87** in the presence of

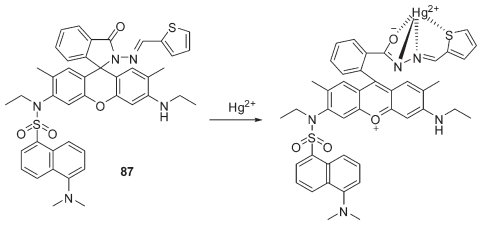

Figure 45. Proposed binding mode of **87** with Hg^{2+}.

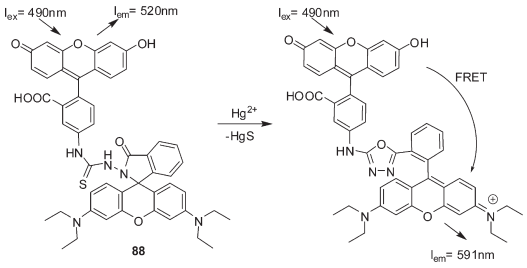

Figure 46. Proposed reaction mechanism of **88** with Hg^{2+}.

Hg^{2+}/Cu^{2+} showed respective emission bands at 555 and 545 nm when excited at 340 nm. By fluorescence titration experiments, the detection limit of sensor **87** for Hg^{2+} was evaluated to be 0.1 ppm. After treatment with **87**, Gram-negative bacterial cells (*Pseudomonas putida*) stained with Hg^{2+} appeared red fluorescent using a confocal microscope with a 405 nm excitation source.

Shang et al. synthesized molecule **88**, composed of a fluorescein fluorophore and a rhodamine B hydrazide linked together by a thiourea spacer.[111] Addition of Hg^{2+} to a solution of **88** caused spirolactam ring-opening and led to the release of a fluorescent rhodamine B moiety. Subsequently, an intramolecular FRET process from fluorescein to the rhodamine group occurred (Figure 46). Due to the fluorescein emission, the free probe exhibited a single emission band centered at 520 nm when excited at 490 nm. The introduction of Hg^{2+} produced another band centered at 591 nm, which corresponds to the emission of the ring-opened rhodamine B moiety. A decrease in the fluorescence intensity at 520 nm and a concomitant increase in the fluorescence intensity at 591 nm took place on addition of increasing amounts of Hg^{2+}. Therefore, the determination of Hg^{2+} could be performed by measuring the ratio of the fluorescence intensities at 591 and 520 nm, respectively. Solution studies revealed a 1:1 reaction stoichiometry of **88** for Hg^{2+}, a detection limit of 0.05 μM, and a linear response up to 10 μM Hg^{2+}. Probe **88** also exhibited a color change from yellow to magenta upon addition of Hg^{2+}, allowing detection with the naked eye. Metal ion selectivity experiments indicated that the emission and color from **88** were unaffected by Fe^{3+}, Co^{2+}, Ni^{2+}, Cr^{3+}, Zn^{2+}, Pb^{2+}, Cd^{2+}, Ca^{2+}, Mg^{2+}, Ba^{2+}, and Mn^{2+}.

Li et al. reported a conjugated polymer sensor, **89**, bearing poly[(*p*-phenyleneethynylene)-*alt*-(thienyleneethynylene)] backbones and rhodamine B units.[112] In the absence of Hg^{2+}, sensor **89** in THF solution showed an absorption band centered at 441 nm and a single fluorescence band with a maximum at 487 nm when excited at 441 nm, which were attributed to the characteristic absorption and emission of the backbone, respectively. Upon addition of Hg^{2+}, a new absorption peak at 552 nm, as well as a visual color change from slightly yellow to orange, was observed, indicating the formation of ring-opened rhodamine

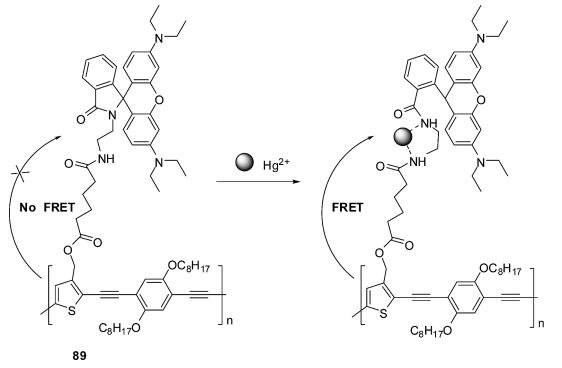

Figure 47. Proposed binding mode of **89** with Hg^{2+}.

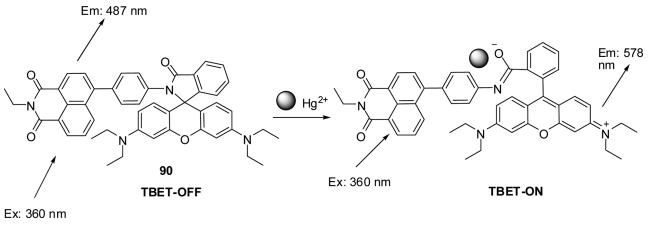

Figure 48. Proposed binding mode of **90** with Hg^{2+}.

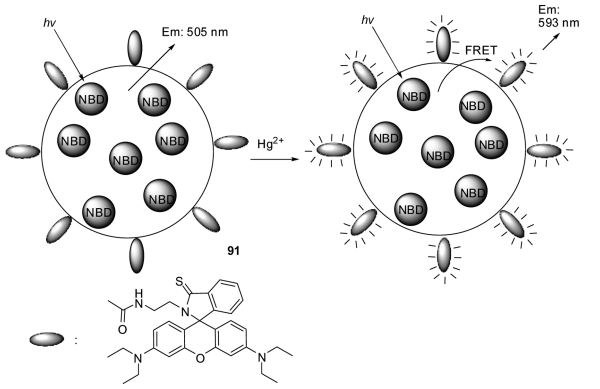

Figure 49. Proposed FRET mechanism of **91** induced by Hg^{2+}.

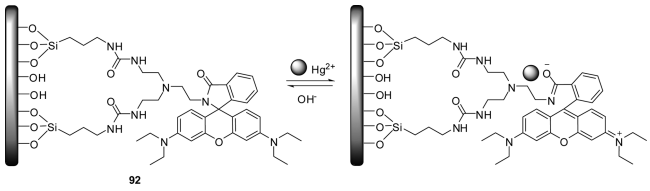

Figure 50. Binding mode of a **92**-coated glass substrate with Hg^{2+}.

(Figure 47). With excitation at 441 nm, an efficient FRET process takes place from polymer backbones to the rhodamine group, resulting in a decrease in the fluorescence intensity at 487 nm and an increase at 575 nm. The addition of Hg^{2+} can lead to an 18.6-fold enhancement in the FRET ratio of the rhodamine to backbone emission intensities. No responses were observed in the presence of other metal ions, indicating good selectivity of **89** toward Hg^{2+}.

To obtain large Stokes shifts, the approach via FRET or through-bond energy transfer (TBET) is applicable. Compared with the FRET mechanism, TBET does not require spectral overlap between the donor emission and acceptor absorption. Most recently, Kumar et al. established a TBET-based chemosensor, **90**, by combining naphthalimide and rhodamine through a conjugated spacer.[113] In THF−H_2O (9.5:0.5, v/v), **90** itself only showed two absorption bands at 320 and 363 nm due to the naphthalimide moiety. Upon addition of Hg^{2+}, a new absorption band appears at 565 nm along with a color change from colorless to pink, and an emission band characteristic of ring-opened rhodamine also appears at 578 nm when the chemosensor is excited at 360 nm (Figure 48). A detection limit of 2×10^{-6} M for Hg^{2+} and a 1:1 stoichiometry for the binding mode with a binding constant of 7.1×10^4 M^{-1} were evaluated. After the prostate cancer (PC3) cell line loaded with sensor **90** was incubated with Hg^{2+}, microscope images showed an intracellular fluorescence change from green to red, indicating that **90** was a potential agent for imaging Hg^{2+} ions in living samples.

A FRET-based ratiometric sensor, **91**, for detecting Hg^{2+} was reported by Wu et al.[114] In their work, a hydrophobic nitrobenzoxadiazolyl (NBD) unit was introduced to the core of nanoparticles by miniemulsion polymerization of methyl methacrylate and acrylic acid, and then a rhodamine moiety was grafted onto the surface of the nanoparticles. In HEPES buffer (pH 7.0), addition of Hg^{2+} induced a ring-opening process of the spirolactam rhodamine. Upon excitation at 420 nm, the excited-state energy of NBD was transferred to the ring-opened rhodamine unit, resulting in a new emission band at 593 nm, as well as a decrease of NBD's emission intensity at 505 nm (Figure 49). The sensing system exhibited high selectivity for the detection of Hg^{2+} in water over other metal ions such as K^+, Na^+, Ca^{2+}, Mg^{2+}, Al^{3+}, Zn^{2+}, Fe^{3+}, Mn^{2+}, Pb^{2+}, Cu^{2+}, Co^{2+}, Ni^{2+}, and Cr^{3+}. The detection limit of the nanoparticle-based system was determined to be 100 nM and can be applied to detect Hg^{2+} in pH 4−8 aqueous solution.

The use of organic−inorganic hybrid materials has attracted considerable interest in the field of ion recognition and sensing. Receptor-immobilized inorganic materials, such as SiO_2, Al_2O_3 and TiO_2, have some important advantages as solid chemosensors in heterogeneous solid−liquid phases.[115,116] The attachment of rhodamine as a signal unit to SiO_2 can be used in a chemosensory kit. Kim, Jung, and co-workers reported a novel mesoporous silica-immobilized rhodamine compound, **92**, anchored by a tren (Figure 50).[117] From fluorescence spectroscopic experiments, **92** shows a high selectivity and sensitivity to Hg^{2+} ions over other metal ions. The interaction between Hg^{2+} and rhodamine on the surface of **92** induces a highly conjugated rhodamine system through the formation of an opened spirolactam to give a strong fluorescence emission and a pink color. In addition, **92** can be easily recovered by treatment with a tetrabutylammonium hydroxide solution. A **92**-coated glass plate has also been developed for Hg^{2+} detection in the environmental field and has shown excellent function in terms of both the visual and fluorescence changes with Hg^{2+}.

Tao and co-workers fabricated a multifunctional material, **93**, based on a rhodamine B immobilized mesoporous silica shell and a magnetic core (Fe_3O_4) for the detection, absorption, and removal of Hg^{2+} in aqueous solution (Figure 51).[118] In CH_3CN−H_2O (1:1, v/v) solution, addition of Hg^{2+} induced an enhancement in the fluorescence intensity of **93** due to the formation of the ring-opened rhodamine fluorophore. Probe **93**

dx.doi.org/10.1021/cr200201z |*Chem. Rev.* 2012, 112, 1910–1956

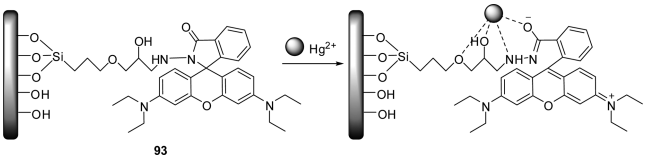

Figure 51. Ring-opening process of a rhodamine derivate immobilized mesoporous silica shell induced by Hg^{2+}.

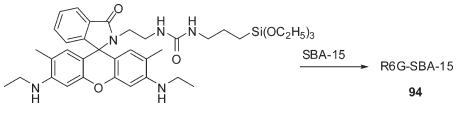

Figure 52. Inorganic−organic hybrid senser **94**.

showed high selectivity toward Hg^{2+} because other metal ions exhibited no significant change in the fluorescence spectra. The detection limit of **93** for Hg^{2+} was found to be 10 ppb. Due to the existence of the magnetic Fe_3O_4 core, **93** can remove Hg^{2+} in 30 s from aqueous solution, and the absorption capability toward Hg^{2+} was evaluated to be 21.05 mg g^{-1}.

By anchoring a rhodamine 6G derivative to the surface of SBA-15, Duan et al. obtained an inorganic−organic hybrid sensor, **94** (Figure 52).[119] In neutral water, free **94** exhibited weak fluorescence. Upon addition of 7.5 equiv of Hg^{2+}, **94** showed an approximately 10-fold enhancement in the fluorescence intensity at about 550 nm. A linear correlation between the emission intensity and the amount of Hg^{2+}, ranging from 1 to 10 ppb, was observed. No significant spectral changes occurred when other metal ions were added, confirming the high selectivity of **94** toward Hg^{2+}. The reversibility and stability over a wide pH range (2−10) suggest that this sensor may be useful in practical applications.

Zhou et al. synthesized a rhodamine-based chemosensor, **95** (Figure 53), for the detection of Hg^{2+}.[120] In DMF−H_2O (1:1, v/v; pH 7), the addition of Hg^{2+} to a solution of **95** induced instantaneous changes from colorless to pink as well as a strong yellow fluorescence. The addition of 1 equiv of Hg^{2+} led to a ca. 26-fold increase compared with sensor **95** itself. The binding constant between sensor **95** and Hg^{2+} was calculated to be 3.4×10^9 M^{-2}, and the 1:2 stoichiometry was confirmed by Job's plot analysis and ESI-MS. A linear relationship between the fluorescence intensities and the concentration of Hg^{2+} ranging from 2 to 20 ppb was observed, indicating the high sensitivity of sensor **95**. The reversibility of **95** was supported by the fact that KI induced decomplexation of Hg^{2+}−**95**. Furthermore, **95**−SBA-15, which was prepared by immobilizing **95** using mesoporous SBA-15, also showed high sensitivity and selectivity toward Hg^{2+} ions in aqueous solution.

By polymerizing monomer **96** (Figure 53), Lin et al. prepared double hydrophilic block copolymer-based multifunctional chemosensor poly-**96** for the detection of Hg^{2+}.[121] Upon addition of 4 equiv of Hg^{2+} (relative to **96** residues), a 22-fold enhancement in fluorescence intensity of polymers as well as a slight red shift of the maximum emission peak from 578 to 584 nm was observed, owing to the formation of ring-opened rhodamine moieties. The polymers have high selectivity toward Hg^{2+}, which was supported by the observation that other metal ions, including K^+, Na^+, Li^+, Co^{2+}, Cd^{2+}, Pb^{2+}, Zn^{2+}, Fe^{2+}, Fe^{3+}, Ca^{2+}, Ag^+, and Cu^{2+}, did not induce any apparent fluorescence enhancement

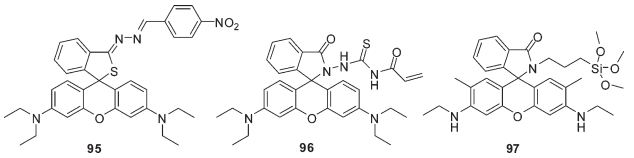

Figure 53. Structures of **95**−**97**.

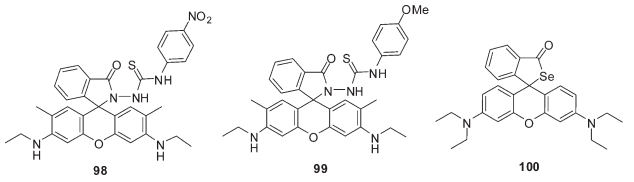

Figure 54. Structures of **98**−**100**.

within 10 min. At room temperature, the detection limit of poly-**96** toward Hg^{2+} was evaluated to be 3.5 ppb. Because **96** is also sensitive to temperature and pH, its application can be explored for use as a sensor in other fields.

Du and co-workers reported a Hg^{2+}-selective fluorescent sensor by immobilizing rhodamine 6G derivative **97** (Figure 53) and CdTe quantum dots onto silica nanoparticles.[122] The inorganic−organic hybrid system showed a selective fluorescence response to Hg^{2+} over other metal ions. The fluorescence intensity is linearly dependent on the concentration of Hg^{2+} ranging from 40 to 800 nM, and the detection limit was found to be 2.6×10^{-9} M. The sensor is stable over the pH range from 5.29 to 9.18. Upon addition of KI to a solution containing the sensor and Hg^{2+} ions, the fluorescence was quenched due to the recovery of the spirolactone form of rhodamine, which indicated the reversibility of the sensor. Furthermore, this system was demonstrated to be useful in detecting Hg^{2+} in water samples.

Methylmercury species, which can readily pass through biological membranes, are much more toxic than inorganic mercury species. Exposure of the human body to methylmercury causes cardiovascular diseases, autoimmune effects, hearing impairment, blindness, and death.[123] The detection of methylmercury is of great interest for both the environment and human health. Shin, Tae, and co-workers reported rhodamine thiosemicarbazides (**73**, **98**, and **99**) (Figure 54) as sensors for detecting CH_3Hg^+.[124] In water containing 1% DMSO at 25 °C, addition of CH_3Hg^+ to solutions (10 mM) of the rhodamine derivatives led to different extents of increase in fluorescence at 560 nm. Probe **73** showed a stronger fluorescence change than the other two rhodamine derivatives, **98** and **99**, with electron-withdrawing or electron-donating groups, respectively. Fluorescence titrations indicated that **73** can detect CH_3Hg^+ at concentrations as low as 200 nM. The 1,3,4-oxadiazole compound **73-I** was obtained as the product of the reaction between **73** and CH_3Hg^+, showing a mechanism similar to that of the Hg^{2+}-induced desulfurization process. Fluorescence imaging of HeLa cells and zebrafish successfully demonstrated that **73** has potential for use in the detection of methylmercury in living cells and organisms.

Owing to the extremely high affinity between mercury and selenium, Yoon and co-workers developed a fluorescent chemodosimeter, **100** (Figure 54), based on rhodamine B selenolactone for inorganic mercury and methylmercury species.[125] The fluorescence enhancement and UV−vis spectral changes induced by mercury/methylmercury species are attributed to a deselenation

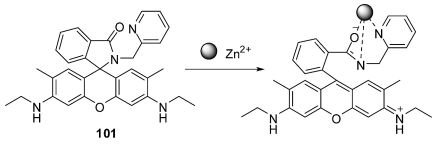

Figure 55. Proposed binding mechanism of probe **101** with Zn^{2+}.

reaction. The fluorescence intensity of **100** is linearly proportional to the Hg^{2+} concentration across the range 0−30 nM, and a concentration of Hg^{2+} as low as about 20 nM can be detected using **100** with a signal-to-noise ratio of 3. Job's plot provided evidence for the binding mode of 1:1 stoichiometry between **100** and Hg^{2+}. The value of this sensor was successfully demonstrated by its use in detecting inorganic mercury/methylmercury species in cells and zebrafish. Using the same compound, Ma's group demonstrated that **100** has corresponding spectral changes for Ag^{+}, even if a high concentration of Cl^{-} exists in the sensing system.[126] The detection limit for Ag^{+} was evaluated to be about 50 nM, and a 1:2 stoichiometric ratio of **100** to Ag^{+} was observed.

2.3. Sensors for Detecting Zn^{2+}

Many of the enzymes available in the human body, as well as in sea organisms, contain zinc as an essential element. Enzymes, in turn, act as catalysts for biological processes such as cellular metabolism. In addition, many pathological processes such as cerebral ischemia, Alzheimer's disease, and infantile diarrhea involve intracellular zinc ions.[127−131] It is very difficult to develop an efficient method for detecting intracellular Zn^{2+} and to obtain optical cellular imaging with high sensitivity and selectivity over biologically abundant cations in living cells.

Mashraqui et al. have synthesized a rhodamine-based chromo- and fluorogenic probe, **101**,[132] which can detect micromolar concentrations of Zn^{2+} by turning the color of the solution from colorless to orange and also by changing the corresponding absorption maximum from 302 to 528 nm. The detection is very selective over other competitive cations such as Li^{+}, Na^{+}, K^{+}, Ba^{2+}, Ca^{2+}, Mg^{2+}, Co^{2+}, Ni^{2+}, Cu^{2+}, and Cd^{2+}. Probe **101** bearing a pyridyl moiety can anchor Zn^{2+} with spiroamide and pyridyl nitrogen, which generates a trigger to open the spiroring of the xanthene moiety as shown in Figure 55.

Zhang et al. have synthesized another probe, **102**,[133] based on the rhodamine framework that can detect Zn^{2+} ratiometrically using the FRET mechanism in aqueous solution (0.1 M HEPES, pH 7.2) with a detection limit of 4×10^{-8} M. The probe contains two moieties, rhodamine B thiohydrazone and fluorescein. The sulfur and nitrogen atoms in the rhodamine moiety, and the oxygen atom in the fluorescein moiety, selectively bind with Zn^{2+}, which acts as a trigger to open the spiroring, producing a long-wavelength rhodamine fluorophore that may act as the energy acceptor for a FRET system (Figure 56). The fluorescein moiety acts as an energy donor as its fluorescence spectrum (band maximum at 520 nm when excited at 490 nm) matches the absorption spectrum of the ring-opened rhodamine moiety (band maximum at 560 nm) well and thus satisfies the primary requirement for intramolecular FRET. The probe shows a high selectivity for Zn^{2+} over other transition-metal ions; even Cd^{2+}, which is known as the strongest competitor for Zn^{2+}, cannot interfere. Having many other features, such as a large-wavelength shift (∼105 nm) between the donor excitation peak and the acceptor emission peak, two emission bands with high resolution, and a reversible response with a short response time, probe **102** is

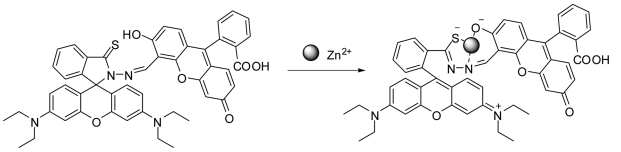

Figure 56. Proposed binding mechanism of probe **102** with Zn^{2+}.

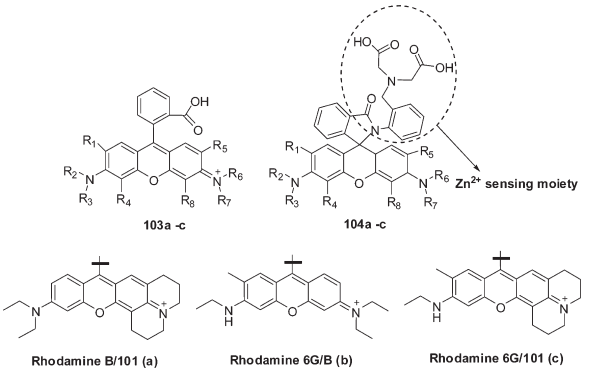

Figure 57. Structures of asymmetric rhodamine derivatives **103a**−**c** and **104a**−**c**.

a potential candidate for the investigation of ratiometric cellular imaging.

Nagano and co-workers have synthesized a series of symmetric and asymmetric rhodamine derivatives,[134] using rhodamine 101, B, and 6G as scaffolds, for investigating the effects of the structure of the xanthene moiety on the spirolactam ring-opening process, and these are suitable candidates for the detection of Zn^{2+} ions in HEPES buffer (pH 7.4) solutions. It is observed that asymmetric rhodamine derivatives are better candidates for sensing Zn^{2+} in aqueous buffer solutions. Among asymmetric derivatives **103a**−**c** and **104a**−**c** (Figure 57), **104c** is the most suitable to be used as a Zn^{2+} sensor. Compound **104c** shows an absorption band that peaks at 571 nm and a fluorescence band that peaks at 595 nm. Absorbance as well as fluorescence enhancement of **104c** occurs by a factor of approximately 12 upon addition of 1.0 equiv of Zn^{2+} to a solution of 100 mM HEPES buffer containing 10 μM **104c**. The apparent dissociation constant, K_d, calculated by the fluorescence method is ∼4 μM, which indicates that it is not suitable for biological applications. Metal ions such as Ni^{2+}, Co^{2+}, and Cu^{2+} interfere with absorption but cannot interfere with the fluorescence enhancement. Ligand **104c** is very selective over other metal ions, including Cd^{2+}. Job's plot indicates a 1:1 (Zn^{2+}:**104c**) stoichiometric complex. The color change (from colorless to pink) and fluorescence enhancement occur due to Zn^{2+}-induced spirocyclic ring-opening of **104c**.

2.4. Sensors for Detecting Fe^{3+}

Fe^{3+} is the most essential metal ion in biological systems and plays a crucial role in many biochemical processes, such as in cellular metabolism, in many enzymatic reactions as a cofactor, and in carrying oxygen by heme. Both its deficiency and overloading induce biological disorders in the living body, such as anemia, liver and kidney damage, heart failure, and diabetes.[135−137] Detection of ferric ions in solution is very difficult using fluorescence techniques because the paramagnetic nature leads

dx.doi.org/10.1021/cr200201z |*Chem. Rev.* 2012, 112, 1910–1956

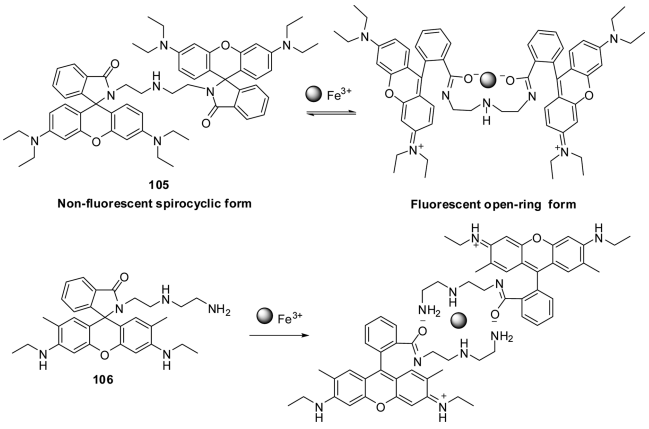

Figure 58. Proposed binding mechanisms of **105** and **106** with Fe^{3+}.

to their fluorescence quenching ability. Fluorescence enhancement through chelation of this metal ion with any fluorophore is a challenging task in vitro as well as in vivo. Several groups have successfully detected Fe^{3+} ions in aqueous environments using xanthene derivatives, which can follow either a metal ion induced spirocyclic ring-opening or a FRET mechanism.

Compound **105** is a rhodamine-based chemosensor,[138] which is very selective for Fe^{3+} in both ethanol and buffered water (Tris−HCl aqueous buffer, pH 7.15) over other metal ions such as Co^{2+}, Ni^{2+}, Cd^{2+}, Ag^{+}, Pb^{2+}, Ba^{2+}, Mg^{2+}, Ca^{2+}, K^{+}, and Na^{+}, but Cr^{3+}, Fe^{2+}, and Cu^{2+} can interfere mildly in ethanol, but not in water. Addition of Fe^{3+} to a colorless solution of **105** (spirocyclic form) in both neutral buffer and ethanol generates a purple color (ring-opened form) and orange fluorescence in the range of 500−650 nm which is visible with the naked eye. The fluorescence spectrum also shifts toward red by ∼25 nm upon addition of Fe^{3+} to a solution of **105**. According to the proposed mechanism, the formation of the open-ring form occurs due to the chelation of Fe^{3+} ions with the oxygen atoms of the amide groups in **105** (Figure 58). Although it can detect 10^{-5} M Fe^{3+} ions, its moderate binding capacity to Fe^{3+} in aqueous medium restricts its use in biochemical applications. Liu et al.[139] reported another xanthene dye, **106**, showing Fe^{3+}-induced fluorescence enhancement as a result of spirolactam ring-opening in aqueous solution. In compound **105**, two rhodamine moieties are linked with diethylenetriamine, whereas it is attached to a single rhodamine moiety in **106**. The stoichiometries for the binding modes between two sensors and Fe^{3+} were speculated to be 1:1 for **105**−Fe^{3+} and 2:1 for $(\mathbf{106})_2$−Fe^{3+} (Figure 58). The stability constants for **105** and **106** with Fe^{3+} are 10 000 and 6428 M^{-1}, respectively, indicating that **105** binds more strongly than **106** with Fe^{3+}.

The uptake of Fe^{3+} ions in biological processes takes place through siderophores,[140−142] such as ferrichrome analogues and enterobactin, which have catecholates or hydroxamates as binding sites. Tae and Bae have designed a rhodamine-based fluorophore, **107**, which couples with a biomimetic hydroxamate binding unit.[143] The probe can detect micromolar concentrations of Fe^{3+} in CH_3OH−CH_3CN (1:1, v/v) solution with high sensitivity and selectivity over other coexistent metal ions by changing the color of the solution from colorless to red-purple with rapid and strong fluorescence, which is the result of spirolactam ring-opening of the xanthene moiety due to binding interactions of Fe^{3+} with the hydroxamate moiety in the probe (Figure 59).

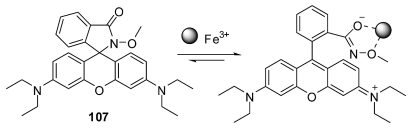

Figure 59. Proposed binding mode of **107** with Fe^{3+}.

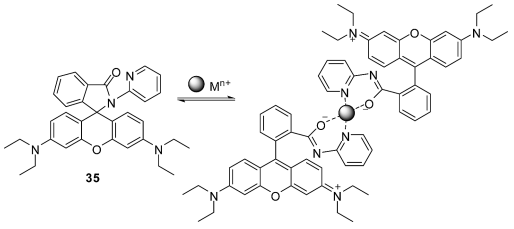

Figure 60. Proposed binding mode of **35** with metal cations.

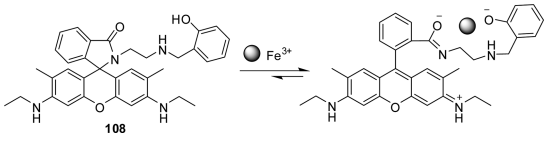

Figure 61. Proposed binding mechanism of **108** with Fe^{3+}.

Compound **35** with a pyridine moiety can detect some heavy- and transition-metal (HTM) cations such as Fe^{3+}, Hg^{2+}, Pb^{2+}, and Fe^{2+} by fluorescence enhancement (turn-on) and quenching (turn-off) mechanisms.[144] Among other metal ions, Zn^{2+} and Cd^{2+} can interfere slightly with the detection of HTM cations. By the Job's plot method, the complex stoichiometry is found to be 1:2 (metal cation:**35**). The carbonyl oxygen and pyridine nitrogen of each of the two probe molecules coordinate with the metal ion and form a six-membered chelate ring which triggers the opening of the spirolactam ring of **35** and forms a new turn-on fluorescent ring-opened form as shown in Figure 60. Using a benzene moiety in place of the pyridine moiety in **35** results in small changes in the absorption and fluorescence spectra upon addition of Fe^{3+} ions, indicating that the pyridyl N of **35** is involved in the coordination of metal ions.

A rhodamine 6G derivative having a phenol moiety, **108**, exhibits Fe^{3+}-induced fluorescence enhancement in ethanol.[145] The sensor is selective for Fe^{3+} over other metal ions, except for Ni^{2+}, Co^{2+}, Mg^{2+}, and Ba^{2+}, which interfere mildly. The deprotonation ability of the Fe^{3+} ion toward the amide group, the radius of the Fe^{3+} ion, and the efficient chelating conformation of the receptor for Fe^{3+} may be probable factors for such selectivity of Fe^{3+} to open the spirolactam ring in the pH range of 5−10 (Figure 61).

Tae et al. have developed rhodamine derivative **109**, which has a flexible bisaminoxy (diethylene glycol) multidentate binding unit for the detection of Fe^{3+} ions.[146] The probe exists predominantly as the spirocyclic form in H_2O−DMSO (99:1, v/v) and changes its color rapidly from colorless to pink with a strong fluorescence that peaks at 557 nm (excitation at 500 nm) upon addition of Fe^{3+} ions to the solution. This is the result of spirocyclic ring-opening due to chelation of the Fe^{3+} ions with the flexible multidentate binding site of the rhodamine fluorophore, maintaining a 1:1 binding stoichiometry (Figure 62).

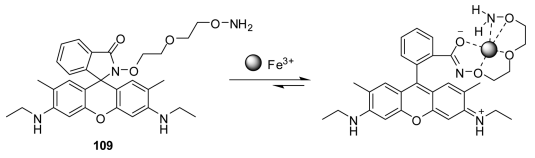

Figure 62. Proposed binding mode of **109** with Fe^{3+} ions.

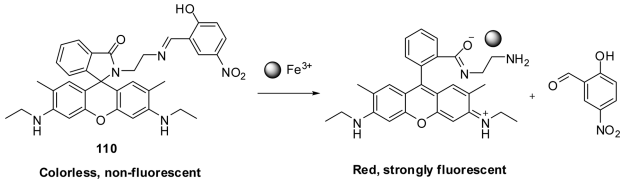

Figure 63. Schematic representation of the Fe^{3+}-induced Schiff base hydrolysis and spirolactam ring-opening of rhodamine moieties in **110**.

Probe **109** works very well in the pH range of 6−9 with a detection limit of 1 μM in aqueous solution.

Kim et al. reported a sensor, **110**, which consists of rhodamine as the main core and ethylenediamine as a spacer that links 2-hydroxy-5-nitrobenzaldehyde with the main core via a hydrolyzable imine linkage.[147] The full moiety has been made in such a way that it may act as a Schiff base. Due to its high affinity toward the ethylenediamine framework, and being a strong Lewis acid, Fe^{3+} selectively binds with **110** as shown in Figure 63 and facilitates hydrolysis of the Shiff base with concomitant opening of the spirocyclic ring, resulting in a red-colored solution and strong yellow fluorescence at 551 nm upon excitation at 528 nm in aqueous solutions. The detection limit of **110** for Fe^{3+} is ~0.1 mM in aqueous medium. Furthermore, after treatment with **110**, the iron-overloaded Hep G2 cells showed red fluorescence enhancement.

Mu et al. have synthesized a fluorescent sensor based on a rhodamine B Shiff base, **111**, which can detect Fe^{3+} ions selectively over commonly coexistent metal ions in neutral ethanol aqueous solution (4:6, v/v; Tris−HCl buffer, pH 7.0) with a detection limit of 0.11 μM.[148] The amide carbonyl groups, enolic hydroxyl oxygen, and nitrogen atom in the acetyl acetone moiety can bind Fe^{3+} ions with simultaneous opening of the spirocyclic ring, turning the solution pink and showing strong fluorescence at 583 nm (Figure 64). The proposed binding mechanism was supported by cyclic voltametry and IR and NMR spectroscopy. After addition of Fe^{3+} to the solution of **111**, the reduction wave shifts from −512 to −551 mV in cyclic voltametry, the amide carbonyl absorption shifts from 1691 to 1614 cm^{-1} in the IR spectrum, and the proton peaks of the rhodamine moiety shift downfield in the NMR spectra.

A rhodamine-based chemosensor, **112** (Figure 64), containing an azacrown ether moiety can behave as a dual-channel fluorescent probe for Hg^{2+} and Fe^{3+} in CH_3CN.[149] Addition of Hg^{2+} leads to the appearance of orange fluorescence at 578 nm, whereas addition of Fe^{3+} shows a highly intense green fluorescence at 525 nm. Addition of Hg^{2+} to the solution of **112** in acetonitrile shows a strong absorption peak at 556 nm, along with a color change from colorless to pink. Other metal ions such as Cu^{2+}, Fe^{2+}, Pb^{2+}, Zn^{2+}, Cd^{2+}, Co^{2+}, Ni^{2+}, Cr^{3+}, Mn^{2+}, Ca^{2+}, Ag^{+}, Li^{+}, Na^{+}, and K^{+} show negligible absorbance, but addition of Fe^{3+} shows a strong blue-shifted absorption peak at 502 nm. When monitored at 580 nm (fluorescence band maximum for **112** with Hg^{2+}),

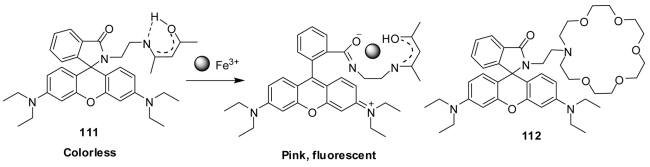

Figure 64. Proposed binding mode of **111** with Fe^{3+} and structure of sensor **112**.

the excitation spectrum of **112** with Hg^{2+}, which peaks at 559 nm, looks similar to the absorption spectrum. The excitation spectrum of **112** with <10 equiv of Fe^{3+} appears at 559 nm, but the increase in concentration of Fe^{3+} (>10 equiv) gives rise to a blue-shifted band at 450−550 nm with a reduced band intensity at 559 nm. Again, 90 equiv of Fe^{3+} gives only the 505 nm band while monitored at 530 nm (fluorescence band maximum for **112** with Fe^{3+}). These findings suggest that the fluorescence, after addition of Fe^{3+} or Hg^{2+}, originates from different ground-state species. As shown from the IR spectra of **112** in CH_3CN, ^1H NMR titration in CD_3CN, and ^{13}C NMR spectra of **112** before and after addition of Hg^{2+} and Fe^{3+}, the metal cations (Hg^{2+} or Fe^{3+}) coordinate with both carbonyl and azacrown ether moieties in **112** and lead to spirocyclic ring-opening, but follow different mechanisms for showing fluorescence which are still not clear.

Ramakrishna, Sinn, and co-workers have synthesized single- and multiple-photon turn-on fluorescent sensors (**113** and **114**) based on bis(rhodamine) dye molecules to enhance the selectivity and sensitivity of the detection of Fe^{3+} ions in aqueous solutions.[150] The structural differences between **113** and **114** are that the two rhodamine dye molecules are linked by pyridine and benzene moieties, respectively. Both **113** and **114** show similar selectivity and sensitivity to Fe^{3+} ions with a detection limit of 70 μM. The addition of Fe^{3+} ions yields a pink solution with a strong red fluorescence signal at 580 nm because of spirocyclic ring-opening induced by Fe^{3+} binding with the amide oxygen, as shown in Figure 65. The ion size, as well as the binding strength of Fe^{3+} to the probe, has made it very selective over other metal ions, except for Cr^{3+}, which interferes mildly. Fluorescence enhancement increases further with two-photon excitation because of reduced absorption interference and the enhanced two-photon cross section by Fe^{3+}-induced ring-opening.

Compound **115** detects micromolar concentrations of Fe^{3+} selectively over other metal ions such as Hg^{2+}, Ag^{+}, Pb^{2+}, Sr^{2+}, Ba^{2+}, Cd^{2+}, Ni^{2+}, Co^{2+}, Fe^{2+}, Mn^{2+}, Cu^{2+}, Zn^{2+}, Ce^{3+}, Mg^{2+}, K^{+}, and Na^{+} in methanol−water (9:1, v/v) by following an Fe^{3+}-induced spirolactam ring-opening mechanism with strong fluorescence turn-on (Figure 66).[151] Compound **115** is colorless and has weak fluorescence at 567 nm when excited at 530 nm. A red shift, as well as 92-fold fluorescence enhancement, occurs at 580 nm after addition of 20 equiv of Fe^{3+} to the solution of **115**.

Heo, Yang, and co-workers reported compound **116**,[152] an Fe^{3+}-selective sensor, using a rhodamine fluorophore. As a nonfluorescent spirocyclic form, free **116** in ethanol shows no significant fluorescence emission. However, the probe displays strong fluorescence emission at 577 nm (205-fold) with addition of Fe^{3+} (10 equiv). No fluorescence enhancement was observed upon treatment with other metal ions, except for Pb^{2+}, indicating the good selectivity of sensor **116** toward Fe^{3+}. Furthermore, compound **116** can detect Fe^{3+} across a broad range of concentrations (100 ppb to 100 ppm) in ethanol selectively over other metal ions (Figure 67).

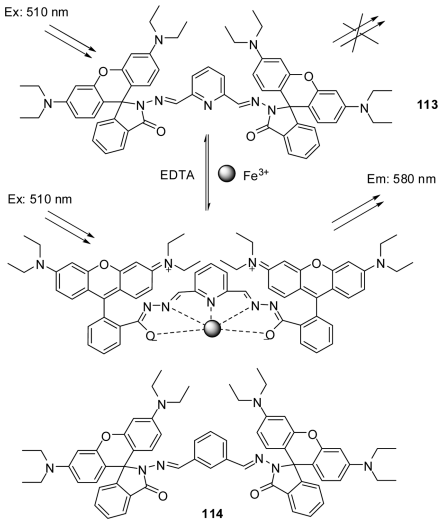

Figure 65. Proposed binding mechanism for the fluorescence turn-on of **113** with spirolactam ring-opening and structure of **114**.

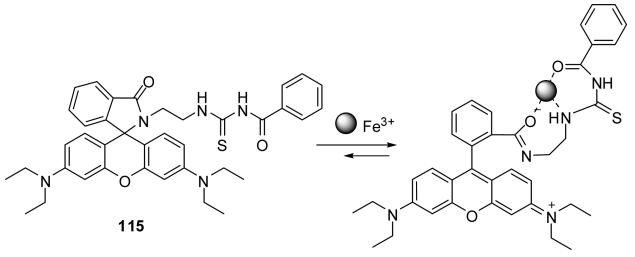

Figure 66. Proposed binding mechanism for the fluorescence enhancement of **115** upon addition of Fe^{3+}.

A fluorescent sensor, **117**, having two rhodamine B moieties linked 1,3-alternately with thiacalix[4]arene can detect Fe^{3+} and Cr^{3+} ions in ethanol−water (3:1, v/v; Tris−HCl, pH 6.0) solutions selectively over other common metal ions such as Na^+, K^+, Ca^{2+}, Mg^{2+}, Sr^{2+}, Co^{2+}, Ni^{2+}, Zn^{2+}, Hg^{2+}, Cd^{2+}, and Mn^{2+} with detection limits of 3.50×10^{-8} for Fe^{3+} and 1.60×10^{-7} M for Cr^{3+}.[153] The possible mechanism involves spirolactam ring-opening of **117** induced by Fe^{3+} or Cr^{3+}, leading to enhancement of the absorption (peak at 557 nm) and emission (peak at 580 nm when excited at 557 nm) intensities along with a color change of the solutions from colorless to pink for Fe^{3+} and to light purple for Cr^{3+} (Figure 68). Job's plot supports a 1:1 (metal ion:ligand) stoichiometric complexation. The IR absorption frequencies of amide carbonyl decrease from 1686 to 1590 cm^{-1} (Fe^{3+}) and 1590 cm^{-1} (Cr^{3+}) upon addition of 20 equiv of metal ions, and ^1H NMR spectra indicate that amide carbonyl oxygens coordinate with Fe^{3+} or Cr^{3+}, supporting the proposed mechanism.

A dual chromo- and fluorogenic chemosensor, **118**, based on a rhodamine framework is very selective and sensitive toward Fe^{3+} in CH_3OH−HEPES buffer solution (3:1, v/v; pH 7.4).[154] Introducing Fe^{3+} to the colorless solution of **118** leads to spirocyclic ring-opening, resulting in a large enhancement in the fluorescence intensity at 580 nm when the chemosensor is excited at 530 nm, which is also accompanied by a color change from colorless to pink in the same medium. The other common metal ions, such as Hg^{2+}, Ag^+, Pb^{2+}, Sr^{2+}, Ba^{2+}, Cd^{2+}, Ni^{2+}, Co^{2+},

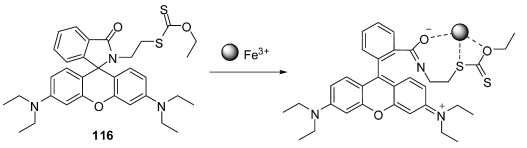

Figure 67. Proposed binding mode of **116** with Fe^{3+}.

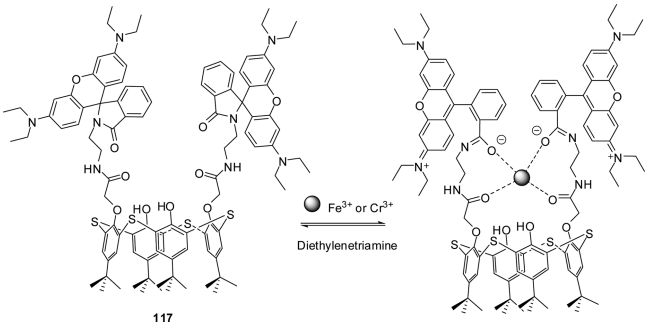

Figure 68. Proposed binding structure of **117** with metal cations.

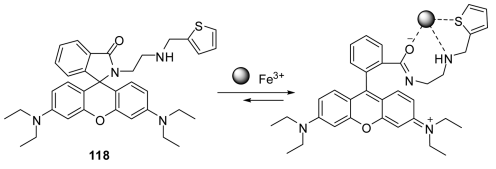

Figure 69. Proposed binding mechanism for the fluorescence enhancement of **118** upon addition of Fe^{3+}.

Fe^{2+}, Mn^{2+}, Cu^{2+}, Zn^{2+}, Ce^{3+}, Mg^{2+}, K^+, and Na^+, do not interfere, while Cr^{3+} interferes mildly in the detection of Fe^{3+}. The proposed mechanism involves Fe^{3+} coordination with the carbonyl oxygen, nitrogen, and thiophene sulfur, inducing spirocyclic ring-opening (Figure 69).

Xu et al. have reported another FRET-based supramolecular sensor, **119**, for ferric ion detection in aqueous solutions.[155] They have used an adamantyl (AD) group as an anchor between the spirolactam rhodamine B derivative (SRhB) and β-CD then linked with a dansyl (DNS) moiety. The spirolactam rhodamine B derivative, after opening of its spirocycle ring induced by Fe^{3+}, produces a long-wavelength rhodamine B fluorophore, which acts as an energy acceptor, with the dansyl group acting as an energy donor (Figure 70). In the absence of Fe^{3+}, the dansyl moiety emits at around 530 nm when excited at 410 nm. In the presence of Fe^{3+}, the intensity of the DNS emission at 530 nm decreases, while the intensity of a new emission band centered at 587 nm increases. Thus, the system ratiometrically detects Fe^{3+} selectively over other competitive metal ions with a detection limit of 1 μM.

Ma et al. have designed a strategy for the detection of ferric ions in aqueous solution by using poly(ethylene oxide)-*b*-polystyrene micelles as scaffolds for the construction of a FRET-based ratiometric sensing system (Figure 71).[156] A hydrophobic fluorescent dye, NBD, resides in the micelle core, acting as an energy transfer donor of the FRET system, and a spirolactam rhodamine derivative (SRhB−OH, **120**), adsorbed at the micelle interface of the core and corona, acts as an energy acceptor after its spiroring-opening induced by Fe^{3+}. By such a method,

dx.doi.org/10.1021/cr200201z |*Chem. Rev.* 2012, 112, 1910–1956

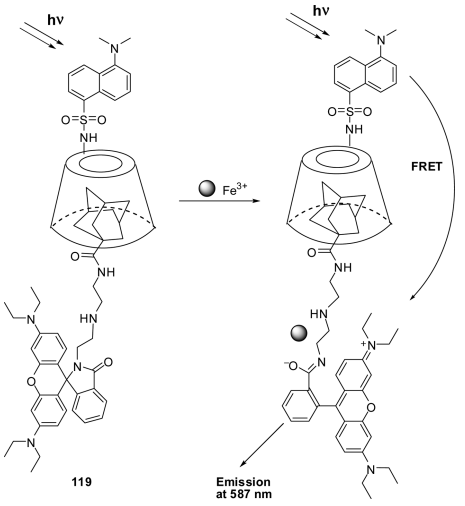

Figure 70. Schematic representation of the formation of an AD−SRhB/β-CD−DNS supramolecular complex and its FRET-based ratiomatric sensing of ferric ions in the aqueous solution.

excitation-induced backscattering effects on fluorescence detection were diminished, and the detection accuracy was enhanced by ratiometric sensing. The detection limit for Fe^{3+} by this method is 1.0 μM in aqueous solutions. This strategy can be useful in the detection of other metal ions by changing the FRET-based acceptor and donor pairs.

Xu et al. have reported a polymeric film sensor, **121**, which can be used like a test paper for the easy detection of Fe^{3+} in aqueous solutions with a detection limit of 1.0 μM.[157] The fluorescent dyad, which consists of a spirolactam rhodamine derivative and a dansyl moiety, is linked with a poly(vinyl alcohol) (PVA) matrix, a low-toxicity biocompatible polymer, forming a ratiometric fluorescence sensing system based on the FRET mechanism. After the film was immersed in the Fe^{3+} aqueous solution, the spirocyclic ring of the rhodamine moiety opened, as seen in Figure 72, and the open form acts as an energy acceptor, while the dansyl moiety acts as an energy donor. The emission intensities of the two bands, 480 nm (for dansyl emission) and 594 nm (for rhodamine B), vary ratiometrically with the Fe^{3+} concentration.

The solubilities of many synthesized organic fluorophores are known to be very poor in water. Poor solubility reduces the detection sensitivity of metal ions, especially in biological media. Yang, Sun, and co-workers have used the concept of nanoparticles to enhance the solubility of the probe and consequently the detection sensitivity.[158] They coupled the probe *N*-(rhodamine 6G lactam)ethylenediamine (**122**) with magnetic Fe_3O_4 nanoparticles modified by polyethylene glycol (PEG). The sensor−nanoparticle conjugate is also capable of separating Fe^{3+} magnetically from the biological solutions, which leads to very selective detection of Fe^{3+} with a detection limit of 2 ppb. The nitrogen atom and the two carbonyl oxygen atoms in the sensor−nanoparticle complex make complexes with Fe^{3+} in a 1:1 binding ratio, as shown in Figure 73, which induces a conversion from the spirolactam ring form to the open cyclic form of **122**. This results in a 58-fold enhancement of the red fluorescence with a shifting of the emission maximum from 544 to 549 nm. After treatment with **122**, HeLa cells stained with Fe^{3+} appeared red fluorescent using a confocal microscope with excitation at 490 nm, indicating that this sensor−nanoparticle

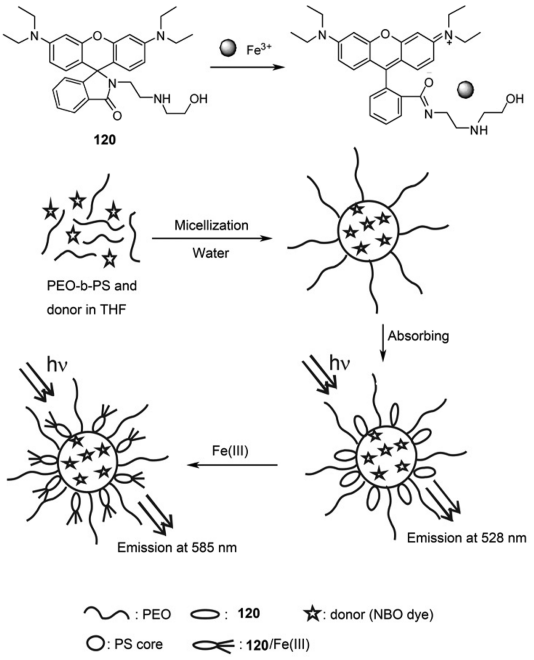

Figure 71. Schematic representation of the formation of the FRET system within a diblock copolymer micelle and its sensing of ferric ions in aqueous solution.

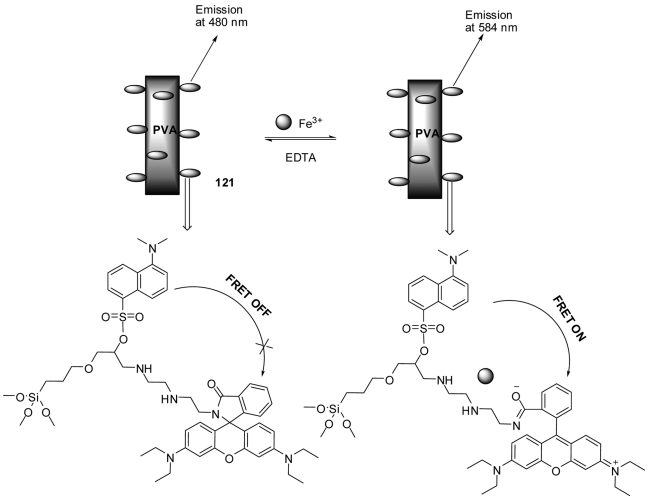

Figure 72. FRET-based PVA chemosensor and its ferric ion sensing.

conjugate is also very efficient for monitoring the intracellular Fe^{3+} concentration in living cells.

2.5. Sensors for Detecting Pb^{2+}

Lead is a poisonous metal, and the key route to poisoning is from ingestion of contaminated food or water. Long-term exposure to lead or its salts can damage nervous connections (especially in young children) and cause blood and brain disorders.[159] In view of ecotoxicological harm of lead(II) salts, considerable efforts have been devoted to developing fluorescent probes for lead(II) ions. Yoon et al. reported a rhodamine B derivative as a fluorescent chemosensor for Pb^{2+} (Figure 74).[160] A single crystal of compound **123** was characterized using X-ray crystallography, which for the first time showed unique

dx.doi.org/10.1021/cr200201z |*Chem. Rev.* 2012, 112, 1910–1956

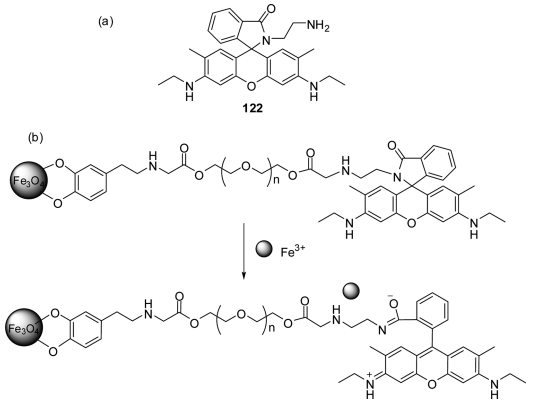

Figure 73. (a) Structure of **122**. (b) Coupling of **122** with PEG−Fe_3O_4 nanoparticles and structural changes after complexation with Fe^{3+}.

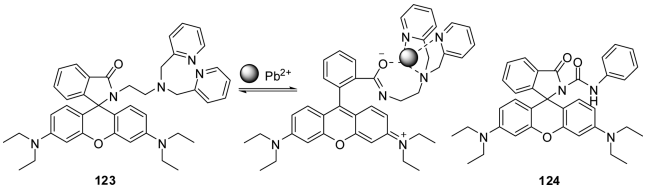

Figure 74. Proposed binding mechanism for the fluorescence enhancement of **123** upon addition of Pb^{2+} and structure of **124**.

spirolactam ring formation. Upon addition of Pb^{2+} to a colorless solution of **123** in acetonitrile, both pink color and fluorescence characteristics of rhodamine B appear. Having been tested with various metal ions, compound **123** showed a significant fluorescence enhancement only with Pb^{2+} in acetonitrile, even though there was a relatively small fluorescence enhancement with Cu^{2+} and Zn^{2+}. Using ESI-MS and IR and ^{13}C NMR spectroscopy, Yoon et al. verified the mechanism of fluorescence enhancement and color change induced by Pb^{2+}. Because both color and fluorescence disappear upon addition of excess cyclen or ethylenediamine, it is believed that the complexation of **123** with Pb^{2+} is reversible.

On the basis of a rhodamine−phenylurea conjugate, Hu et al. developed a turn-on fluorescent sensor, **124**, that can detect both Pb^{2+} and Hg^{2+} in different media (Figure 74).[161] Probe **124** displayed remarkably enhanced fluorescence intensities and clear color changes upon addition of Pb^{2+} in CH_3CN or Hg^{2+} in CH_3CN−H_2O (3:7, v/v) solution. In these respective conditions, Job's plot analysis afforded a 2:1 stoichiometry for the **124**−Pb^{2+} complex and a 1:1 stoichiometry for the **124**−Hg^{2+} complex. By fluorescence titration assays, the detection limits of **124** were further evaluated to be about 7×10^{-9} M for Pb^{2+} and 3.5×10^{-8} M for Hg^{2+}.

2.6. Sensors for Detecting Cr^{3+}

Cr^{3+} is an essential metal ion involved in many biochemical processes, such as metabolism of nucleic acids, proteins, carbohydrates, and fats, by activating certain enzymes and stabilizing nucleic acids and proteins.[162] A deficiency of chromium in the body may cause various diseases, including diabetes and cardiovascular diseases.[163] However, high levels of Cr^{3+} may affect cellular structures.[164] Due to agricultural and industrial activities, Cr^{3+} is accumulated in the environment as a pollutant. Having a

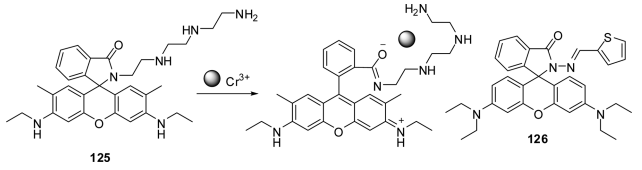

Figure 75. Proposed binding mechanism for the fluorescence enhancement of **125** upon addition of Cr^{3+} and structure of **126**.

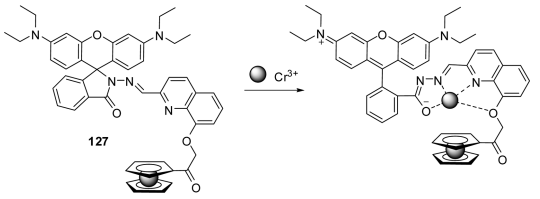

Figure 76. Proposed complexation mechanism of **127** with Cr^{3+}.

paramagnetic nature, Cr^{3+} is well-known to cause fluorescence quenching. In addition, lacking a proper recognition moiety for Cr^{3+} makes its detection very difficult by fluorimetric methods. Therefore, there is very little literature available describing xanthene-based Cr^{3+} sensors for either in vitro or in vivo systems.

Compound **125** is a rhodamine-based chemosensor for the detection of Cr^{3+} at biological pH in aqueous solutions.[139] A possible mechanism for the binding of Cr^{3+} with **125**, which induces spirolactam ring-opening of **125**, involves a 1:1 stoichiometry (Figure 75). Spirocyclic ring-opening upon addition of Cr^{3+} gives strong fluorescence that peaks at 560 nm with excitation at 500 nm in HEPES buffer.

Sinn et al. have reported a very simple rhodamine-based fluorescent turn-on chemosensor, **126**, for the detection of Cr^{3+} in acetonitrile (Figure 75).[165] Compound **126** is very selective for Cr^{3+} over other metal ions, except for Hg^{2+}, which shows a smaller effect. The perchlorate salt of Hg^{2+} does not interfere with the detection of Cr^{3+}. Addition of Cr^{3+} results in spirolactam ring-opening of **126**, probably due to chelation with oxygen, the imine nitrogen, and the thiophene sulfur. As a result, the colorless solution (for the ring-closed rhodamine) becomes pink (for the ring-opened rhodamine), and a large enhancement of the fluorescence intensity occurs at 583 nm.

Li et al. have reported a rhodamine B based multisignal chemosensor with a ferrocene substituent, **127**, for the detection of Cr^{3+} in ethanol−water (1:1, v/v) solutions.[166] Addition of Cr^{3+} induces spirolactam rhodamine ring-opening (Figure 76) that leads to fluorescence enhancement over a wide pH range (5−10) and a color change from colorless to pink. As the ring-opening phenomenon may affect the ferrocene substituent, the electrochemical parameter also changes. A probable complexation mechanism (Figure 76) has been checked by X-ray photoelectron spectroscopy (XPS) and ESI-MS measurements. Differential pulse voltammetric (DPV) curves of **127** recorded in an ethanol solution containing 0.1 M *n*-tetrabutylammonium hexafluorophosphate as a supporting electrolyte, in the absence and presence of Cr^{3+}, show that the peak shifts cathodically by ~140 mV with reduced electric currency in its reversible ferrocene/ferricinium redox cycles upon complexation with Cr^{3+}. The XPS measurements for the **127**−Cr^{3+} system indicate the presence of Cr^{3+} in the system; i.e., complexation of Cr^{3+} with **127** occurs, rather than reduction of Cr^{3+}. The ESI-MS spectrum for a

dx.doi.org/10.1021/cr200201z |*Chem. Rev.* 2012, 112, 1910–1956

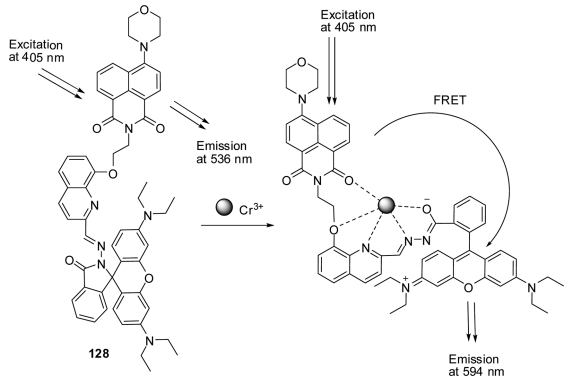

Figure 77. Proposed mechanism for FRET-based chemosensing of **128** for Cr^{3+}.

mixture of **127** and 200 μM $CrCl_3$ shows a peak at m/z 962.0 corresponding to $[\mathbf{127} + Cr^{3+} + 2Cl^-]^+$. The sensor is very selective for Cr^{3+} over other coexistent metal ions, except for Hg^{2+}, which causes mild interference. By laser scanning confocal microscopy, after incubation with **127**, HeLa cells treated with Cr^{3+} showed a significant increase in the fluorescence from the intracellular area; thus, the subcellular distribution of Cr^{3+} can be detected.

Ligand **128** is a FRET-based chemosensor which consists of rhodamine and naphthalimide moieties, acting as a fluorophore dyad for the detection of Cr^{3+} in ethanol−water (2:1, v/v) solutions.[167] Adding Cr^{3+} to a solution of **128** induces ring-opening of the rhodamine moiety, and consequently, the color of the solution turns from weak yellow to red-orange. The naphthalimide moiety, which shows an absorption band that peaks at 380 nm in the ethanol−water solution, behaves as an energy donor for the FRET system, and the open form of the rhodamine moiety, which shows an absorption band that peaks at 568 nm in the same solution, acts as an energy acceptor (Figure 77). The intensity of the fluorescence band peaks at 544 nm (for the naphthalimide moiety), and the intensity of the fluorescence band that peaks at 592 nm varies ratiometrically with the concentration of Cr^{3+}, when the probe is excited at 405 nm. By laser scanning confocal microscopy, a significant increase in the fluorescence from the intracellular area was observed in HeLa cells treated with Cr^{3+} after being stained with **128**.

Two-photon-excited fluorescence (TPEF) has many advantages over one-photon-excited fluorescence, such as low background noise because of the large spectral separation of the excitation light and the fluorescence emission signal, the excitation wavelength being in the near-infrared (NIR) region, so light penetrates deeply into the biological tissue, reducing photodamage. Wang, Xia, and co-workers[168] have made a rhodamine-based fluorophore dyad, **128**, containing a naphthalimide moiety which can detect Cr^{3+} by following the FRET mechanism for both in vivo and in vitro systems with a detection limit of 1.0 μM. Herein, **128** can show two-photon-excited fluorescence, which makes it more sensitive and selective for the detection of Cr^{3+} over other metal ions. The addition of Cr^{3+} to the solution of **128** induces spirocyclic ring-opening of the rhodamine moiety, and the open form acts as an energy acceptor whereas the naphthalimide moiety behaves as an energy donor in the FRET system. The absorption and fluorescence bands are located around 400 and 515 nm, respectively, whereas the open form of the rhodamine moiety absorbs in the 500−600 nm region and has an

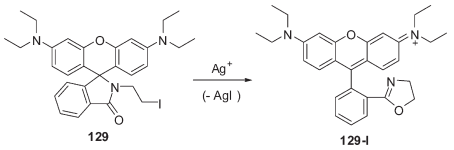

Figure 78. Proposed reaction mechanism of **129** with Ag^+.

emission maximum at 583 nm when excited at 515 nm in ethanol−water (2:1, v/v) solution. The calculated FRET rate ratio between free **128** and **128**−Cr^{3+} is 0.25, which indicates a large enhancement of the intramolecular FRET effect upon binding of Cr^{3+} with **128**. The compound is able to detect Cr^{3+} in the pH range of 5−10 in ethanol−water solution.

2.7. Sensors for Detecting Noble-Metal Ions

Noble metals, such as gold, silver, platinum, and palladium, are widely used for the preparation of dental materials, catalysts, fuel cells, jewelry, and anticancer drugs. However, their frequent use can result in high levels of residual noble-metal ions, which may result in the contamination of water systems and soil and therefore cause a health hazard.[169−171] For example, Au^{3+} is known to be highly toxic in biological systems due to its strong affinity for DNA and can even cause DNA cleavage,[172−174] excessive silver ion intake can lead to the long-term accumulation of insoluble precipitates in the skin and eyes,[175] platinum salts can cause DNA alteration, cancers, autoimmune disorders, respiratory and hearing problems, and damage to organs, such as the intestines, kidneys, and bone marrow,[176] and palladium ions can bind to thiol-containing amino acids, proteins, DNA, or other macromolecules and disturb a variety of cellular processes.[177] Selective sensing methods would be very useful for the real-time monitoring of these metal ions in environmental and biological samples.

Ahn et al. developed an intelligent system using the rhodamine-based fluorogenic and chromogenic probe **129** for Ag^+ ions in 20% ethanolic water solution.[178] The sensing mechanism is based on the irreversible tandem ring-opening and -formation processes of **129-I** promoted by Ag^+ coordinated to the iodide of the probe (Figure 78). As **129** reacted with Ag^+, both a color change to pink and a turn-on-type fluorescence change to orange were observed. Counteranions of silver salts had a negligible effect on the sensing process, as AgOAc and $AgClO_4$ gave similar results. Probe **129** showed remarkably high selectivity over other metal ions and could detect silver ions at concentrations down to 14 ppb. Furthermore, the sensing protocol can be applied to the quantification of silver nanoparticles in consumer products.

In 2009, a rhodamine alkyne derivative, **130**, was reported by Kim, Lee, Yoon, and co-workers as the first fluorescent and colorimetric chemodosimeter for Au^{3+} (Figure 79).[179] Probe **130** displayed a highly selective fluorescence enhancement (over 100-fold) and colorimetric change (from colorless to pink) with Au^{3+} in EtOH−HEPES buffer (0.01 M; pH 7.4; 1:1, v/v), which was attributed to the transformation of the propargylamide moiety of **130** to the oxazolecarbaldehyde **130-I** in the presence of Au^{3+}. There was also a large enhancement (~6-fold) in the UV absorption (λ_{max} = 562 nm) of probe **130** upon addition of Au^{3+}. The rate constant for the conversion of **130** (5 μM) to **130-I** was measured in the presence of Au^{3+} (10 equiv) and estimated to be $K_{obsd} = (4.5 \pm 0.20) \times 10^{-4}\ s^{-1}$ on the basis of the initial kinetic analysis. From the fluorescence responses of **130** (1 μM) in EtOH−water (1:1, v/v) toward various amounts of Au^{3+}, the

dx.doi.org/10.1021/cr200201z |Chem. Rev. 2012, 112, 1910–1956

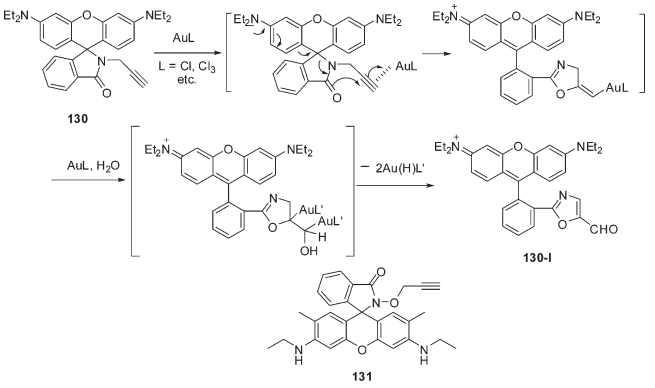

Figure 79. Proposed reaction mechanism of **130** with Au^{+}/Au^{3+} and structure of **131**.

detection limit was estimated to be 63 ppb. Finally, probe **130** was successfully applied to the cell imaging of Au^{3+}. During the same period, Ahn et al. further applied probe **130** to the detection of Au^{+}. They demonstrated that probe **130** shows both color and turn-on fluorescence changes only toward Au^{+}/Au^{3+} among various metal species.[180] A formyloxazole compound was formed as the major product in aqueous medium, presumably via a vinylgold intermediate, which has new mechanistic implications for vinylgold intermediates (Figure 79).

Similarly, Tae et al. utilized a rhodamine B alkyne derivative, **131**, as a fluorescent chemosensor for Au^{3+} (Figure 79).[181] This sensor, **131**, exhibits reversible dual chromo- and fluorogenic changes for Au^{3+} in PBS buffer (1% MeOH) solution at pH 7.4 in a highly selective and sensitive manner. The probe can sense Au^{3+} selectively over other biologically relevant metal ions, and ~50 nM Au^{3+} could be readily detected in aqueous medium. HeLa cells stained with **131** showed strong red fluorescence after incubation with Au^{3+}. In contrast, the cells without treatment using Au^{3+} show no fluorescence.

Lin et al. described rhodamine derivative **132** as a fluorescent sensor for the detection of gold ion through Au^{3+}-mediated hydrolysis of acylsemicarbazide to carboxylic acid (Figure 80).[182] **132** displayed no fluorescence in PBS (pH 7.4, containing 0.3% DMF) due to it being in the spirocyclic form. Upon addition of Au^{3+}, **132** exhibited a 233-fold enhancement in the fluorescence intensity. A linear relationship between the fluorescence intensity at 549 nm and the concentration of Au^{3+} from 0.5 to 70 mM was observed, and the detection limit was determined to be 290 nM (S/N = 3). In contrast, **133** only showed a 12-fold fluorescence enhancement with the addition of 10 equiv of Au^{3+}, although it also responds to gold ions under the same conditions. Other metal species such as Ag^{+}, Ca^{2+}, Cd^{2+}, Co^{2+}, Cr^{3+}, Cu^{2+}, Zn^{2+}, Fe^{2+}, Fe^{3+}, Hg^{2+}, Mg^{2+}, Mn^{2+}, Ni^{2+}, Pb^{2+}, Na^{+}, and K^{+} induced little variation in the fluorescence of solutions containing **133**, indicating good selectivity of **133** toward Au^{3+}. Furthermore, after incubation with Au^{3+}, HeLa cells preloaded with the probe displayed intense fluorescence, demonstrating that probe **132** is potentially useful for Au^{3+} imaging in living cells.

Peng and co-workers reported a fluorescence-enhanced probe, **134**, which can selectively detect palladium in both Pd^{2+} and Pd^{0} states (Figure 81).[183] The recognition of Pd by **134** is based on the p-affinity of Pd to allyl groups, which further induced the well-known transformation from spirolactam to the ring-opened form of rhodamine. In ethanol−H_2O (1:1, v/v; 25 °C) solution, upon addition of Pd^{2+}, **134** displayed a brilliant purple

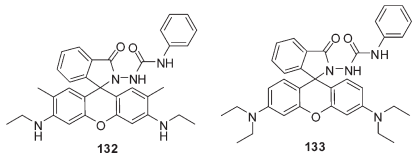

Figure 80. Structures of **132** and **133**.

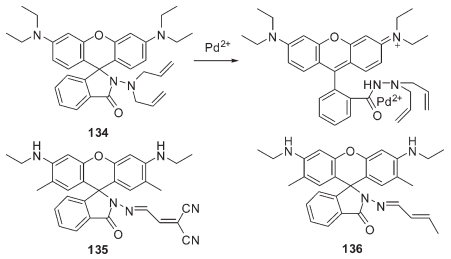

Figure 81. Proposed binding mechanism of **134** with Pd^{2+} and structures of **135** and **136**.

coloration as well as a strong absorption band centered at 560 nm. The strong fluorescence enhancement at 580 nm was only observed in the presence of Pd^{2+}, and not other metal ions, indicating the high selectivity of **134** toward Pd^{2+}. The fluorescence intensities are linearly related to the amount of Pd^{2+} over the range of 0−1 ppm, and the detection limit was evaluated to be 1.85×10^{-7} M. By the Job's plot method, a 1:1 stoichiometry for the binding between **134** and Pd^{2+} was demonstrated. In the presence of excess PPh_3, Pd^{2+} can be reduced to Pd^{0}. The fluorescence intensity of **134** gradually increased after addition of Pd^{2+} to PPh_3−**134** solution, which showed that **134** is also useful as a sensor for detecting Pd^{0}. However, **134** is imperfect in that the presence of Hg^{2+} can quench the fluorescence of **134**−Pd^{2+}. The modified molecules **135** and **136** (Figure 81) showed similar color changes and fluorescence enhancement in the presence of Pd^{2+} in 50% ethanolic water solution,[184] even in the presence of Hg^{2+}. Among the three sensors, **135** displays the best specificity toward Pd^{2+} and affords convenient detection by the naked eye, owing to richer electron density and a more suitable stereo effect in the allylidenehydrazone group. The 2:1 stoichiometries between the probe and Pd^{2+} for both **135** and **136** were supported by Job's plots. The fluorescence intensities of **135** and **136** are both linearly proportional to the amount of Pd^{2+} added (0−1.0 ppm), with detection limits of 1.80×10^{-7} M for **135** and 1.70×10^{-6} M for **136**.

Ahn and Jun also reported a rhodamine derivative, **137**, bearing an iodophenyl group as an efficient fluorogenic and chromogenic sensor for palladium species.[185] The mechanism is described as shown in Figure 82: The oxidative insertion of Pd^{0} species into probe **137** generated the palladium intermediate **137-I**, which subsequently underwent a transformation from the spirolactam to the ring-opened form owing to the coordination between the carboxamide oxygen and palladium. A further reductive elimination process led to the generation of fluorescent benzoxazole **137-II**. At 85 °C, when a solution of probe **137** in acetonitrile was treated with $PdCl_2$ and $[(t\text{-Bu})_3PH]BF_4$, where $[(t\text{-Bu})_3PH]BF_4$ was used as an agent for reducing Pd^{2+} to Pd^{0}, the colorless solution became pink with an absorption band centered at 560 nm. The fluorescence of **137** also underwent a transformation from dark to bright orange with an emission band

dx.doi.org/10.1021/cr200201z |*Chem. Rev.* 2012, 112, 1910–1956

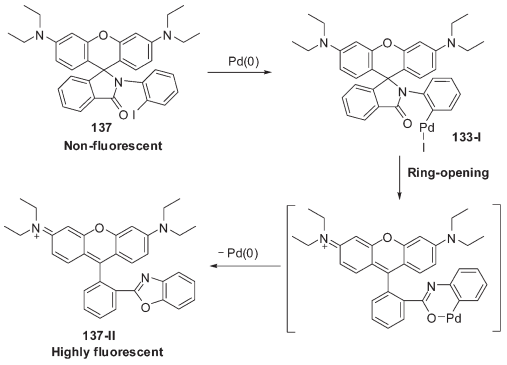

Figure 82. Proposed binding mechanism of **137** with Pd(0).

centered at 580 nm. The selectivity of this system for palladium species over other metal ions is remarkably high, and the detection limit was evaluated to be 10.2 ppm. Probe **137** was demonstrated to be useful for determining the residual palladium content in chemical products.

Tae et al. utilized a rhodamine 6G triazole, **138**, as a fluorescent chemosensor for Pt^{2+} in aqueous solution (Figure 83).[186] The dual binding unit composed of a hydroxamate and a triazole showed high selectivity and sensitivity toward Pt^{2+} over a range of other metal ions in water. Probe **138** shows neither color nor fluorescence in H_2O (DMSO, 1%, v/v), indicating that it exists predominantly in the spirocyclic form, as expected. Upon addition of Pt^{2+}, probe **138** (5 μM) exhibits strong fluorescence at 562 nm as well as a color change from colorless to pink-red in H_2O (DMSO, 1%, v/v). This suggests that the triazole group accelerates the ring-opening of the spirolactam, thereby allowing it to play an important role as a Pt^{2+} sensor. Probe **138** could be used to monitor Pt(II) ions in the pH range of 5−9.

2.8. Sensors for Detecting Other Metal Ions

Lanthanides can emit NIR radiations, which are very useful for biomedical imaging and optical communications because of the high penetration power of NIR through living tissues, less harm to living cells, low background fluorescence due to long luminescence lifetimes of lanthanides, and sharp emission bands.[187−194] A sensitizing chromophore, **139**,[195] containing the rhodamine 6G unit linked to 8-hydroxyquinoline-2-carboxaldehyde by a carbohydrazone linker, can donate its excitation energy in the visible range (~500 nm) to Yb^{3+}, which then emits near-infrared radiation at around 1000 nm. Yb^{3+}, when coordinated with the rhodamine 6G moiety of **139**, induces spirolactam ring-opening of closed and nonfluorescent rhodamine 6G moieties to give the fluorescent ring-opened form, which has an absorption band maximum around 525 nm and an emission band maximum around 560 nm in acetonitrile. The ring-opening is associated with a proton being lost from the 8-hydroxyquinoline unit, leading to the formation of a tetradentate ligand and the subsequent Yb^{3+} complexes (Figure 84). The rigid tetradentate ligand occupies eight coordination sites and thus eliminates the possibility of solvent participation in the coordination and gives efficient NIR radiation while coupled with the triplet excited state of the rhodamine moiety.

Wu et al. have reported a fluorescent chemosensor, **140**,[196] based on the rhodamine framework containing a homotrioxacalix[3]arene skeleton as an ionophore for the detection of HTM ions in neutral (pH 7) aqueous acetonitrile solutions. Upon addition of metal ions (Sb^{3+}, Fe^{3+}, or Ni^{2+}) to solutions of probe **140**, the spirolactam ring opens due to the coordination of metal

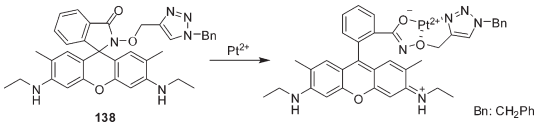

Figure 83. Proposed binding mode of **138** with Pt^{2+}.

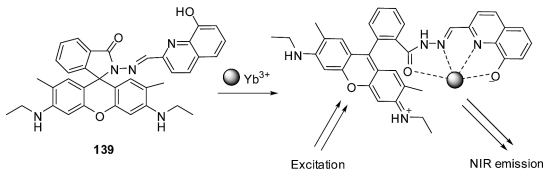

Figure 84. Schematic binding mechanism of **139** with Yb^{3+}.

ions to the amide carbonyl oxygen, as shown in Figure 85, resulting in a pink color and strong orange fluorescence. Job's plot indicates a 3:1 (metal ion:ligand) binding stoichiometry. The addition of 50 equiv of metal ions, including Sb^{3+}, Fe^{3+}, and Ni^{2+}, to the solution of **140** provides 353-fold, 164-fold, and 51-fold absorbance enhancement in UV−vis spectra, respectively. Similarly, upon addition of the same number of equivalents of Sb^{3+}, Fe^{3+}, and Ni^{2+} to a solution of **140**, fluorescence enhancement at 587 nm occurs by factors of 527, 357, and 224, respectively. For Fe^{2+} and Cu^{2+}, fluorescence enhancement occurs by factors of 40 and 57, respectively, while other metal ions such as Co^{2+}, Ag^{+}, Zn^{2+}, Cd^{2+}, Hg^{2+}, Mg^{2+}, Na^{+}, and K^{+} show almost no enhancement in either UV−vis or fluorescence spectra. The IR absorption peak of the amide carbonyl at 1685 cm^{-1}, upon addition of 10 equiv of of Sb^{3+}, Fe^{3+}, and Ni^{2+}, shifts to 1618 cm^{-1} (Sb^{3+}), 1633 cm^{-1} (Fe^{3+}), and 1632 cm^{-1} (Ni^{2+}), indicating that the amide carbonyl oxygen is involved in the coordination of metal ions.

3. DETECTION OF ANIONS BASED ON XANTHENES AND RELATED DERIVATIVES

3.1. Detection of CN^-

The extreme toxicity of cyanide in physiological systems, as well as the continuing environmental concern caused by its widespread industrial use, has led to the development of methods for cyanide detection. The chemosensing ensemble method in conjunction with a rhodamine fluorophore was also applied to detect thiols in aqueous solution. In the chemosensing ensemble method, the fluorescent dye is first bound with the receptor through noncovalent interactions, resulting in either quenching or enhancement of fluorescence. When the analyte was added to the dye−receptor solution, the fluorescence of the dye could be recovered. By this strategy, Li et al. reported a colorimetric chemosensor using the ensemble **4**−Cu^{2+} for the detection of cyanide (Figure 86).[197] In 50% (v/v) buffered (10 mM Tris−HCl, pH 7.0) water−CH_3CN, **4**−Cu^{2+} displayed an obvious magenta color with an absorption band at around 555 nm. Upon addition of cyanide, the magenta color of the sensing system faded to colorless, and the peak at 555 nm decreased immediately. Due to the much higher affinity between cyanide and copper ions, the added cyanide caused dissociation of copper ions from the complex, resulting in decreased intensity in absorption as well as a color change. The detection limit was evaluated to be 0.013 ppm by absorption changes. Other anions, such as

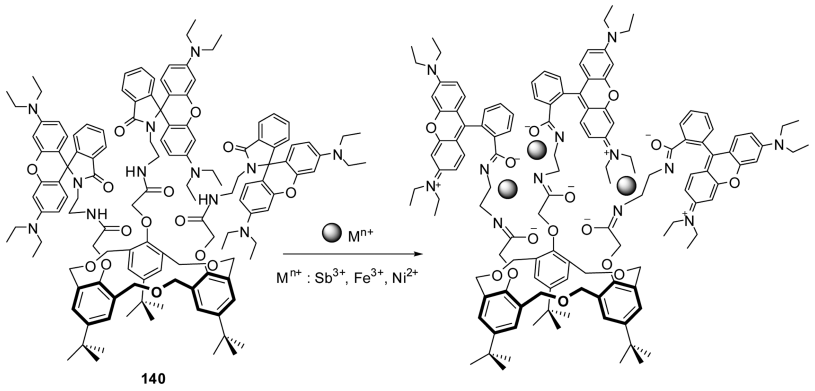

Figure 85. Proposed binding mode of **140** with HTM ions.

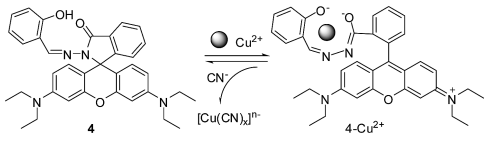

Figure 86. Schematic representation of CN^- sensing by the **4**−Cu^{2+} ensemble.

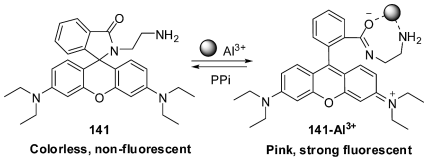

Figure 87. Schematic representation of PPi sensing by the **141**−Al^{3+} ensemble.

Cl^-, I^-, IO_3^-, SO_4^{2-}, NO_2^-, Br^-, $H_2PO_4^-$, F^-, SCN^-, HSO_4^-, and ClO_4^-, had almost no influence on the sensing system, indicating high selectivity of this system toward CN^-.

3.2. Detection of $P_2O_7^{4-}$

Nucleoside triphosphates, including ATP, which takes part in cell metabolism and its regulation, produce pyrophosphate (PPi) on hydrolysis.[198−200] Biological processes involved with the hydrolysis of nucleoside triphosphates can be monitored by quantitative and selective PPi detection in intracellular environments. Although several reports on PPi sensors are available in the literature,[201−213] sensors based on xanthene dyes are rarely reported.

Yoon, Lee, and co-workers[214] have developed a chemical ensemble system for the detection of PPi in aqueous solution. The ensemble is based on a complex between the rhodamine derivative **141** and Al^{3+}. The spirolactam ring form of **141** is colorless and nonfluorescent, and Al^{3+} induces spirocyclic ring-opening (Figure 87), resulting in a color change from colorless to pink as well as strong fluorescence. The addition of PPi to a solution of the ensemble system changes the solution color from pink to colorless and causes fluorescence quenching. This is probably due to the dissociation of Al^{3+} from the ensemble system, which closes the ring of the rhodamine moiety. ESI-MS experiments were carried out before and after addition of PPi to the solution of the **141**−Al^{3+} ensemble, and the results reveal the nature of the interaction between the **141**−Al^{3+} ensemble and PPi. After addition of 10 equiv of PPi, the peak at m/z 617.20 corresponding to $[\mathbf{141} - AlCl_3 + H^+]^+$ disappears, while the peak at m/z 485.21 corresponding to $[\mathbf{141} - H^+]^+$ remains intact, which indicates that the binding affinity between PPi and Al^{3+} is stronger than that between **141** and Al^{3+}. Thus, the ensemble system detects PPi in neutral (pH 7.4) aqueous solution selectively over other biological competitors such as AMP, ADP, ATP, and phosphate ions.

3.3. Detection of CH_3COO^- and Other Anions

Kim et al. have reported a colorimetric and fluorescent chemosensor, *N*-(2′,7′-dichlorofluorescein lactam)-*N*′-phenylthiourea

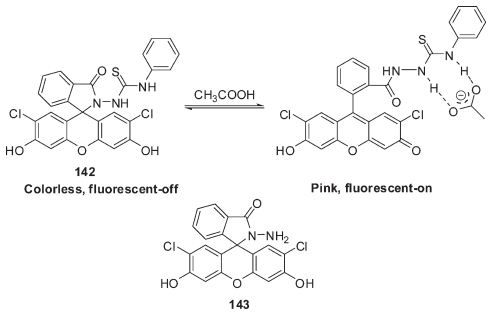

Figure 88. Proposed mechanism for CH_3COO^--induced ring-opening of **142** and structure of **143**.

(**142**),[215] for the detection of anions such as CH_3COO^-, F^-, and $H_2PO_4^-$ in acetonitrile. A thiourea moiety has been attached to the fluorescein moiety as it can bind some specific anions through H-bonding. The addition of CH_3COO^-, F^-, or $H_2PO_4^-$ induces spirolactam ring-opening (Figure 88) as these anions can form H-bonds with the amide-*N*-thiourea, which results in a color change of the solution from colorless to pink, and a new absorption band is observed at 530 nm. The ring-opened form gives strong fluorescence at 550 nm, and the fluorescence intensity increases with increasing concentration of anions (CH_3COO^-, F^-, or $H_2PO_4^-$). Due to the lack of a thiourea unit in **143**, ring-opening of the fluorescein moiety does not occur in the presence of CH_3COO^-; instead, only phenoxide ions are formed, giving rise to one absorption band that peaks at 323 nm and no absorption band at 530 nm or any fluorescence change. This indicates that the thiourea unit is responsible for interacting (H-bond) with the acetate ions rather than deprotonating the phenolic OH. Other anions such as Cl^-, Br^-, I^-, and HSO_4^- do not interfere with the detection of CH_3COO^-, F^-, or $H_2PO_4^-$ ions.

Chemosensor **144** bearing rhodamine and naphthalene moieties can detect CH_3COO^- ions in acetonitrile through the

dx.doi.org/10.1021/cr200201z |*Chem. Rev.* 2012, 112, 1910–1956

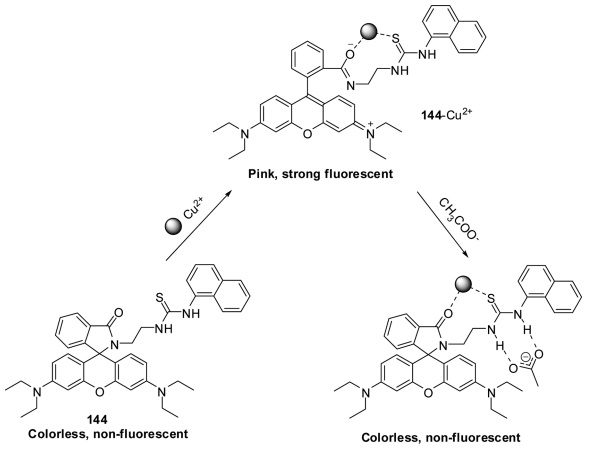

Figure 89. Proposed Cu^{2+}-induced ring-opening and CH_3COO^--induced ring-closing of **144**.

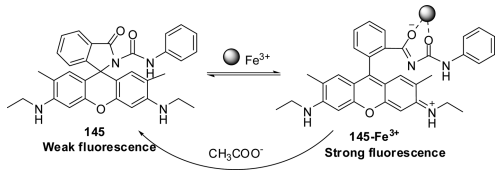

Figure 90. Proposed binding mode of the **145**$-Fe^{3+}$ complex with acetate ions.

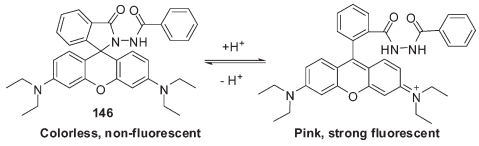

Figure 91. Proposed mechanism for the fluorescence enhancement of **146** upon addition of H^+.

excimer fluorescence resonance energy transfer (Em-FRET) mechanism.[216] Compound **144** has a binding affinity toward anions such as CH_3COO^-, F^-, $H_2PO_4^-$, and $PhCOO^-$. Binding takes place through H-bonding interactions with the two N−H fragments of the thiourea and the anions. The absorption band of **144** undergoes a red shift by ∼95 nm after binding with the anions. The addition of Cu^{2+} ions to the solution of **144** induces spirolactam ring-opening of **144** and gives a color change from colorless to pink. The open form of the rhodamine moiety can, in turn, accept the excitation energy from the naphthalene excimer which is formed after excitation at 300 nm. Thus, the Em-FRET system operates, and the intensity of the acceptor emission centered at 584 nm increases with increasing concentration of Cu^{2+}. The Em-FRET becomes switched off selectively after the addition of CH_3COO^- to the solution of **144**$-Cu^{2+}$ because of ring-closing of the rhodamine moiety (Figure 89). This phenomenon is very selective for CH_3COO^- over other anions, such as Cl^-, Br^-, I^-, NO_3^-, and ClO_4^-, but not F^-, $H_2PO_4^-$, and $PhCOO^-$ ions, which have some influence over this phenomenon.

A rhodamine 6G−phenylurea conjugate derivative, **145**, can selectively detect Fe(III) ions in aqueous medium.[217] In the presence of Fe^{3+}, **145** complexes with Fe^{3+} ions. The metal ion complex **145**$-Fe^{3+}$ can detect CH_3COO^- ions in aqueous acetonitrile (1:1, v/v) solutions with a very high sensitivity and selectivity over a wide range of coexistent anions, including F^-, Cl^-, Br^-, I^-, HSO_4^-, $H_2PO_4^-$, NO_3^-, and CO_3^{2-} (Figure 90). The addition of CH_3COO^- to a solution of **145**$-Fe^{3+}$ results in a remarkable reduction in the absorption and emission peak intensities and also a change in color from pink to colorless. The spectral changes should be attributed to the release of free **145** in the presence of CH_3COO^-, which can be proved by checking the ^1H NMR signal for the xanthene proton in **145**.

4. SENSORS FOR DETECTING PH

Various cellular events, such as cell growth,[218] cell adhesion,[219] chemotaxis,[220] endocytosis,[221] calcium regulation,[222] etc., are monitored by following the intracellular pH. Abnormal pH regulation (e.g., low pH, 4.5−6) in some specific and localized areas of the cell, which is an indication of abnormal cell events, can be useful for the diagnosis of some specific diseases, such as neurodegenerative disorders,[223] cystic fibrosis,[224] colorectal and breast cancer, etc. Fluorescence-based techniques are popular for the measurement of intracellular pH and cell imaging. Fluorescent probes should be highly selective and sensitive to the change in pH of the intracellular compartment as minor variations can cause cellular dysfunction. Efficient acidic fluorescent probes, which may work in the pH range of 4.5−6 and can be useful for studying acidic organelles, are rarely reported in the literature.

Tang et al. have synthesized the rhodamine-based fluorescent probe **146** for optical imaging of intracellular H^+ in vivo.[225] The spirocyclic form of **146** is colorless and nonfluorescent. The addition of H^+ to the probe solution leads to spirocyclic ring-opening (Figure 91), which results in a pink-colored solution with a strong fluorescence emission that peaks at around 582 nm (excitation at 525 nm) in buffer solutions (10% ethanol cosolvent, 0.1 M NaCl, pH 3.55−7.01). The probe is very sensitive in the pH range of 4.2−6.0 with a pK_a value of 4.85, which is very important for studying acidic organelles. Compound **146** is also very selective for H^+ over other metal ions, such as Cu^{2+}, Zn^{2+}, Fe^{3+}, Ca^{2+}, and Mg^{2+}. The probe is very efficient for fluorescence microscopy imaging of H^+ in HepG2 cells (human hepatocellular liver carcinoma cell line).

Rhodamine hydrazide based chemosensors **147** and **148**[226] in the solid state can detect volatile acids, such as HF, HCl, HBr, and HNO_3. They can even detect acid precursors, such as CH_3COCl, $POCl_3$, $SOCl_2$, PBr_3, and acryloyl chloride, which can produce HCl or HBr indirectly by reactions with nucleophiles (e.g., hydrazide). They can also detect chemical warfare agents such as diethyl chlorophosphate and are very selective for acid vapors over volatile organic bases and other volatile organic compounds. The spirolactam forms of **147** and **148** are colorless and nonfluorescent, whereas their open forms are colored and fluorescent. The protonation of the hydrazide moieties in **147** or **148** induces spirolactam ring-opening (Figure 92), which results in the appearance of a pink color and strong red fluorescence.

Compounds **149** and **150** are two rhodamine B based chemosensors for monitoring the pH in HeLa cells, where the rhodamine B moiety and β-CD are linked by ethylenediamine and tetraethylenepentamine, respectively (Figure 93).[227] Compound **149** can also be used for detecting low pH (<5) in cell organelles such as lysosome due to its low cytotoxicity. At low pH the spirolactam ring of **149** or **150** opens, giving rise to a new absorption band at 560 nm and strong fluorescence at 590 nm in aqueous solution.

dx.doi.org/10.1021/cr200201z |*Chem. Rev.* 2012, 112, 1910–1956

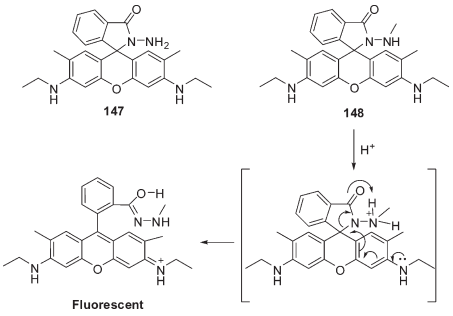

Figure 92. Structure of **147** and proposed mechanism for the spirocyclic ring-opening of **148** upon addition of H^+.

Dyer et al. have synthesized a series of structurally similar rhodamine B based chemosensors, which can behave differently for the detection of the pH in solution, depending upon the nucleophilicity and steric hindrance of the amine moiety attached.[228] The probes **151**−**153** are nonfluorescent under basic conditions and fluorescent under acidic conditions. Compound **154** is fluorescent in both the basic and acidic regions, but the fluorescence is stronger under acidic conditions. For **151**−**153** there is no absorption at basic pH (e.g., at pH 8), but a new band arises at around 570 nm in 15% ethanol−water (v/v) solutions, and the absorbance increases on going from the basic to the more acidic region. Probe **154** shows strong absorption under both acidic and basic conditions, and the change of absorbance is invariant with the pH. To explain this result, the authors have proposed a PET mechanism for explaining the pH sensing properties of **154**, where fluorescence quenching by the nitrogen lone pair in the amine moiety is disrupted after protonation of the amine moiety under acidic conditions. For **151**−**153**, as shown in Figure 94, the spirolactam ring opens after protonation of the amine moiety, and the opened form shows strong absorption and fluorescence in acidic medium.

Bojinov et al. have constructed a bichromophoric FRET system, **155**, based on rhodamine 6G and a 1,8-napthalimide attached to the *N*-methylpiperazine moiety. 4-(*N*-Methylpiperazinyl)-1,8-naphthalimide moieties are used as donor dyes, and rhodamine 6G is used as an acceptor dye.[229] The PET process, which involves electron transfer from the *N*-methylpiperazine moiety to the excited state of the fluorophore, quenches the fluorescence emission of the 1,8-naphthalimide unit, leading to the off state of the system. The protonation of the piperazine *N*-amine does not allow the electron transfer, causing the donor to be "switched on" for fluorescence emission. Thus, the dyad system can be used as a sensor for the detection of the pH. At pH 8.0, the system is weakly fluorescent owing to the PET effect and the spirolactam form of rhodamine 6G. However, at pH 2.5, the spirolactam ring of rhodamine is opened, while the PET process is inhibited, which results in a new absorption band at 522 nm, and emission occurs at 562 nm when the system is excited at 390 nm in water−DMF (4:1, v/v) solution, indicating energy transfer from the donor 1,8-naphthalimide to the ring-opened form of the acceptor (Figure 95).

5. SENSORS FOR DETECTING REACTIVE OXYGEN AND NITROGEN SPECIES

Reactive oxygen species (ROS) and reactive nitrogen species (RNS) play positive roles in diverse physiological and in pathogenic processes and are also connected to many diseases,

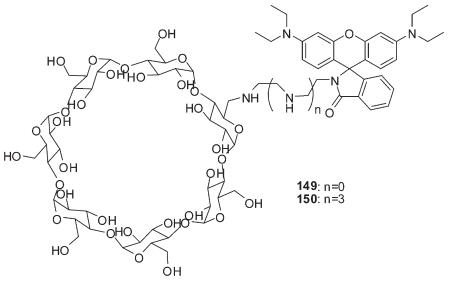

Figure 93. Structures of **149** and **150**.

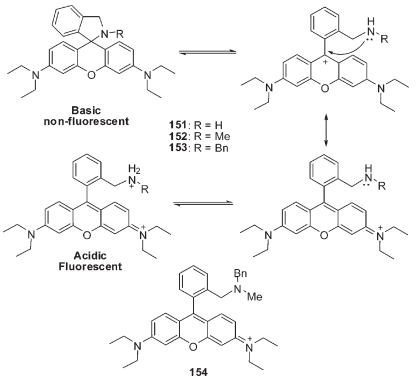

Figure 94. Quenching mechanism for probes **151**−**153** and structure of **154**.

including cancer and neurodegeneration disorders.[230] Sensitive and selective detection methods by fluorescent and luminescent chemosensors for ROS/RNS are useful for monitoring in vivo production of these species and elucidating the functions of these species.[10]

As described previously, compound **1** can serve as a sensor for both Hg^{2+} and Cu^{2+} on the basis of the ring-opened mechanism induced by coordination with respective metal ions. Guo et al. reported that **1** responds to peroxynitrite in aqueous solution.[231] In the presence of peroxynitrite, **1** was oxidized to form strongly fluorescent rhodamine B. The response time of the probe to peroxynitrite is less than 30 s, and a linear relationship was observed between the fluorescence intensity and the concentration of peroxynitrite in the range from 7.5×10^{-8} to 3.0×10^{-6} M with a detection limit of 2.4×10^{-8} M. **1** has also been demonstrated to show potential for the detection of NO_2^- and NO at acidic pH.[232] When $NaNO_2$ solution was added to a citrate buffer (pH 3.0) containing **1** and the mixture was incubated for 1 h at 60 °C, a large increase in the absorbance at 561 nm and an emission band at 581 nm were observed. The absorbance at 561 nm is linearly proportional to the concentration of NO_2^- in the range from 0.5 to 30 μM. Besides, in neutral solution, **1** showed a strong fluorescence when NOC 7 (a source of NO) was added, indicating the potential of **1** for bioimaging endogenous NO under physiological conditions.

Hypochlorous acid (HOCl) is an important ROS that exists in equilibrium with hypochlorite ($^-$OCl) at physiological pH. The regulated production of microbicidal HOCl is highly beneficial for host innate immunity during microbial invasion.[233,234] However, as a result of the highly reactive and diffusible nature of HOCl, its uncontrolled production within phagocytes is involved in a variety of human diseases.[235−239] Rhodamine-based compound

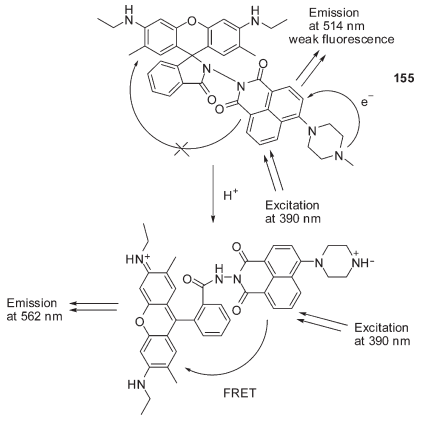

Figure 95. Schematic representation of the proposed energy transfer in **155** through the FRET mechanism.

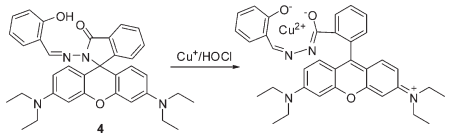

Figure 96. Proposed sensing mechanism of **4** toward HOCl in the presence of Cu^{+}.

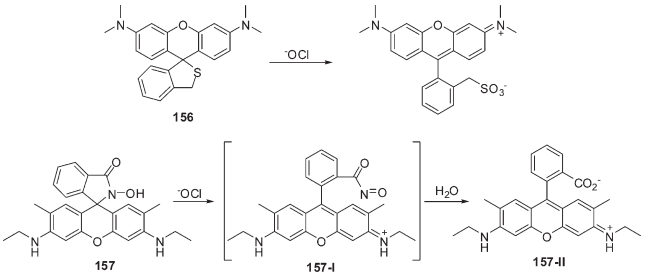

Figure 97. Proposed reaction mechanisms of **156** and **157** with $^{-}$OCl.

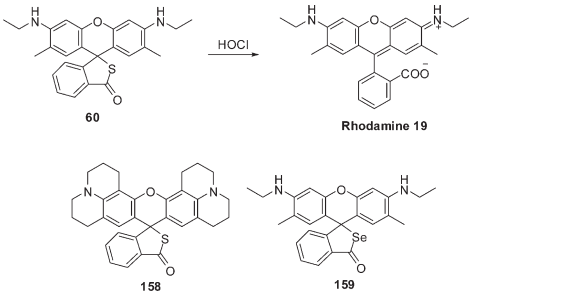

Figure 98. Proposed reaction mechanism of **60** with HOCl and structures of **158** and **159**.

4 has been reported as a good copper ion sensor with high sensitivity and selectivity by Tong et al.[33] However, Li and co-workers developed further HOCl-sensitive sensors by using the same compound in conjunction with cuprous ions (Figure 96).[240] In Tris−HCl (10 mM, pH 7.0) buffer containing 50% (v/v) CH_3CN, the solution containing compound **4** and cuprous ions was colorless in the presence of sodium ascorbate (as a stabilizer of cuprous ions). Upon addition of hypochlorite, a new absorption peak centered at 555 nm appeared, suggesting Cu^{2+}-induced ring-opening of the spirolactam form. The enhancement of absorption at 555 nm is proportional to the concentration of $^{-}$OCl in the range from 0 to 7.0×10^{-5} M with a detection limit as low as 8.1×10^{-7} M. Furthermore, the sensing system was demonstrated to be applicable in the detection of hypochlorites even in real water samples.

Nagano and co-workers prepared the tetramethylrhodamine-based fluorescent probe **156** for detecting hypochlorous acid with good selectivity (Figure 97).[241] Hypochlorous acid oxidized the thioether group in **156** to generate the corresponding sulfonate. This process leads to the opening of the spiroring system, resulting in a concomitant increase in fluorescence. Probe **156** also exhibits high tolerance to autoxidation and excellent selectivity for HOCl over other ROS/RNS. Importantly, findings arising from imaging experiments have demonstrated that **156** is useful in a system designed to visualize HOCl generation inside phagosomes in real time.

Tae and Shin's group have developed the rhodamine hydroxamic acid based fluorescent probe **157** for detection of $^{-}$OCl (Figure 97).[242] The hydroxamic acid group in this probe reacts with HOCl to form the ring-opened rhodamine derivatives **157-I** and **157-II**, which are highly fluorescent. In aqueous solutions, probe **157** displays a high selectivity for HOCl over other ROS/RNS, such as hydrogen peroxide, NO, hydroxyl radicals, peroxyl radicals, and superoxide radicals. A linear relationship between the fluorescence response of the probe and the concentrations of HOCl was observed in the range from 0 to 0.3 μM, and the detection limit was evaluated to be 25 nM. Bioimaging experiments were employed to show that this probe is useful for detecting HOCl in living cells and organisms.

Yoon and Lee et al. developed three rhodamine-based compounds, **60**, **158**, and **159**, as sensors for the detection of HOCl (Figure 98).[243] In KH_2PO_4 buffer (pH 5.5, 1% CH_3CN), adding 10 μM of HOCl to **60** resulted in an approximately 65-fold fluorescence increase, which was attributed to oxidant-mediated ring-opening through sulfur oxidation. Other ROS/RNS including H_2O_2, $NO^{\bullet}$, $^{\bullet}OH$, $ROO^{\bullet}$, $ONOO^{-}$, $^{1}O_2$, and $O_2^{\bullet-}$, induced little fluorescence enhancement. Similar results were also observed in the case of **158** with treatment with various ROS/RNS. In contrast, owing to the higher susceptibility of selenolactone than thiolactone, **159** showed less selectivity for HOCl compared to **60** and **158**. Furthermore, the fluorescence intensities of three rhodamine derivates were linearly proportional to the concentrations of HOCl in the range of 0−12 μM for **60**, 0−10 μM for **158** and 0−20 μM for **159**. The detection limits of the three sensors for HOCl were evaluated to be 0.4 μM for **60**, 0.6 μM for **158**, and 2 μM for **159**, respectively. Using **60** in conjunction with genetic analyses, bacteria-mediated microbicidal HOCl production can be visualized in the mucosal epithelia of fruit fly though DUOX enzymatic activity.

Ma and co-workers developed a rhodamine-based fluorescent probe, **160**, for detecting $^{-}$OCl (Figure 99).[244] When NaOCl was added to a $Na_2B_4O_7$−NaOH solution (pH 12, 0.03 M, 30% THF) containing **160**, the hydrazide moiety of the probe

dx.doi.org/10.1021/cr200201z |*Chem. Rev.* 2012, 112, 1910–1956

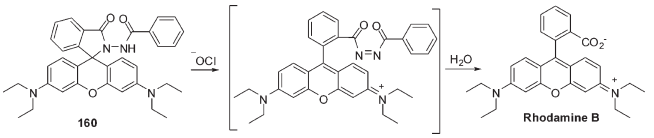

Figure 99. Proposed reaction mechanism of **160** with $^{-}$OCl.

was oxidized to form a diimide, which underwent further hydrolysis to produce strongly fluorescent rhodamine B. A good selectivity was observed for detecting $^{-}$OCl over other oxidants. The intensity in fluorescence is linearly dependent on the concentration of the $^{-}$OCl across the range from 1 to 10 μM with a detection limit of 27 nM.

A rhodamine-based probe, **161**, for detection of NO was recently developed by Xu and co-workers (Figure 100).[245] This probe is composed of a rhodamine B spirolactam as the fluorophore and an *o*-phenylenediamine as an NO-reactive group. Upon reaction of **161** with NO in the presence of oxygen, the amine group is converted to a diazonium group through an azotization reaction that leads to spiroring-opening to produce a rhodamine B acylbenzotriazole intermediate. Although this intermediate exhibits strong fluorescence emission in a way similar to that of rhodamine B, it undergoes further hydrolysis to generate rhodamine B and benzotriazole in aqueous solution. Therefore, **161**, which fluorescently detects the ROS via an induced spiroring-opening mechanism of a rhodamine spirolactam scaffold, selectively responds to NO in aqueous solutions over a wide pH range.

By masking a copper sensor, **162**, with a boronic ester, Franz developed a strategy for probing metal-mediated oxidative stress by fluorescence (Figure 101).[246] In organic solvents, high levels of hydrogen peroxide first trigger the deprotection of a boronic ester, releasing a Cu^{2+}-sensitive rhodamine derivative, **7**. The addition of Cu^{2+} and water further leads to opening of the ring of rhodamine, thus activating fluorescence. It is noted that the deprotection reaction of the arylboronic ester needs to be carried out in organic solvents. In aqueous solutions, the imide bond of the Shiff base in **162** will be hydrolyzed to produce fluorescein hydrazide **2**, which produces a greater increase in fluorescence emission due to formation of fluorescein upon interaction with Cu^{2+} or H_2O_2.

Various H_2O_2-specific fluorescent probes, which were based on the conversion of arylboronates to phenols induced by H_2O_2, have been developed by many groups. The group headed by Chang pioneered the H_2O_2-selective probe **163**,[247] which features two boronic ester groups at the 3′ and 6′ positions of a xanthene moiety (Figure 102). The initial sensor is nonfluorescent, however, upon addition of H_2O_2, the solution containing **163** results in the hydrolysis of the boronic ester groups and further leads to ring-opening of spirolactone fluorescein, producing strong fluorescence. This probe exhibits a >500-fold higher fluorescence response to H_2O_2 over other ROS/RNS, such as *tert*-butyl hydroperoxide, superoxide radicals, NO, and hypochlorite, has been applied to detect H_2O_2 within living cells. Conjugation with FRET mechanism, Wang and co-workers prepared a conjugated polymer-based sensing system that serves as a H_2O_2 sensor by combining PFP-NMe_3^+ and **163** (Figure 103).[248] In the absence of H_2O_2, the polymeric sensor exhibits blue fluorescence due to nonexistence of electrostatic interactions between the cationic PFP-NMe_3^+ and neutral **163**. However, upon

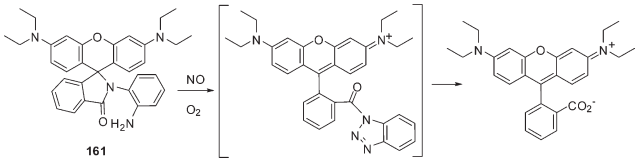

Figure 100. Proposed reaction mechanism of **161** with NO.

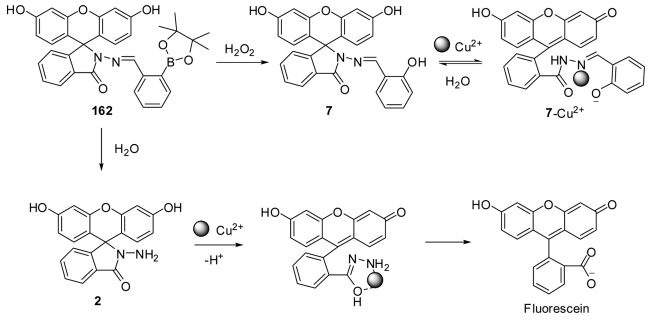

Figure 101. Proposed reaction mechanism of **162** with H_2O_2.

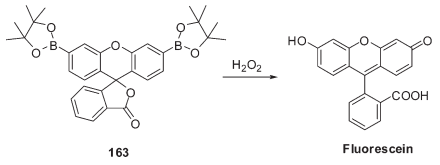

Figure 102. Fluorescence response of boronated probe **163** in the presence of H_2O_2.

addition of H_2O_2, the boronic ester groups in the polymer is hydrolyzed to produce anionic and ring-opening fluorescein which interact with PFP-NMe_3^+. In this state, due to the existence of overlap between the absorption band of fluorescein and the emission band of PFP-NMe_3^+, efficient FRET from PFP-NMe_3^+ to fluorescein takes place. By using the polymeric fluorescent probe, H_2O_2 in aqueous buffer can be detected in the range from 15 to 600 nM.

163 was further covalently conjugated to cationic polyfluorene for obtaining higher FRET efficiency, affording a new sensor **164** (Figure 103).[249] Similarly, in the absence of H_2O_2, **164** only exhibited a blue emission upon excitation of the fluorene chromophore. However, upon treatment with H_2O_2, the probe displayed green fluorescence because FRET from fluorene chromophore to fluorescein moiety occured. Furthermore, probe **164** enabled detecting H_2O_2 at concentrations ranging from 4.4 to 530 μM.

Using boronate-based fluorescein, Trogler and his co-workers prepared a polymeric film, **165** (Figure 104), that enable monitoring H_2O_2 in liquid or vapor phase.[250] The film showed little response under ambient conditions and UV light. However, upon exposure to even low concentrations of H_2O_2, it exhibited a large increase in fluorescence intensity. In addtion, the detection limit of **165** for H_2O_2 was determined to be as low as 3 ppb.

Five new monoboronate-based probes, **166-170**, were prepared by Chang's group, and their spectral properties and selective response to H_2O_2 were examined (Figure 104).[251]

dx.doi.org/10.1021/cr200201z |*Chem. Rev.* 2012, 112, 1910–1956

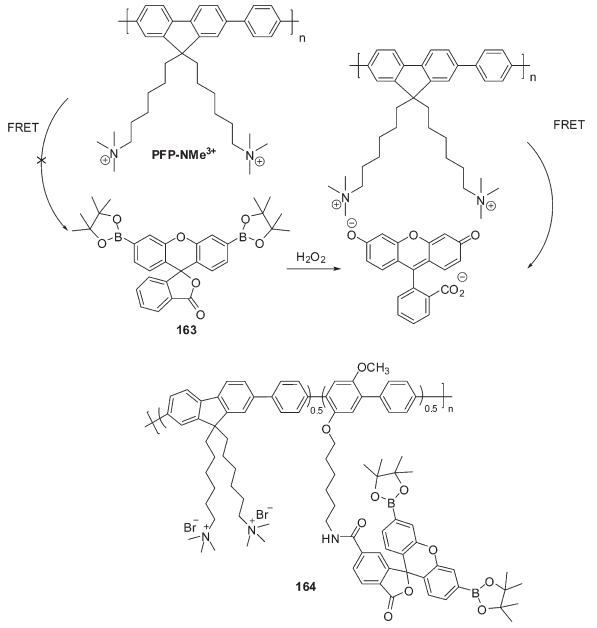

Figure 103. Conjugated polymer-based H_2O_2 sensing systems.

In aqueous buffer (pH 7), treating these probes with H_2O_2 resulted in marked increases in the fluorescence intensities with emission colors ranging from green to yellow to orange. In addition, all of these sensors showed high selectivity for H_2O_2 over other ROS/RNS. By imaging experiments, **167**, **169** and **170** were demonstrated that can be employed to detect the H_2O_2 produced in cells during immune response and growth factor stimulation. Moreover, using **170** and 3′-(*p*-aminophenyl) fluorescein (a $^{-}$OCl-selective probe), the dual-color imaging means enabled discrimination between changes in H_2O_2 and hypochlorite levels in macrophages.

On the basis of the FRET mechanism, Chang and co-workers developed the ratiometric fluorescent H_2O_2 sensor **171**, which contains a coumarin moiety as donor and a boronate-protected fluorescein as acceptor (Figure 105).[252] Sensor **171** itself showed blue donor emission upon excitation of the coumarin chromophore. However, upon addition of H_2O_2, the deprotection of boronic ester leads to the ring-opening of spirolactone. Furthermore, the intensity of the green fluorescence associated with the fluorescein acceptor increases via a FRET process when the donor coumarin is excited. The concentration changes of H_2O_2 are readily determined by measuring the ratio of the blue and green fluorescence intensities. This FRET-based probe shows high selectivity for H_2O_2 over other ROS. Further experiments with viable mitochondria indicated that **171** could be used to detect and quantify H_2O_2 produced endogenously in cells.

Maeda's group developed the highly specific fluorescent probe **172** for detection of $O_2^{\bullet-}$; the probe is based on a nonredox mechanism.[253] As shown in Figure 106, upon treatment with $O_2^{\bullet-}$ generated by the xanthine oxidase/hypoxanthine system or KO_2, the benzenesulfonate groups in **172** are removed, following a ring-opened process, resulting in the formation of strongly fluorescent **172-I**. Using enzymatic reactions of hypoxanthine and xanthine oxidase at 37 °C for 10 min in a 96-well microplate assay, this probe was demonstrated to be highly sensitive to $O_2^{\bullet-}$ with a detection limit of as low as 1.0 pmol/well.

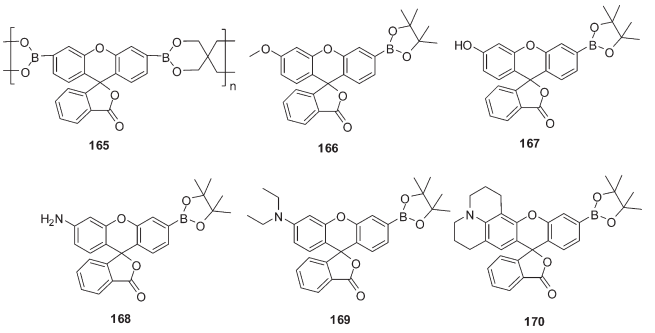

Figure 104. Structures of **165**−**170**.

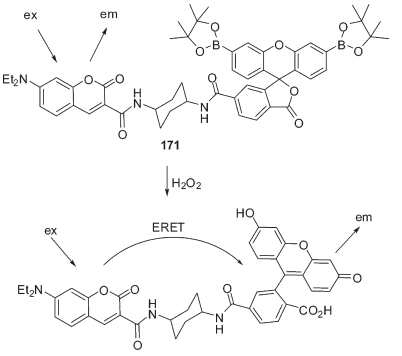

Figure 105. Proposed mechanism for the reaction of **171** with H_2O_2.

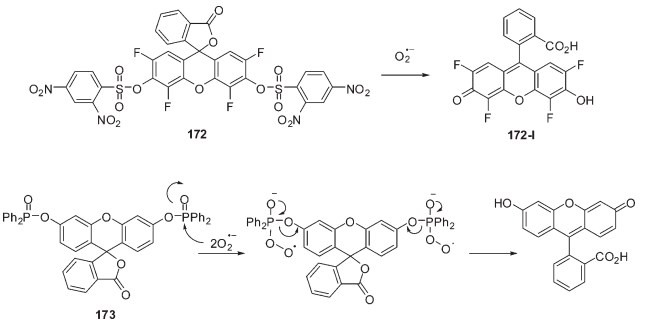

Figure 106. Proposed reaction mechanisms of probes **172** and **173** with $O_2^{\bullet-}$.

Tang and co-workers designed the fluorescent probe **173**, whose operation is based on the nucleophilic properties of $O_2^{\bullet-}$; the probe mediates deprotection of a diphenylphosphinate moiety, leading to ring-opening of spirolactone fluorescein (Figure 106).[254] In aqueous solution (pH 7.4), **173** displays high sensitivity with a detection limit of 4.6 pM. In addition, it has an excellent selectivity toward $O_2^{\bullet-}$ over other ROS/RNS and biologically relevant compounds, such as hydrogen peroxide, hypochlorite, singlet oxygen, *tert*-butyl peroxide radicals, 1,4-hydroquinone, hydroxyl radicals, peroxynitrite, glutathione, and NO. The results of fluorescence imaging experiments show that **173** can be used to detect micromolar changes in the concentration of $O_2^{\bullet-}$ in mouse peritoneal macrophages.

Peroxynitrite, produced by the reaction of nitric oxide with superoxide radicals, is a highly reactive oxidant that causes serious damage to living cells and is the cause of a series of human diseases.[255] Yang and co-workers designed the peroxynitrite-selective probe

dx.doi.org/10.1021/cr200201z |*Chem. Rev.* 2012, 112, 1910–1956

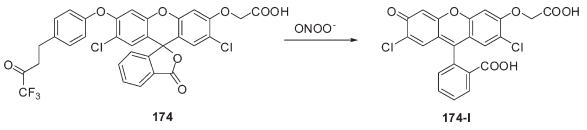

Figure 107. Proposed reaction mechanism of **174** with $ONOO^-$.

174, which contains a dichlorofluorescein moiety linked a ketone unit via an aryl ether spacer (Figure 107).[256] Upon reaction with peroxynitrite, the ketone group in **174** is oxidized to form a dioxirane intermediate, which subsequently undergoes a cleavage of the ether bond to afford the ring-opening product **174-I** with strong fluorescence. In aqueous buffer (pH 7.3), incubation this probe with 15 equiv of peroxynitrite induced a 7−8-fold increase in fluorescence intensity, whereas other ROS/RNS, including NO, $^1O_2$, $O_2^{\bullet-}$, and H_2O_2, only led to <1-fold increase, indicating that this probe is highly selective for peroxynitrite. In experiments using primary cultured neuronal cells, **174** was demonstrated to have potential for the detection of peroxynitrite in living cells.

6. SENSORS FOR DETECTING THIOLS

Intracellular thiols, such as cysteine (Cys), homocysteine (Hcy), and glutathione (GSH), play many crucial roles in physiological matrixes.[257] Generally, alterations in the level of these thiols have been linked to a number of diseases, such as leukocyte loss, psoriasis, liver damage, cancer, and AIDS.[258] Due to the biological importance of thiols, the development of optical probes for thiols has been an active research area in recent years.[4]

Using the chemosensing ensemble method, Yang et al. developed a thiol-selective sensing system using **4**−Cu^{2+} and rhodamine B (Figure 108).[259] In 40% ethanol aqueous solution at pH 7.1 in Tris−HCl buffer, **4**−Cu^{2+} itself is colorful but only weakly fluorescent due to the paramagnetic nature of Cu^{2+}. When rhodamine B was added to a solution containing **4**−Cu^{2+}, the fluorescence of rhodamine B was dramatically quenched due to the inner filter effect. Upon addition of cysteine to the above solution, the complexation of Cu^{2+} and cysteine led to the dissociation of **4**−Cu^{2+} accompanied by the cancellation of the inner filter effect, which induced an increase in the fluorescence of the sensing system. Except for Cys, Hcy, and GSH, other amino acids did not induce fluorescence recovery of the solution, indicating the high selectivity of this sensing system toward thiols. Furthermore, the detection limit for cysteine was determined to be 1.4×10^{-7} M^{-1}.

Yang and co-workers also reported a turn-on fluorescence sensing system, **175**, based on a rhodamine−Au−sugar for the recognition of thiol-containing amino acids (Figure 109).[260] In H_2O (CH_3OH, 1%), when **175** was treated with amino acids, only Cys and Hcy induced dramatic enhancements in fluorescence intensities, indicating the high selectivity of the **175**−Au^+ system. Furthermore, the 1:1 stoichiometry of binding between **175** and cysteine was found, and the association constant was calculated to be 6.65×10^3 M^{-1} from the UV titration. The fluorescence titration experiment exhibited that the detection limit for Cys is at the 100 nM level.

Peng and co-workers also reported a chemodosimeter, **176**, which can effectively discriminate Cys from Hcy and GSH in aqueous solution and living cells (Figure 110).[261] Probe **176** itself was weakly fluorescent in ethanol-PBS (0.1 M; pH = 7.00; 3 : 7, v/v) solution, however, when

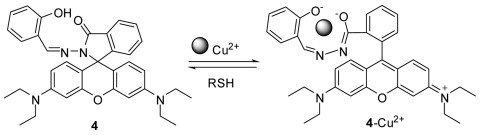

Figure 108. Schematic representation of thiol sensing by a **4**−Cu^{2+} ensemble.

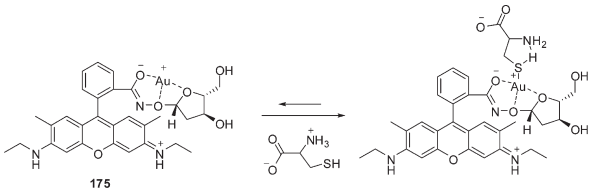

Figure 109. Proposed binding mode of **175** with Cys.

200 μM Cys was added to the solution containing **176**, a ca. 20-fold enhancement in fluorescent intensity at 531 nm was observed. The fluorescence intensity of **176** was linearly proportional to the amount of Cys added at micromolar levels and a detection limit of 73.5 nM was evaluated. The proposed mechanism for the specific selectivity for Cys over Hcy is illustrated in Figure 110. Upon addition of Cys to the colorless solution of **176**, thiazolidine **176-I** was first formed, followed by a ring-opening process and a hydrolysis reaction that led to the formation of rhodamine 19. The reactions induced strong fluorescence accompanied by a color change from colorless to pink. In the case of Hcy, **176-II** was colorless and nonfluorescent, which ensured the selectivity for Cys over Hcy. Furthermore, probe **176** was also successfully used in the quantitative estimation of levels of Cys in human urine.

Selective cleavage of the selenium−nitrogen bond by thiols was adopted for the design of thiol probes by Tang et al.[262] A rhodamine-based fluorescent probe, **177**, containing Se−N bonds displayed fluorescence enhancement with GSH in PBS (pH 7.4, 15 mM), which was induced by nucleophilic substitution of sulfhydryl (Figure 111). Upon addition of GSH, probe **177** showed a high signal-to-noise ratio (up to 170-fold) with a detection limit of 144 pM. The response time was within 5 min, and imaging of thiols was demonstrated using both HL-7702 cells and HepG2 cells.

Chmielewski et al. reported a rhodamine derivative, **178**, bearing two disulfide units, and this sensor displayed a large fluorescence enhancement upon reaction with cellular thiols such as GSH in vitro (Tris-HCl buffer, 80 mM, pH 8.0 at 37 °C) and in cyto (Figure 112).[263] The reduction of disulfide bonds by intracellular GSH revealed nucleophilic sulfhydryl groups that caused the breakdown of the neighboring carbamate bonds, leading to the formation of ring-opening rhodamine 110. After HeLa cells were incubated with **178**, strong fluorescence was exhibited inside the cells. However, when the cells were pretreated with *N*-ethylmaleimide, which is a trapping reagent of thiol species, a remarkable decrease in fluorescence intensity was observed, indicating the specific detection of thiols by **178**.

Abe et al. synthesized a 4-dinitrobenzenesulfonyl group with a rhodamine 110 derivative, **179**, as a fluorescent probe for biological thiols (Figure 113).[264] In Tris−HCl buffer (50 mM, pH 7.4),

dx.doi.org/10.1021/cr200201z |*Chem. Rev.* 2012, 112, 1910–1956

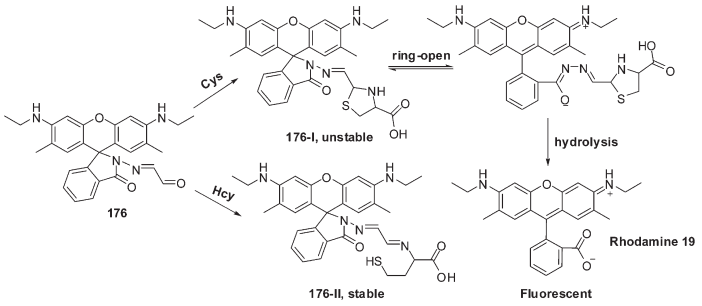

Figure 110. Proposed mechanisms of sensor **176** with Cys and Hcy.

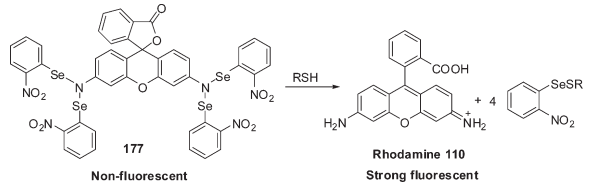

Figure 111. Proposed reaction mechanism of **177** with thiols.

after addition of Cys to the solution containing probe **179**, strong fluorescence at around 520 nm appeared and the emission intensity was enhanced by about 5800-fold with a detection limit of 100 μM. Usually mixtures of monodeprotected and fully deprotected rhodamine 110 were observed in different ratios depending on the thiol being detected. By confocal microscopy, a marked increase in fluorescence was observed when HeLa cells were treated with **179**, while no fluorescence appeared in cells pretreated with *N*-methylmaleimide and then incubated with **179**.

Yoon and Shin et al. reported a new fluorescein-based fluorescent probe, **180**, for the detection of thiol-containing molecules with high selectivity and sensitivity (Figure 114).[265] In HEPES buffer (20 mM, pH 7.4, 1% CH_3CN), addition of thiols such as Cys, Hcy, and GSH led to a 1,4-addition reaction of α,β-unsaturated ketone in the probe followed by the spiroring-opening of fluorescein. Concomitantly, a strong new emission peak at 520 nm and an enhancement of the fluorescence intensity were observed. By fluorescence titration experiments, the detection limits were estimated to be less than 50 nM for Cys, about 100 nM for Hcy, and 53 nM for GSH. When incubated with the probe, murine P19 embryonic carcinoma cells and a 3-day-old zebrafish showed significant fluorescence signals. In contrast, when cells and zebrafish were pretreated with the thiol blocking reagent *N*-methylmaleimide and then incubated with the probe in a similar manner, no fluorescence signal was observed. These results indicated that **180** can enter the cells and zebrafish and reacts with thiols to form the fluorescent product.

7. DETERMINATION OF ENZYME ACTIVITY USING XANTHENE DERIVATES

Dipeptidyl peptidase (DP IV), a serine protease, is involved in the cleavage of dipeptides from the N-terminus of oligo- and polypeptides,[266] the activation and proliferation of immune cells, and also HIV infection.[267] A highly fluorescent xanthene dye, rhodamine 110 (Rh 110), is used to synthesize the DP IV substrate, Gly(Ala)-Pro-Rh 110-R (**181a**−**181i**, Figure 115), where R is a reactive anchor group of varying length, hydrophobicity,

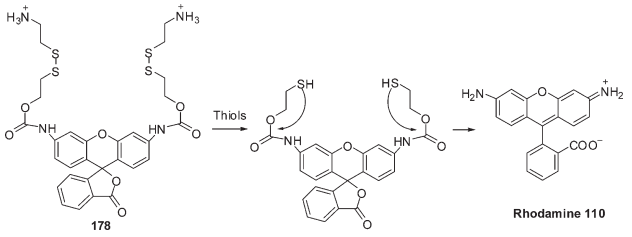

Figure 112. Mechanism of unmasking for **178** in the presence of thiols.

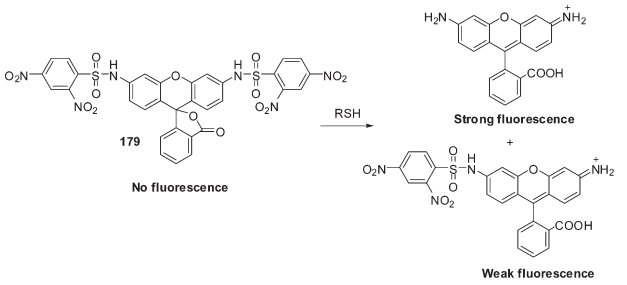

Figure 113. Proposed reaction mechanism of **179** with thiols.

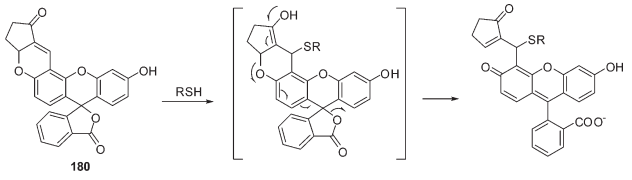

Figure 114. Proposed reaction mechanism of **180** with thiols.

and reactivity, which helps Rh 110 to bind on the cell surface.[268] The substrates are colorless and nonfluorescent; however, when they were hydrolyzed by DP IV, the products Rh 110-R, which exist as ring-opened forms, provide strong emission bands centered at 525 nm and absorption peaks at 467 and 494 nm (two peaks). Compounds **181a**−**181i** were hydrolyzed by isolated DP IV from pig kidney, with k_{cat}/K_M values between 1.14×10^6 and 3.33×10^6 M^{-1} s^{-1}, where k_{cat} and K_M are, respectively, the rate constant for the catalytic reaction and the Michaelis constant. The quantification of DP IV activity on single cells can be achieved.

Apoptosis is a normal physiological process, where programmed cell death occurs during embryonic development and tissue homeostasis and aging. Excessive apoptosis may cause

dx.doi.org/10.1021/cr200201z |*Chem. Rev.* 2012, 112, 1910–1956

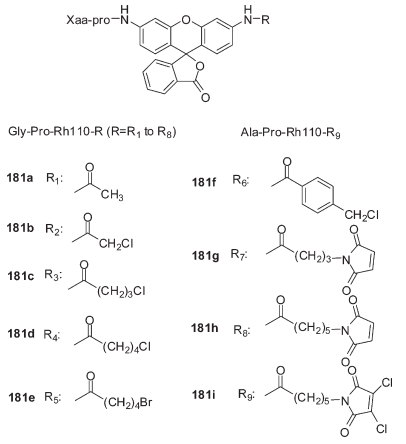

Figure 115. Structures of DP IV substrates Xaa-Pro-Rh 110-R (**181a**−**181i**).

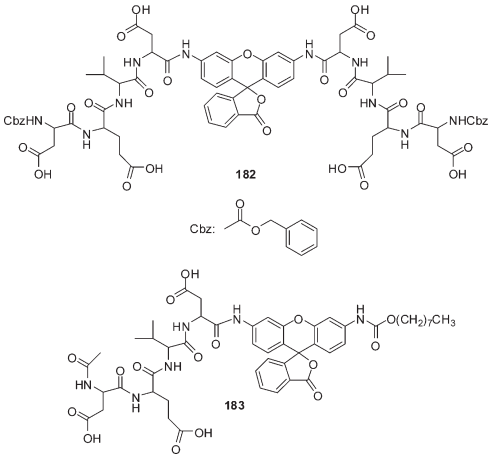

Figure 116. Structures of **182** and **183**.

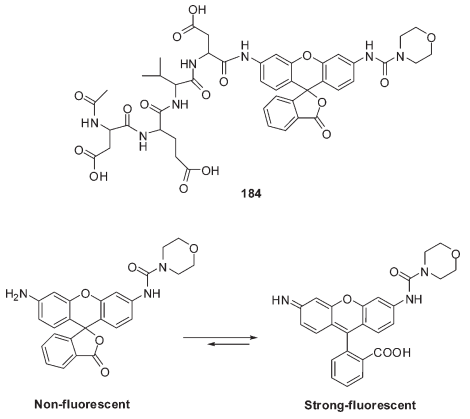

Figure 117. Structure of **184** and proposed mechanism for the fluorescence enhancement of *N*-MC-Rh 110.

congestive heart failure, liver failure, ischemic stroke, and neurodegenerative diseases, and insufficient apoptosis may cause cancer.[269,270] Apoptosis can be monitored by the activation of caspases, especially by caspase-3 in the caspase family. (Z-Asp-Glu-Val-Asp)$_2$-rhodamine 110 (**182**) has been developed as a fluorogenic substrate for the determination of casepase-3 activity (Figure 116).[271] Compound **182** is nonfluorescent but produces highly fluorescent Rh 110 upon cleavage of the Z-Asp-Glu-Val-Asp blocking groups of **182** by the caspase. Similarly, compound **183** has also been used as a caspase-3 substrate, which can be cleaved by human recombinant caspase-3 and lysates from apoptotic cells.

N-Ac-DEVD-*N*′-MC-Rh 110 (**184**) is a fluorogenic, cell-permeable caspase-3 substrate which cleaves in a single step.[272] Compared to other fluorogenic substrates, **184** has a higher enzyme turnover rate and sensitivity for detecting caspase-3 activity both in solution and in living cells. Compound **184** is nonfluorescent in buffer solution and shows strong fluorescence at about 525 nm due to the formation of *N*-morpholinecarbonyl-Rh 110 (*N*-MC-Rh 110) after cleavage by caspase-3 in aqueous solutions. *N*-MC-Rh 110 produces fluorescence due to the opening of its spirocyclic ring in aqueous solution, as shown in Figure 117.

A profluorophore or pig liver esterase (PLE) substrate, **185**,[273] shows near baseline excitation and emission in PBS. The introduction of PLE to a solution of **185** shows strong fluorescence that peaks at about 520 nm (excitation at 492 nm) with apparent kinetic parameters of $k_{cat}/K_M = 1.9 \times 10^3\ M^{-1}\ s^{-1}$. The trimethyl lock **185-I** is an *o*-hydroxycinnamic acid derivative in which unfavorable steric interactions between three methyl groups enhance the nucleophilicity of the phenolic oxygen and lead to lactonization, which results in the formation of hydrocoumarin **185-II**. Lactonization occurs in **185** in the presence of esterase, producing **185-II** and Rh 110 (open form) (Figure 118). HeLa cells incubated with **185** also display strong fluorescence, which can be observed in fluorescence microscopy.

DT diaphorase (DTD), a protective enzyme, can catalyze the two-electron reduction of various quinones, quinone epoxides, and aromatic nitro compounds, using NADH or NADPH as an electron donor.[274−276] The reduction of quinones by enzymes results in detoxification in living cells.[277,278] Huang and Lin have designed a DTD substrate, **186**,[279] which is constructed from quinone acid and Rh 110. Compound **186** is nonfluorescent in the rhodamine lactone form. In the presence of DTD and NADH (as a cofactor) the reduction of the quinine moiety in **186** occurs, producing highly reactive phenol, followed by rapid lactone formation with concomitant release of fluorescent rhodamine 110 (open form) (Figure 119). The apparent kinetic parameters, k_{cat}/K_M and K_M, determined for **186** with DTD, are, respectively, $2.35 \times 10^5\ M^{-1}\ s^{-1}$ and 26.8 μM.

Bioactive polymers are used for many purposes, such as in drug carriers,[280−283] as substrates for cell growth,[284−287] in therapeutics,[288−292] and in many other biological applications. Ring-opening metathesis polymerization can be used to generate biologically active polymers. Polymers bearing labels fluoresce only upon endocytosis and thus can provide information on the processes of internalization and trafficking. A trimethyl lock can be used to mask the fluorescence until esterases liberate the fluorophore from the labeled polymer. Dinitrophenyl (DNP)-substituted lysin has been conjugated to polymer backbones to convert polymers to antigens that can bind to DNP-specific B cell receptors. A rhodamine derivative condensed with a trimethyl lock derivative is attached to an azide-terminated polymer to obtain the profluorophores **187** or **188** (Figure 120). When polymer **187** is exposed to esterase (5 μM), the fluorophore is released with $k_{cat}/K_M = 5.8 \times 10^6\ M^{-1}\ s^{-1}$, which indicates that the fluorogenic label can be used to monitor cellular uptake processes of polymers that occur on the time scale of several minutes.[293]

dx.doi.org/10.1021/cr200201z |*Chem. Rev.* 2012, 112, 1910–1956

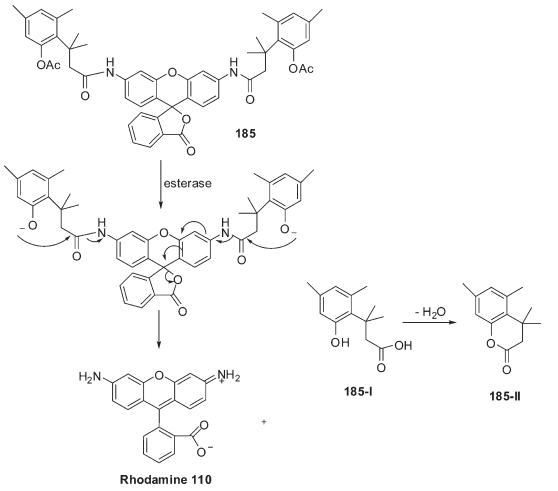

Figure 118. Schematic representation of the cleavage of **185** by esterase.

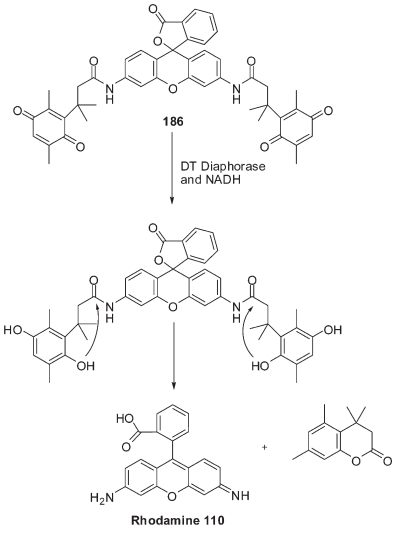

Figure 119. Schematic representation of the cleavage of **186** by DTD.

A Rh 110 based profluorophore, **189**,[294] has been reported for monitoring the activity of cytochrome P450 enzyme, which plays an important role in the metabolic activation of chemical carcinogens in human lungs.[295,296] Here the phenolic oxygen of the *o*-hydroxycinnamic acid has been modified in such a way that it can act as a substrate unit for the cytochrome P450 enzyme as well being attached to rhodamine dye by the condensation of its carboxyl group with the amine group of the rhodamine dye. The cleavage of the ether bond of the modified *o*-hydroxycinnamic acid unit in **189** by cytochrome P450 generates phenolic oxygen, which leads to rapid lactonization with concomitant release of the open form of rhodamine dye from the profluorophore **189** (Figure 121). In vitro, probe **189** releases a fluorescence when exposed to human isoenzyme with $k_{cat}/K_M = 8.8 \times 10^3\ M^{-1}\ s^{-1}$ and $K_M = 0.09\ \mu M$.

Cathepsin C, a lysosomal cysteine protease, is called dipeptidyl peptidase I. It functions as a homotetramer, with each subunit containing an N-terminal exclusion domain, a heavy chain harboring the catalytic Cys234, and a C-terminal light chain.

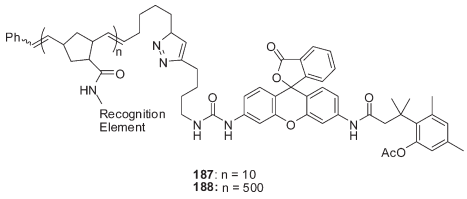

Figure 120. Structures of **187** and **188**.

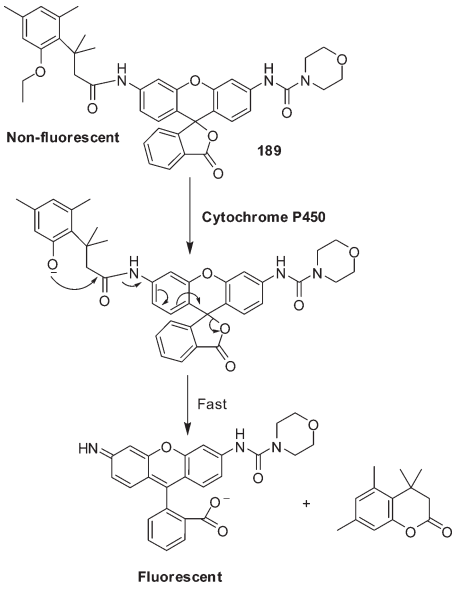

Figure 121. Schematic representation of the cleavage of **189** by cytochrome P450.

Rhodamine derivate **190** (Figure 122) is very reactive and selective for developing a flow cytometry assay to monitor the proteolytic activity of cathepsin C in living cells and has been tested using the B721 human B-lymphoblastoid cell line.[297]

Being a colorless and nonfluorescent probe in the spirolactam form, rhodamine B derivative **4** exhibits a color change from colorless to pink and a strong absorption peak at 555 nm upon addition of Cu^{2+} to its solutions; the pink color reverts to colorless upon addition of α-amino acids to the solution of the **4**$-Cu^{2+}$ complex.[298] The **4**$-Cu^{2+}$ complex is very sensitive and selective for α-amino acids over β- and γ-amino acids. As α-amino acids are produced by the hydrolysis of proteins in the presence of protease, protease can also be detected by this method. Bovine serum albumin (BSA) produces α-amino acids on hydrolysis catalyzed by trypsin, and the **4** $-Cu^{2+}-$BSA system can act as a trypsin sensor (Figure 123).

8. OTHER SENSORS BASED ON XANTHENES AND RELATED DERIVATES

8.1. Determination of Cytochrome *c*

Cytochrome *c*, which is located in the mitochondrial membrane, is a water-soluble protein that takes part in producing cellular energy. Measurement of cytochrome *c* helps to identify some diseases. Rhodamine B hydrazide (**1**), a colorless and nonfluorescent probe in the spirocyclic form, in sodium dodecylbenzenesulfonate (SDBS) surfactant micelles, has been used

dx.doi.org/10.1021/cr200201z |*Chem. Rev.* 2012, 112, 1910–1956

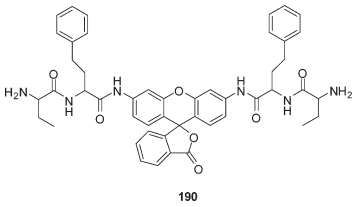

Figure 122. Structure of **190**.

for the determination of cytochrome *c*.[299] **1** is decomposed in SDBS micellar medium, which is catalyzed by cytochrome *c*, producing spiroring-opened rhodamine B, which changes the solution color to pink and gives strong fluorescence as well. The ring-opened form of rhodamine B shows a strong absorption peak at 556 nm and gives a fluorescence emission peak at 589 nm. The optimum conditions are achieved when the concentrations of SDBS and **1** are, respectively, 0.4 mM and 3.2 μM at pH 4. The dynamic range and detection limit for the determination of cytochrome *c* are respectively 4−120 and 0.87 ng mL^{-1}. The method is very selective for cytochrome *c* over other coexistent substances.

8.2. Detection of Nucleic Acids

Kool and Franzini have developed a scheme for the detection of nucleic acids, which is based on the delivery of a *p*-mercuriobenzoate (HgBA) group from one DNA strand to a fluorogenic, mercury-sensitive reagent, rhodamine B phenylthiosemicarbazide, attached to the second DNA strand (Figure 124).[300] The rhodamine unit in this system is nonfluorescent; however, the thiosemicarbazide functionality undergoes a cyclization reaction, producing oxadiazole, which triggers the opening of the rhodamine spirolactam ring, resulting in a large enhancement in the fluorescence. Incubation of 1 μM Rhops−DNA1 (the sequence is 5′-Rhops-$(CH_2)_3$-OPO_3^--TGT GGG CAA GAG T-3′) with 5 μM Hg−DNA1 (5′-CCG TCG G-OPO_3^--$(CH_2)_3$HgBA-3′, where HgBA = *p*-mercuriobenzamide) in the presence of a 1 μM concentration of the complementary template *mut AA* (15 h at 37 °C in 70 mM Tris−borate and 10 mM $MgCl_2$, pH 7) shows strong fluorescence (150-fold increase) that peaks at 600 nm when the system is excited at 530 nm. The sequence of *mut AA* is 5′-GCA *CTC TTG CCC ACA* AAC CGA CGG CG-3′, where italic letters indicate probe hybridization sites. An organomercury-functionalized DNA probe, which induces the fluorogenic unmasking of a rhodamine−phenylthiosemicarbazide−DNA conjugate in the presence of another DNA target strand, can be used as a fluorogenic reporter of the nucleic acid sequence in solution, and it would be capable of giving readable signals with single nucleotide discrimination in minutes.

8.3. Sensor for Detecting Organophosphate

Organophosphates, the active elements of nerve gas, can inhibit the activity of acetylcholinesterase, leading to neuromuscular paralysis and eventual death.[301] The development of a sensitive detection method for organophosphates has received great attention due to the considerations of public security. Recently, Han's group reported an organophosphate-sensitive sensor using rhodamine derivate **191** (Figure 125).[302] In DMF-containing triethylamine (3%, v/v), after incubation with diethyl chlorophosphate for 20 min, **191** displayed an enhancement in the fluorescence intensity at 590 nm with a colorimetric transformation from yellow to red, and the fluorescence response is

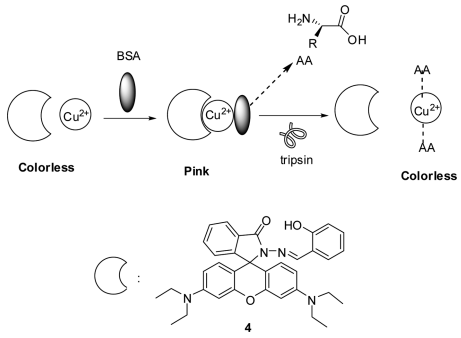

Figure 123. Schematic representation of the detection of trypsin.

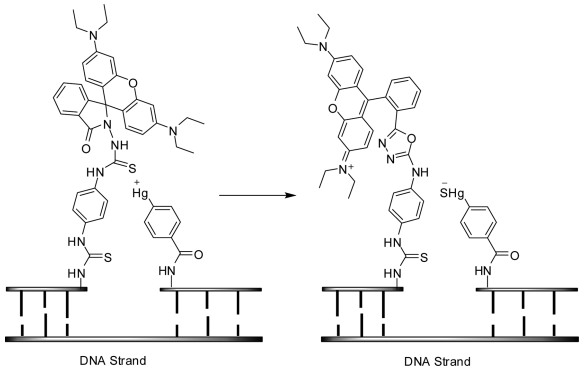

Figure 124. Schematic representation of the DNA-template activation of Rhops fluorescence by phenylmercury−DNA conjugates.

sensitive to levels of diethyl chlorophosphate as low as 25 ppm. The ring-opening process via a Lossen rearrangement was supported by high-resolution mass spectrometry.

8.4. Sensing Alcohols Using Xanthenes

Nagamura et al. have developed a method for sensing alcohol using the guided wave mode geometry, which is composed of low refractive index polymer (e.g., fluorocarbon polymer, Cytop) and dye-doped polymer (tricyclodecane polymer, ARTON) layers.[303] Rhodamine B has been used as a dye as it shows reversible changes in absorption and emission spectra in polar and nonpolar environments by a spirolactam ring-closing and -opening mechanism. The ethanol reacts with the lactone dye, rhodamine B, resulting in changes in the absorption and emission properties. Sensitive fluorescence intensity changes, as well as reflectance changes, with ethanol concentration, can be used for the detection of dilute ethanol with a detection limit on the order of parts per million and a rapid response time (<5 s) in the aqueous solution and gas phases.

Hydrotalcite (Ht), a clay material capable of anion exchange, has been used to prepare a hybrid material with rhodamine 6G as a vapor sensor for the detection of alcohol.[304] The spectral shape and fluorescence intensity of the Rh6G−Ht material remains almost the same either in vacuo or in air. When the material is exposed to alcohol vapor, the spectral shape, as well as fluorescence intensity, changes enormously. The fluorescence intensity decreases by about 80% compared to that in air. The removal of alcohol vapor recovers the spectral shape and intensity, indicating that the phenomenon is reversible. The fluorescence intensity decrease in the presence of alcohol vapors is specific over other

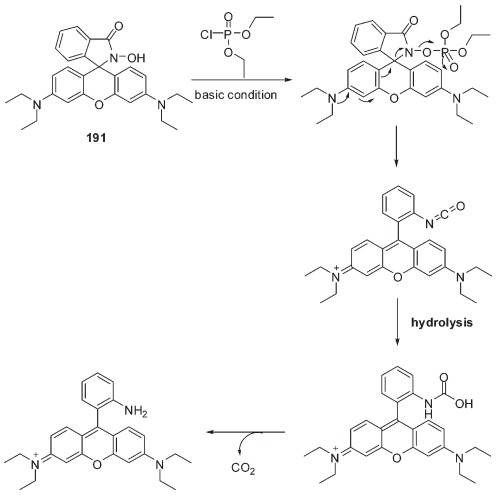

Figure 125. Proposed reaction mechanism for **191** in the presence of chlorophosphate.

solvents, such as acetonitrile, acetone, and benzene, as vapors from these solvents enhance fluorescence intensity.

1,2-Amino alcohol is a structural unit in many drugs and asymmetric catalysts.[305,306] The stereochemistry of 1,2-amino alcohols controls the catalytic activity in the catalysts, as well as the pharmaceutical activity in drugs. The equilibrium between the neutral rhodamine lactone and zwitterion forms is sensitive to its local microenvironment. Inspired by this mechanism, a fluorescence assay based on commercially available xanthene dyes, such as rhodamine B and fluorescein, which can distinguish diastereomeric 1,2-amino alcohols, such as ephedrine, pseudoephedrine, and methylephedrine, over a range of concentrations has been developed by Shimizu et al.[307] They proposed that the diastereoselectivity arises due to the differences in the strength of an intermolecular lone pair−π interaction within the analyte−rhodamine zwitterion complex (Figure 126). Another method, which is based on the mixture of rhodamine B and fluorescein, can detect the structure as well as being able to estimate the concentration of a 1,2-amino alcohol solution. The cationic ring-opened form of rhodamine B shows an emission band maximum at 587 nm in acetonitrile solutions when excited at 470 nm. A weak band that peaks at 565 nm, which appears in the presence of diastereomeric ephedrine or pseudoephedrine in acetonitrile solutions, is very sensitive to the structure of 1,2-amino alcohols. The differences in the emission intensity at 565 nm distinguish the various 1,2-aminophenols. Fluorescence of fluorescein turns on in the presence of base and shows an emission maximum at 535 nm when it is excited at 470 nm in acetonitrile, and the emission intensity increases with increasing concentration of 1,2-amino alcohols, for which both rhodamine B and fluorescein can be monitored simultaneously for detecting the structure as well as the concentrations of 1,2-aminophenols in solution.

8.5. Temperature Sensor Related to Rhodamine Derivate

Temperature, as an environmental condition, may change the structure as well as permeability of cell membranes. As temperature can affect various noncovalent bonds, such as hydrogen bonds, electrostatic interactions, and hydrophobic interactions, between amino acid residues within a protein and between a protein and a solvent, the structural and kinetic properties of proteins may change. High temperature may destroy the

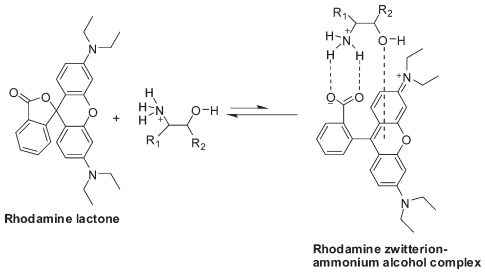

Figure 126. Proposed mechanism for the complex formation between 1,2-ammonium alcohols and rhodamine zwitterion.

proteins, which is called protein denaturation. Enzymes, which are also proteins, function most efficiently within a physiological temperature range. Any deviations from the normal temperature range may negatively affect many vital biochemical reactions in the cells.

N-Isopropylacrylamide (NIPAM) and rhodamine moieties can make a copolymer, poly(NIPAM-*co*-Rh), which can behave as a fluorescent thermometer in the temperature range of 25−35 °C in water.[308] Poly(NIPAM-*co*-Rh) in water shows a reversible phase transition, coil-to-globule, which is associated with the hydration or dehydration of the polymer chain by temperature variation. Increases in temperature enhance the hydrophobicity of the polymer chain and the size of the polymer particles, which in turn control the fluorescence properties of the rhodamine moiety. Rhodamine emits at around 540−640 nm. If the emission intensity is monitored at 571 nm against temperature, it is observed that the fluorescence intensity increases drastically after 25 °C and reaches a maximum at 33 °C. Above 33 °C the intensity decreases rapidly and becomes very low above 40 °C. In the temperature range of 10−25 °C, as supported by turbidity measurements and ^{1}H NMR analysis, the polymer exists in the coil state (nonfluorescent), and above 25 °C the polymer starts to be aggregated (globular formation, fluorescent) in aqueous solution (pH 2) (Figure 127). Fluorescence quenching above 33 °C is explained by considering the lowering of the incident light absorption by the rhodamine moiety due to strong polymer aggregation (size >143 μm).

8.6. Application of Ring-Opening Processes to Optically Controlled Ca^{2+} Chelator and Molecular Logic Gates

A spiroamidorhodamine derivative, **192**, containing 1,2-bis(*o*-aminophenoxy)ethane-*N*,*N*,*N*′,*N*′-tetraacetic acid (BAPTA) was developed as an optically controlled Ca^{2+} chelator by the Marriott group.[309] In a buffered solution (10 mM MOPS, 100 mM KCl, pH 7.2), with 312 nm UV light irradiation for 30 s, compound **192** underwent a ring-opening process to provide the red-colored and fluorescent isomer **192-I**, resulting in a decrease of the electron density of the BAPTA moiety. Correspondingly, the affinity of the open isomer for Ca^{2+} (K_d = 181 μM) was much lower than that of the closed form (K_d = 509 nm). Following thermal treatment, **192-I** can return to the closed state of **192**; thus, the affinity for Ca^{2+} is restored (Figure 128). By an optical-thermal switch, the process can be repeated for several cycles. Most importantly, the system also exhibited excellent selectivity for Ca^{2+} over Mg^{2+}, indicating its potential to mimic calcium oscillations and to monitor the release of Ca^{2+} in a biological sample.

Yoon, Park, and co-workers have constructed several molecular logic gates,[310] such as AND, XOR, and INHIBIT, in microfluidic

dx.doi.org/10.1021/cr200201z |*Chem. Rev.* 2012, 112, 1910–1956

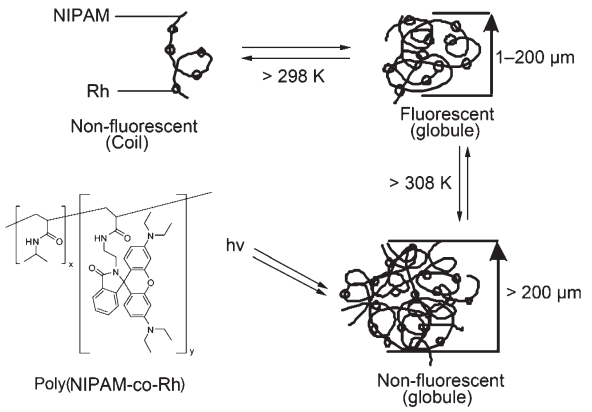

Figure 127. Schematic representation of the temperature-dependent changes in the structure of poly(NIPAM-*co*-Rh).

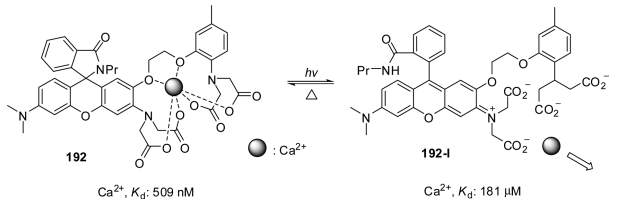

Figure 128. Photoreversible Ca^{2+} chelator **192**.

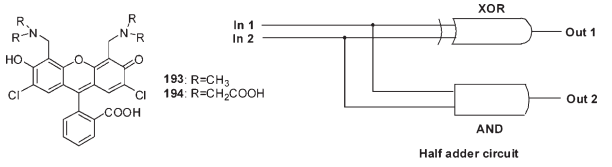

Input		Output	
In_1 (H^+)	In_2 (H^+)	XOR/Out_1 (green)	AND/Out_2 (red)
0	0	0 (low, 10.4)	0(low,12.1)
0	1	1(high,100)	0(low, 16.2)
1	0	1 (high, 100)	0 (low, 16.2)
1	1	0 (low, 21.6)	1 (high,100)

Figure 129. A half-adder circuit and a truth table of XOR and AND logic gates.

systems, which are based on fluorescent xanthene derivatives, such as fluorescein derivates (**193** and **194**) and a rhodamine derivative (**141**). These are then added to more advanced combinatorial circuits, such as half-adder (Figure 129). The inputs for the molecular logic gates are pH and metal ions, whereas the outputs are changes in the fluorescence intensity (intensity enhancement or quenching) (Figure 129, truth table). In a microfluidic device two or more fluids are mixed. Fluorescein derivative **193** is used for the XOR gate in the microfluidic device. Compound **193** shows a strong green fluorescence emission peak at 525 nm in the neutral range and a fluorescence quenching effect in the acidic and basic ranges. The fluorescence quenching of **193** at basic pH can be explained by considering PET from benzylic amine. Quenching in the acidic region is explained by considering the formation of a fluorescein cation. Rhodamine B derivative **141** shows strong red fluorescence at acidic pH and fluorescence quenching at neutral and basic pH, which may be due to spirolactam ring-opening (fluorescent) in the acidic region and ring-closing to spirolactam (nonfluorescent) in both neutral and basic regions. Thus, XOR and AND logic gates together make a half-adder, where the XOR logic gate produces a sum digit and the AND logic gate produces a carry digit. Another fluorescein derivative, **194**, similarly makes an INHIBIT logic gate, where the inputs are Cu^{2+} and OH^-.

9. CONCLUSIONS AND FUTURE PERSPECTIVES

Remarkable progress in the design and synthesis of fluorescent chemosensors based on various platforms has been made over the past several years. The approach of using spiroring-opening of xanthenes and related derivatives has provided a new strategy for the design of novel chemosensors. This review has dealt with xanthenes and related derivatives used as fluorescent reagents for sensing cations, anions, biological species, enzyme activity, etc., with a focus on the major mechanisms that control luminescence behavior, while many prospects for the utilization of sensors in biological imaging have been demonstrated. The modified xanthenes and related derivatives from the published literature mentioned in this review are indeed good candidates for selective responses to metal ions, anions, and biological species. For sensors derived from rhodamine B and rhodamine 6G, the modification of the molecules was most commonly concentrated on the N-terminus of spiroamide, which was linked to various receptors for targets of interest, such as metal ions, thiols, ROS/RNS, organophosphates, etc. A few sensors based on rhodamine thiolactone/selenolactone have also been explored. However, unlike spiroamide derivates, the further derivatization toward thiolactone/selenolactone is difficult owing to the natures of sulfur and selenium. In contrast, the transformation toward fluorescein and Rh 110 derivates placed emphasis on the hydroxyl or amino group on the ring of xanthene, in which the cleavage reaction induced by analytes led to the release of free phenol groups in fluorescein or free amino groups in Rh 110, resulting in the transformation of spirolactones to the open cycle form.

Though an increasing number of probes have been developed based on spiroring-opening of the xanthene platform, further developments in the design and fabrication of the sensing system with high sensitivity and selectivity are still desired. The incorporation of the xanthene platform and nanomaterials or polymers has provided opportunities for rapid and efficient detection of heavy-metal ions in the environment. In addition, by linking an additional fluorophore or quantum dots to the xanthene moiety, ratiometric sensing via the FRET approach can be built up. On the other hand, for exploring the biological application of xanthene derivatives, other factors should be considered in the design of probes for biological systems, such as high photostability, high quantum yield, good solubility in aqueous and lipid environments, good cell permeability, and low interference from biological environments. Besides, fluorescent probes that selectively respond to diverse analytes, such as volatile gases, explosive gases, and biologically relevant species, should be devised to expand the applications of xanthene derivatives.

AUTHOR INFORMATION

Corresponding Author

*Phone: 82-2-3277-2400 (J.Y.); 82-2-3290-3143 (J.S.K.). Fax: 82-2-3277-2384 (J.Y.); 82-2-3290-3121 (J.S.K.). E-mail: jyoon@ewha.ac.kr (J.Y.); jongskim@korea.ac.kr (J.S.K.).

BIOGRAPHIES

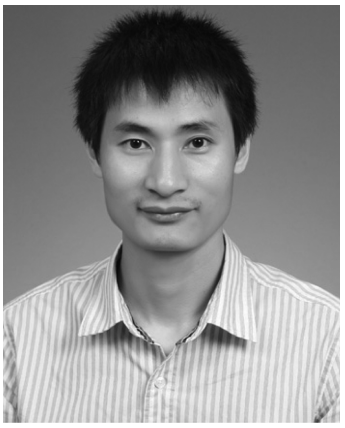

Xiaoqiang Chen was born in China in 1980. He received his Ph.D. in Applied Chemistry from the Dalian University of Technology (China) in 2007. In 2008, he joined Professor Yoon's group at Ewha Womans University (Korea) as a postdoctoral fellow. In March 2010, he moved to the Nanjing University of Technology (China). His current research interests mainly focus on fluorescent chemosensors.

Tuhin Pradhan completed his Ph.D. in Physical Chemistry in 2009 under the supervision of Professors Ranjit Biswas and Jaydeb Chakrabarti at the S. N. Bose National Centre for Basic Sciences (Jadavpur University, India). After nearly $1^1/_2$ years of postdoctoral research at the same institute, he joined the laboratory of Professor Jong Seung Kim at Korea University, Republic of Korea, as a Research Professor in 2010. His major interests are in time-resolved fluorescence spectroscopy, electrochemistry, computational photochemistry, nonlinear optical materials, and chemosensors in supramolecular chemistry.

Fang Wang was born in Jilin, China, in 1981. She obtained her B.S. degree in Chemical Engineering at YanBian University in 2005 and her M.S. degree in the College of Pharmacy, Kyung Hee University, in 2008. Subsequently, she joined Prof. Juyoung Yoon's group at Ewha Womans University as a Ph.D. student.

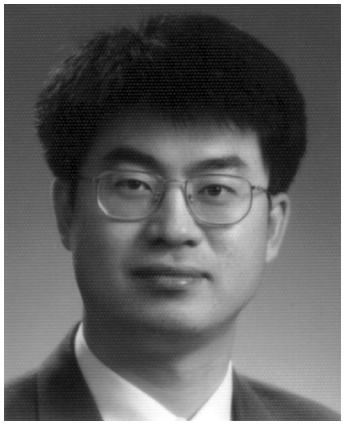

Jong Seung Kim was born in Daejon, Korea, in 1963. He received his Ph.D. from the Department of Chemistry and Biochemistry at Texas Tech University. After a 1 year postdoctoral fellowship at the University of Houston, he joined the faculty of Konyang University in 1994 and transferred to Dankook University in 2003. In 2007, he moved to the Department of Chemistry at Korea University in Seoul as a Professor. To date, his research has resulted in 260 scientific publications and 25 domestic and international patents.

Juyoung Yoon received his Ph.D. (1994) from The Ohio State University. After completing postdoctoral research at UCLA and at Scripps Research Institute, he joined the faculty at Silla University in 1998. In 2002, he moved to Ewha Womans University, where he is currently a Professor in the Departments of Chemistry and Nano Science and of Bioinspired Science. His research interests include investigations of fluorescent chemosensors, molecular recognition, and organo-EL materials.

ACKNOWLEDGMENT

J.Y. acknowledges the National Research Foundation (NRF; Grants 2011-0020450 and 2011-0001334) and WCU (Grant R31-2008-000-10010-0). J.S.K. acknowledges the CRI project (Grant 2010-0000728). X.C. acknowledges NSFY of China

(Grant 21002049). J.Y. and J.S.K. deeply thank previous and present group members.

ABBREVIATIONS

AD adamantyl
ADP adenosine diphosphate
AIDS acquired immunodeficiency syndrome
AMP adenosine monophosphate
ATP adenosine diphosphate
BAPTA 1,2-bis(*o*-aminophenoxy)ethane-*N*,*N*,*N*′,*N*′-tetraacetic acid
BODIPY boron dipyrromethene difluoride
BSA bovine serum albumin
β-CD *β*-cyclodextrin
CHEF chelation-enhanced fluorescence
Cys cysteine
DFT density functional theory
DNP dinitrophenyl
DNS dansyl
DP IV dipeptidyl peptidase
DPV differential pulse voltammetry
DUOX dual oxidase
DTD DT diaphorase
EDTA ethylenediaminetetraacetic acid
Em-FRET excimer fluorescence resonance energy transfer
ESI-MS electrospray-ionization mass spectrometry
FRET fluorescence resonance energy transfer
GSH glutathione
Hcy homocysteine
HEPES 4-(2-hydroxyethyl)-1-piperazineethanesulfonic acid
HgBA *p*-mercuriobenzoate
HOCl hypochlorous acid
Ht hydrotalcite
HTM heavy- and transition-metal
IR infrared radiation
MOPS 3-(*N*-morpholino)propanesulfonic acid
NADH nicotinamide adenine denucleotide reduced form
NADPH nicotinamide adenine denucleotide phosphate reduced form
NBD nitrobenzoxadiazolyl
NC nanocrystal
NIPAM *N*-isopropylacrylamide
NIR near-infrared
NMR nuclear magnetic resonance
PBS phosphate-buffered saline
PEG polyethylene glycol
PET photoinduced electron transfer
PFP poly(fluorene-*co*-phenylene)
PLE pig liver esterase
PPi pyrophosphate ion
PVA poly(vinyl alcohol)
Rh 110 rhodamine 110
RNS reactive nitrogen species
ROS reactive oxygen species
SDBS sodium dodecylbenzenesulfonate
TBET through-bond energy transfer
TMR tetramethylrhodamine
TPEF two-photon-excited fluorescence
Tris−HCl tris(hydroxymethyl)aminomethane hydrochloride
XPS X-ray photoelectron spectroscopy

REFERENCES

(1) Quang, D. T.; Kim, J. S. *Chem. Rev.* **2010**, *110*, 6280.
(2) Kim, J. S.; Quang, D. T. *Chem. Rev.* **2007**, *107*, 3780.
(3) Nolan, E. M.; Lippard, S. J. *Chem. Rev.* **2008**, *108*, 3443.
(4) Chen, X.; Zhou, Y.; Peng, X.; Yoon, J. *Chem. Soc. Rev.* **2010**, *39*, 2120.
(5) Zhou, Y.; Xu, Z.; Yoon, J. *Chem. Soc. Rev.* **2011**, *40*, 2222.
(6) Kim, H. N.; Guo, Z.; Zhu, W.; Yoon, J.; Tian, H. *Chem. Soc. Rev.* **2011**, *40*, 79.
(7) Xu, Z.; Kim, S. K.; Yoon, J. *Chem. Soc. Rev.* **2010**, *39*, 1457.
(8) Martinez-Manez, R; Sancenon, F. *Chem. Rev.* **2003**, *103*, 4419.
(9) de Silva, A. P.; Gunaratne, H. Q. N.; Gunnlaugsson, T.; Huxley, A. J. M.; McCoy, C. P.; Rademacher, J. T.; Rice, T. E. *Chem. Rev.* **1997**, *97*, 1515.
(10) Chen, X.; Tian, X.; Shin, I.; Yoon, J. *Chem. Soc. Rev.* **2011**, *40*, 4783.
(11) Butler, O. T.; Cook, J. M.; Harrington, C. F.; Hill, S. J.; Rieuwerts, J.; Miles, D. L. *J. Anal. At. Spectrom.* **2006**, *21*, 217.
(12) Li, Y.; Chen, C.; Li, B.; Sun, J.; Wang, J.; Gao, Y.; Zhao, Y.; Chai, Z. *J. Anal. At. Spectrom.* **2006**, *21*, 94.
(13) Leermakers, M.; Baeyens, W.; Quevauviller, P.; Horvat, M. *Trends Anal. Chem.* **2005**, *24*, 383.
(14) Czarnik, A. W. *Fluorescent Chemosensors for Ion and Molecule Recognition*; American Chemical Society: Washington, DC, 1992.
(15) Lakowicz, J. R. *Principles of Fluorescence Spectroscopy*; Plenum Press: New York, 1983.
(16) Lakowicz, J. R. Fluorescence spectroscopy of biomolecules. In *Encyclopedia of Molecular Biology and Molecular Medicine*; Meyers, R. A., Ed.; VCH Publishers: New York, 1995.
(17) Szmacinski, H.; Gryczynski, I.; Lakowicz, J. R. *Photochem. Photobiol.* **1993**, *58*, 341.
(18) Yanagida, T.; Ishii, Y. *Single Molecule Dynamics in Life Science*; Wiley-VCH: Weinheim, Germany, 2009.
(19) Duke, R. M.; Veale, E. B.; Pfeffer, F. M.; Kruger, P. E.; Gunnlaugsson, T. *Chem. Soc. Rev.* **2010**, *39*, 3936.
(20) Beija, M.; Afonso, C. A. M.; Martinho, J. M. G. *Chem. Soc. Rev.* **2009**, *38*, 2410.
(21) Noelting, E.; Dziewonsky, K. *Ber. Dtsch. Chem. Ges.* **1905**, *38*, 3516.
(22) Haugland, R. P. *Handbook of Fluorescent Probes and Research Chemicals*, 9th ed.; Molecular Probes: Eugene, OR, 2002.
(23) Amat-Guerri, F.; Costela, A.; Figuera, J. M.; Florido, F.; Sastre, R. *Chem. Phys. Lett.* **1993**, *209*, 352.
(24) Dujols, V.; Ford, F.; Czarnik, A. W. *J. Am. Chem. Soc.* **1997**, *119*, 7386.
(25) von Bayer, A. *Chem. Ber.* **1871**, *5*, 255.
(26) Gonçalves, M.; Sameiro, T. *Chem. Rev.* **2009**, *109*, 190.
(27) Kuo, Y.-M.; Zhou, B.; Cosco, D.; Gitschier, J. *Proc. Natl. Acad. Sci. U.S.A.* **2001**, *98*, 6836.
(28) Multhaup, G.; Schlicksupp, A.; Hesse, L.; Beher, D.; Ruppert, T.; Masters, C. L.; Beyreuther, K. *Science* **1996**, *271*, 1406.
(29) Lovstad, R. A. *BioMetals* **2004**, *17*, 111.
(30) Que, E. L.; Domaille, D. W.; Chang, C. J. *Chem. Rev.* **2008**, *108*, 1517.
(31) Chen, X.; Ma, H. *Anal. Chim. Acta* **2006**, *575*, 217.
(32) Xie, P.; Guo, F.; Li, D.; Liu, X.; Liu, L. *J. Lumin.* **2011**, *131*, 104.
(33) Xiang, Y.; Tong, A.; Jin, P.; Yong, J. *Org. Lett.* **2006**, *8*, 2863.
(34) Huo, F.-J.; Su, J.; Sun, Y.-Q.; Yin, C.-X.; Tong, H.-B.; Nie, Z.-X. *Dyes Pigm.* **2010**, *86*, 50.
(35) Xiang, Y.; Li, Z.; Chen, X.; Tong, A. *Talanta* **2008**, *74*, 1148.
(36) Chen, X.; Li, Z.; Xiang, Y.; Tong, A. *Tetrahedron Lett.* **2008**, *49*, 4697.
(37) Zhou, Y.; Wang, F.; Kim, Y.; Kim, S.; Yoon, J. *Org. Lett.* **2009**, *11*, 4442.
(38) Zhang, J. F.; Zhou, Y.; Yoon, J.; Kim, Y.; Kim, S. J.; Kim, J. S. *Org. Lett.* **2010**, *12*, 3852.
(39) Mei, L.; Xiang, Y.; Li, N.; Tong, A. *Talanta* **2007**, *72*, 1717.

(40) Yu, F.; Zhang, W.; Li, P.; Xing, Y.; Tong, L.; Ma, J.; Tang, B. *Analyst* **2009**, *134*, 1826.
(41) Zhao, Y.; Zhang, X.-B.; Han, Z.-X.; Qiao, L.; Li, C.-Y.; Jian, L.-X.; Shen, G.-L.; Yu, R.-Q. *Anal. Chem.* **2009**, *81*, 7022.
(42) Chen, X.; Jou, M. J.; Lee, H.; Kou, S.; Lim, J.; Nam, S.-W.; Park, S.; Kim, K.-M.; Yoon, J. *Sens. Actuators, B* **2009**, *B137*, 597.
(43) Swamy, K. M. K.; Ko, S.-K.; Kwon, S. K.; Lee, H. N.; Mao, C.; Kim, J.-M.; Lee, K.-H.; Kim, J.; Shin, I.; Yoon, J. *Chem. Commun.* **2008**, 5915.
(44) Yu, C.; Zhang, J.; Wang, R.; Chen, L. *Org. Biomol. Chem.* **2010**, *8*, 5277.
(45) Huang, L.; Chen, F.; Xi, P.; Xie, G.; Li, Z.; Shi, Y.; Xu, M.; Liu, H.; Ma, Z.; Bai, D.; Zeng, Z. *Dyes Pigm.* **2011**, *90*, 265.
(46) Zeng, X.; Dong, L.; Wu, C.; Mu, L.; Xue, S.-F.; Tao, Z. *Sens. Actuators, B* **2009**, *B141*, 506.
(47) Li, T.; Yang, Z.; Li, Y.; Liu, Z.; Qi, G.; Wang, B. *Dyes Pigm.* **2011**, *88*, 103.
(48) Xi, P.; Dou, J.; Huang, L.; Xu, M.; Chen, F.; Wu, Y.; Bai, D.; Li, W.; Zeng, Z. *Sens. Actuators, B* **2010**, *B148*, 337.
(49) Chen, X.; Jia, J.; Ma, H.; Wang, S.; Wang, X. *Anal. Chim. Acta* **2009**, *632*, 9.
(50) Tang, L.; Li, F.; Liu, M.; Nandhakumar, R. *Bull. Korean Chem. Soc.* **2010**, *31*, 3212.
(51) Xiang, Y.; Tong, A. *Luminescence* **2008**, *23*, 28.
(52) Zhang, X.; Shiraishi, Y.; Hirai, T. *Org. Lett.* **2007**, *9*, 5039.
(53) Kim, Y.-R.; Kim, H. J.; Kim, J. S.; Kim, H. *Adv. Mater.* **2008**, *20*, 4428.
(54) Lee, M. H.; Kim, H. J.; Yoon, S.; Park, N.; Kim, J. S. *Org. Lett.* **2008**, *10*, 213.
(55) He, G.; Zhang, X.; He, C.; Zhao, X.; Duan, C. *Tetrahedron* **2010**, *66*, 9762.
(56) Yu, M.; Shi, M.; Chen, Z.; Li, F.; Li, X.; Gao, Y.; Xu, J.; Yang, H.; Zhou, Z.; Yi, T.; Huang, C. *Chem.—Eur. J.* **2008**, *14*, 6892.
(57) Zhao, M.; Yang, X.-F.; He, S.; Wang, L. *Sens. Actuators, B* **2009**, *B135*, 625.
(58) Hua, Z.-Q.; Wang, X.-M.; Feng, Y.-C.; Ding, L.; Lu, H.-Y. *Dyes Pigm.* **2011**, *88*, 257.
(59) Valko, M.; Morris, H.; Cronin, M. T. D. *Curr. Med. Chem.* **2005**, *12*, 1161.
(60) Buettner, G. R.; Jurkiewicz, B. A. *Radiat. Res.* **1996**, *145*, 532.
(61) Chevion, M. *Free Radical Biol. Med.* **1988**, *5*, 27.
(62) Ruan, Y.-B.; Li, C.; Tang, J.; Xie, J. *Chem. Commun.* **2010**, *46*, 9220.
(63) Xie, X.; Li, X.; Ge, Y.; Qin, Y.; Chen, H.-Y. *Sens. Actuators, B* **2010**, *B151*, 71.
(64) *Mercury Update: Impact on Fish Advisories*; EPA Fact Sheet EPA-823-F-01-011; Office of Water, Environmental Protection Agency: Washington, DC, 2001.
(65) Kim, K. N.; Choi, M. G.; Noh, J. H.; Ahn, S.; Chang, S.-K. *Bull. Korean Chem. Soc.* **2008**, *29*, 571.
(66) Suresh, M.; Shrivastav, A.; Mishra, S.; Suresh, E.; Das, A. *Org. Lett.* **2008**, *10*, 3013.
(67) Kim, H. N.; Nam, S.-W.; Swamy, K. M. K.; Jin, Y.; Chen, X.; Kim, Y.; Kim, S.-J.; Park, S.; Yoon, J. *Analyst* **2011**, *136*, 1339.
(68) Huang, W.; Zhou, P.; Yan, W.; He, C.; Xiong, L.; Li, F.; Duan, C. *J. Environ. Monit.* **2009**, *11*, 330.
(69) Tang, L.; Li, F.; Liu, M.; Nandhakumar, R. *Spectrochim. Acta, Part A* **2011**, *78*, 1168.
(70) Wu, D.; Huang, W.; Duan, C.; Lin, Z.; Meng, Q. *Inorg. Chem.* **2007**, *46*, 1538.
(71) Wu, D.; Huang, W.; Lin, Z.; Duan, C.; He, C.; Wu, S.; Wang, D. *Inorg. Chem.* **2008**, *47*, 7190.
(72) Huang, W.; Wu, D.-Y.; Duan, C.-Y. *Inorg. Chem. Commun.* **2010**, *13*, 294.
(73) Yang, H.; Zhou, Z.; Huang, K.; Yu, M.; Li, F.; Yi, T.; Huang, C. *Org. Lett.* **2007**, *9*, 4729.
(74) Du, J.; Fan, J.; Peng, X.; Sun, P.; Wang, J.; Li, H.; Sun, S. *Org. Lett.* **2010**, *12*, 476.
(75) Shiraishi, Y.; Sumiya, S.; Kohno, Y.; Hirai, T. *J. Org. Chem.* **2008**, *73*, 8571.
(76) Kwon, S. K.; Kim, H. N.; Rho, J. H.; Swamy, K. M. K.; Shanthakumar, S. M.; Yoon, J. *Bull. Korean Chem. Soc.* **2009**, *30*, 719.
(77) Jana, A.; Kim, J. S.; Jung, H. S.; Bharadwaj, P. K. *Chem. Commun.* **2009**, 4417.
(78) Kim, S. K.; Swamy, K. M. K.; Chung, S.-Y.; Kim, H. N.; Kim, M. J.; Jeong, Y.; Yoon, J. *Tetrahedron Lett.* **2010**, *51*, 3286.
(79) Soh, J. H.; Swamy, K. M. K.; Kim, S. K.; Kim, S.; Lee, S.-H.; Yoon, J. *Tetrahedron Lett.* **2007**, *48*, 5966.
(80) Lee, M. H.; Wu, J.-S.; Lee, J. W.; Jung, J. H.; Kim, J. S. *Org. Lett.* **2007**, *9*, 2501.
(81) Bhalla, V.; Tejpal, R.; Kumar, M. *Sens. Actuators, B* **2010**, *151*, 180.
(82) Zhao, Y.; Sun, Y.; Lv, X.; Liu, Y.; Chen, M.; Guo, W. *Org. Biomol. Chem.* **2010**, *8*, 4143.
(83) Huang, J.; Xu, Y.; Qian, X. *J. Org. Chem.* **2009**, *74*, 2167.
(84) Shi, W.; Ma, H. *Chem. Commun.* **2008**, 1856.
(85) Zhan, X.-Q.; Qian, Z.-H.; Zheng, H.; Su, B.-Y.; Lan, Z.; Xu, J.-G. *Chem. Commun.* **2008**, 1859.
(86) Chen, X.; Nam, S.-W.; Jou, M. J.; Kim, Y.; Kim, S.-J.; Park, S.; Yoon, J. *Org. Lett.* **2008**, *10*, 5235.
(87) Huang, W.; Song, C.; He, C.; Lv, G.; Hu, X.; Zhu, X.; Duan, C. *Inorg. Chem.* **2009**, *48*, 5061.
(88) Huang, W.; Zhu, X.; Wua, D.; He, C.; Hu, X.; Duan, C. *Dalton Trans.* **2009**, 10457.
(89) Lin, W.; Cao, X.; Ding, Y.; Yuan, L.; Long, L. *Chem. Commun.* **2010**, *46*, 3529.
(90) Lin, W.; Cao, X.; Ding, Y.; Yuan, L.; Yu, Q. *Org. Biomol. Chem.* **2010**, *8*, 3618.
(91) Zhou, Y.; You, X.-Y.; Fang, Y.; Li, J.-Y.; Liu, K.; Yao, C. *Org. Biomol. Chem.* **2010**, *8*, 4819.
(92) Zheng, H.; Qian, Z.-H.; Xu, L.; Yuan, F.-F.; Lan, L.-D.; Xu, J.-G. *Org. Lett.* **2006**, *8*, 859.
(93) Ma, Q.-J.; Zhang, X.-B.; Zhao, X.-H.; Jin, Z.; Mao, G.-J.; Shen, G.-L.; Yu, R.-Q. *Anal. Chim. Acta* **2010**, *663*, 85.
(94) Lee, M. H.; Kang, G.; Kim, J. W.; Ham, S.; Kim, J. S. *Supramol. Chem.* **2009**, *21*, 135.
(95) Yang, Y.-K.; Yook, K.-J.; Tae, J. *J. Am. Chem. Soc.* **2005**, *127*, 16760.
(96) Ko, S.-K.; Yang, Y.-K.; Tae, J.; Shin, I. *J. Am. Chem. Soc.* **2006**, *128*, 14150.
(97) Yang, Y.-K.; Ko, S.-K.; Shin, I.; Tae, J. *Nat. Protoc.* **2007**, *2*, 1740.
(98) Gil, D. B.; Rodriguez-Cáceres, M. I.; Hurtado-Sánchez, M. D. C.; de la Peña, A. M. *Appl. Spectrosc.* **2010**, *64*, 520.
(99) Yang, X.-F.; Li, Y.; Bai, Q. *Anal. Chim. Acta* **2007**, *584*, 95.
(100) Page, L. E.; Zhang, X.; Jawaid, A. M.; Snee, P. T. *Chem. Commun.* **2011**, *47*, 7773.
(101) Zhang, J. F.; Lim, C. S.; Cho, B. R.; Kim, J. S. *Talanta* **2010**, *83*, 658.
(102) Wu, J. S.; Hwang, I. C.; Kim, K. S.; Kim, J. S. *Org. Lett.* **2007**, *9*, 907.
(103) Xi, P.-X.; Huang, L.; Liu, H.; Jia, P.-F.; Chen, F.-J.; Xu, M.; Zeng, Z.-Z. *J. Biol. Inorg. Chem.* **2009**, *14*, 815.
(104) Yuan, M.; Zhou, W.; Liu, X.; Zhu, M.; Li, J.; Yin, X.; Zheng, H.; Zuo, Z.; Ouyang, C.; Liu, H.; Li, Y.; Zhu, D. *J. Org. Chem.* **2008**, *73*, 5008.
(105) Othman, A. B.; Lee, J. W.; Wu, J.-S.; Kim, J. S.; Abidi, R.; Thuéry, P.; Strub, J. M.; Dorsselaer, A. V.; Vicens, J. *J. Org. Chem.* **2007**, *72*, 7634.
(106) Lee, Y. H.; Lee, M. H.; Zhang, J. F.; Kim, J. S. *J. Org. Chem.* **2010**, *75*, 7159.
(107) Fang, G.; Xu, M.; Zeng, F.; Wu, S. *Langmuir* **2010**, *26*, 17764.
(108) Zhang, X.; Xiao, Y.; Qian, X. *Angew. Chem., Int. Ed.* **2008**, *47*, 8025.
(109) Yu, H.; Xiao, Y.; Guo, H.; Qian, X. *Chem.—Eur. J.* **2011**, *17*, 3179.
(110) Suresh, M.; Mishra, S.; Mishra, S. K.; Suresh, E.; Mandal, A. K.; Shrivastav, A.; Das, A. *Org. Lett.* **2009**, *11*, 2740.

(111) Shang, G.-Q.; Gao, X.; Chen, M.-X.; Zheng, H.; Xu, J.-G. *J. Fluoresc.* **2008**, *18*, 1187.
(112) Zhu, M.; Zhou, C.; Zhao, Y.; Li, Y.; Liu, H.; Li, Y. *Macromol. Rapid Commun.* **2009**, *30*, 1339.
(113) Kumar, M.; Kumar, N.; Bhalla, V.; Singh, H.; Sharma, P. R.; Kaur, T. *Org. Lett.* **2011**, *13*, 1422.
(114) Ma, C.; Zeng, F.; Huang, L.; Wu, S. *J. Phys. Chem. B* **2011**, *115*, 874.
(115) John, G.; Mason, M.; Ajayan, P. M.; Dordick, J. S. *J. Am. Chem. Soc.* **2004**, *126*, 15012.
(116) Tran-Thi, T.-H.; Dagnelie, R.; Crunaire, S.; Nicole, L. *Chem. Soc. Rev.* **2011**, *40*, 621.
(117) Lee, M. H.; Lee, S. J.; Jung, J. H.; Lim, H.; Kim, J. S. *Tetrahedron* **2007**, *63*, 12087.
(118) Wang, C.; Tao, S.; Wei, W.; Meng, C.; Liu, F.; Han, M. *J. Mater. Chem.* **2010**, *20*, 4635.
(119) Zhou, P.; Meng, Q.; He, G.; Wu, H.; Duan, C.; Quan, X. *J. Environ. Monit.* **2009**, *11*, 648.
(120) Song, C.; Zhang, X.; Jia, C.; Zhou, P.; Quan, X.; Duan, C. *Talanta* **2010**, *81*, 643.
(121) Hu, J.; Li, C.; Liu, S. *Langmuir* **2010**, *26*, 724.
(122) Liu, H.; Yu, P.; Du, D.; He, C.; Qiu, B.; Chen, X.; Chen, G. *Talanta* **2010**, *81*, 433.
(123) *ATSDR, Toxicological Profile for Mercury*; U.S. Department of Health and Human Services: Atlanta, GA, 1999.
(124) Yang, Y.-K.; Ko, S.-K.; Shin, I.; Tae, J. *Org. Biomol. Chem.* **2009**, *7*, 4590.
(125) Chen, X.; Baek, K.-H.; Kim, Y.; Kim, S.-J.; Shin, I.; Yoon, J. *Tetrahedron* **2010**, *66*, 4016.
(126) Shi, W.; Sun, S.; Li, X.; Ma, H. *Inorg. Chem.* **2010**, *49*, 1206.
(127) Cuajungco, M. P.; Lees, G. J. *Neurobiol. Dis.* **1997**, *4*, 137.
(128) Choi, D. W.; Koh, J. Y. *Annu. Rev. Neurosci.* **1998**, *21*, 347.
(129) Weiss, J. H.; Sensi, S. L.; Koh, J. K. *Trends Pharmacol. Sci.* **2000**, *21*, 395.
(130) Suh, S. W.; Jensen, K. B.; Jensen, M. S.; Silva, D. S.; Kesslak, P. J.; Danscher, G.; Frederickson, C. J. *Brain Res.* **2000**, *852*, 274.
(131) Bush, A. I. *Alzheimer Dis. Assoc. Disord.* **2003**, *17*, 147.
(132) Mashraqui, S. H.; Khan, T.; Sundaram, S.; Betkar, R.; Chandiramani, M. *Chem. Lett.* **2009**, *38*, 730.
(133) Han, Z.-X.; Zhang, X.-B.; Li, Z.; Gong, Y.-J.; Wu, X.-Y.; Jin, Z.; He, C.-M.; Jian, L.-X.; Zhang, J.; Shen, G.-L.; Yu, R.-Q. *Anal. Chem.* **2010**, *82*, 3108.
(134) Sasaki, H.; Hanaoka, K.; Urano, Y.; Terai, T.; Nagano, T. *Bioorg. Med. Chem.* **2011**, *19*, 1072.
(135) Brugnara, C. *Clin. Chem.* **2003**, *49*, 1573.
(136) Beutler, E.; Felitti, V.; Gelbart, T.; Ho, N. *Drug Metab. Dispos.* **2001**, *29*, 495.
(137) Cairo, G.; Pietrangelo, A. *Biochem. J.* **2000**, *352*, 241.
(138) Xiang, Y.; Tong, A. *Org. Lett.* **2006**, *8*, 1549.
(139) Mao, J.; Wang, L.; Dou, W.; Tang, X.; Yan, Y.; Liu, W. *Org. Lett.* **2007**, *9*, 4567.
(140) Guerinot, M. L. *Annu. Rev. Microbiol.* **1994**, *48*, 743.
(141) Matzanke, B. F.; Müller-Matzanke, G.; Raymond, K. N. *Iron Carriers and Iron Proteins*; VCH: New York, 1989; Vol. 5, pp 1−121.
(142) Winkelmann, G.; van der Helm, D.; Neilands, J. B. *Iron Transport in Microbes, Plants and Animals*; VCH Verlagsgesellschaft mbH: Weinheim, Germany, 1987.
(143) Bae, S.; Tae, J. *Tetrahedron Lett.* **2007**, *48*, 5389.
(144) Zhang, X.; Shiraishi, Y.; Hirai, T. *Tetrahedron Lett.* **2007**, *48*, 5455.
(145) Zhang, L.; Fan, J.; Peng, X. *Spectrochim. Acta, Part A* **2009**, *73A*, 398.
(146) Moon, K.-S.; Yang, Y.-K.; Ji, S.-H.; Tae, J.-S. *Tetrahedron Lett.* **2010**, *51*, 3290.
(147) Lee, M. H.; Giap, T. V.; Kim, S. H.; Lee, Y. H.; Kang, C.; Kim, J. S. *Chem. Commun.* **2010**, *46*, 1407.
(148) Dong, L.; Wu, C.; Zeng, X.; Mu, L.; Xue, S.-F.; Tao, Z.; Zhang, J.-X. *Sens. Actuators, B* **2010**, *B145*, 433.
(149) Zhang, X.; Shiraishi, Y.; Hirai, T. *Tetrahedron Lett.* **2008**, *49*, 4178.
(150) Weerasinghe, A. J.; Schmiesing, C.; Varaganti, S.; Ramakrishna, G.; Sinn, E. *J. Phys. Chem. B* **2010**, *114*, 9413.
(151) Tang, L.; Li, Y.; Nandhakumar, R.; Qian, J. *Monatsh. Chem.* **2010**, *141*, 615.
(152) Gao, T.; Lee, K. M.; Heo, J.; Yang, S. I. *Bull. Korean Chem. Soc.* **2010**, *31*, 2100.
(153) Zheng, X. Y.; Zhang, W. J.; Mu, L.; Zeng, X.; Xue, S. F.; Tao, Z.; Yamatob, T. *J. Inclusion Phenom. Macrocyclic Chem.* **2010**, *68*, 139.
(154) Tang, L.; Li, Y.; Qian, J. *J. Chem. Res.* **2010**, *34*, 216.
(155) Xu, M.; Wu, S.; Zeng, F.; Yu, C. *Langmuir* **2010**, *26*, 4529.
(156) Ma, B.; Wu, S.; Zeng, F.; Luo, Y.; Zhao, J.; Tong, Z. *Nanotechnology* **2010**, *21*, 195501/1.
(157) Ma, B.; Wu, S.; Zeng, F. *Sens. Actuators, B* **2010**, *B145*, 451.
(158) Wang, B.; Hai, J.; Liu, Z.; Wang, Q.; Yang, Z.; Sun, S. *Angew. Chem., Int. Ed.* **2010**, *49*, 4576.
(159) Needleman, H. L. *Human Lead Exposure*; CRC Press: Boca Raton, FL, 1992.
(160) Kwon, J. Y.; Jang, Y. J.; Lee, Y. J.; Kim, K. M.; Seo, M. S.; Nam, W.; Yoon, J. *J. Am. Chem. Soc.* **2005**, *127*, 10107.
(161) Hu, Z.-Q.; Lin, C.-s.; Wang, X.-M.; Ding, L.; Cui, C.-L.; Liu, S.-F.; Lu, H. Y. *Chem. Commun.* **2010**, *46*, 3765.
(162) Arakawa, H.; Ahmad, R.; Naoui, M.; Tajmir-Riahi, H.-A. *J. Biol. Chem.* **2000**, *275*, 10150.
(163) Vincent, J. B. *Nutr. Rev.* **2000**, *58*, 67.
(164) Singh, A. K.; Gupta, V. K.; Gupta, B. *Anal. Clim. Acta* **2007**, *585*, 171.
(165) Weerasinghe, A. J.; Schmiesing, C.; Sinn, E. *Tetrahedron Lett.* **2009**, *50*, 6407.
(166) Huang, K.; Yang, H.; Zhou, Z.; Yu, M.; Li, F.; Gao, X.; Yi, T.; Huang, C. *Org. Lett.* **2008**, *10*, 2557.
(167) Zhou, Z.; Yu, M.; Yang, H.; Huang, K.; Li, F.; Yi, T.; Huang, C. *Chem. Commun.* **2008**, 3387.
(168) Wan, Y.; Guo, Q.; Wang, X.; Xia, A. *Anal. Chim. Acta* **2010**, *665*, 215.
(169) Hodge, V. F.; Stallard, M. O. *Environ. Sci. Technol.* **1986**, *20*, 1058.
(170) Liu, T. Z.; Lee, S. D.; Bhatnagar, R. S. *Toxicol. Lett.* **1979**, *4*, 469.
(171) Wataha, J. C.; Hanks, C. T. *J. Oral Rehabil.* **1996**, *23*, 309.
(172) Goodman, C. M.; McCusker, C. D.; Yilmaz, T.; Rotello, V. M. *Bioconjugate Chem.* **2004**, *15*, 897.
(173) Habib, A.; Tabata, M. *J. Inorg. Biochem.* **2004**, *98*, 1696.
(174) Nyarko, E.; Hara, T.; Grab, D. J.; Habib, A.; Kim, Y.; Nikolskaia, O.; Fukuma, T.; Tabata, M. *Chem.-Biol. Interact.* **2004**, *148*, 19.
(175) Ratte, H. T. *Environ. Toxicol. Chem.* **1999**, *18*, 89.
(176) Schiller, J. H.; Bittner, G. *Clin. Cancer Res.* **1999**, *5*, 4287.
(177) *International Programme on Chemical Safety. Palladium*; Environmental Health Criteria Series 226; World Health Organization: Geneva, Switzerland, 2002.
(178) Chatterjee, A.; Santra, M.; Won, N.; Kim, S.; Kim, J. K.; Kim, S. B.; Ahn, K. H. *J. Am. Chem. Soc.* **2009**, *131*, 2040.
(179) Jou, M. J.; Chen, X.; Swamy, K. M. K.; Kim, H.; N.; Kim, H.-J.; Lee, S,-g.; Yoon, J. *Chem. Commun.* **2009**, 7218.
(180) Egorova, O. A.; Seo, H.; Chatterjee, A.; Ahn, K. H. *Org. Lett.* **2010**, *12*, 401.
(181) Yang, Y.-K.; Lee, S.; Tae, J. *Org. Lett.* **2009**, *11*, 5610.
(182) Yuan, L.; Lin, W.; Yang, Y. *Chem. Commun.* **2011**, *47*, 6275.
(183) Li, H.; Fan, J.; Du, J.; Guo, K.; Sun, S.; Liu, X.; Peng, X. *Chem. Commun.* **2010**, *46*, 1079.
(184) Li, H.; Fan, J.; Song, F.; Zhu, H.; Du, J.; Sun, S.; Peng, X. *Chem.—Eur. J.* **2010**, *16*, 12349.
(185) Jun, M. E.; Ahn, K. H. *Org. Lett.* **2010**, *12*, 2790.
(186) Kim, H.; Lee, S.; Lee, J.; Tae, J. *Org. Lett.* **2010**, *12*, 5342.
(187) Albrecht, M.; Osetska, O.; Frohlich, R.; Bünzli, J.-C. G.; Aebischer, A.; Gumy, F.; Hamacek, J. *J. Am. Chem. Soc.* **2007**, *129*, 14178.

(188) Banerjee, S.; Huebner, L.; Romanelli, M. D.; Kumar, G. A.; Riman, R. E.; Emge, T. J.; Brennan, J. G. *J. Am. Chem. Soc.* **2005**, *127*, 15900.
(189) Pope, S. J. A.; Coe, B. J.; Faulkner, S.; Bichenkova, E. V.; Yu, X.; Douglas, K. T. *J. Am. Chem. Soc.* **2004**, *126*, 9490.
(190) Imbert, D.; Cantuel, M.; Unzli, J. C. G. B.; Bernardinelli, G.; Piguet, C. *J. Am. Chem. Soc.* **2003**, *125*, 15698.
(191) Unzli, J. C. G. B. *Acc. Chem. Res.* **2006**, *39*, 53.
(192) Unzli, J. C. G. B.; Piguet, C. *Chem. Soc. Rev.* **2005**, *34*, 1048.
(193) Ward, M. D. *Coord. Chem. Rev.* **2007**, *251*, 1663.
(194) Wong, K. L.; Wok, W. M. K.; Wong, W. T.; Phillips, D. L.; Cheah, K. W. *Angew. Chem., Int. Ed.* **2004**, *43*, 4659.
(195) Huang, W.; Wu, D.; Guo, D.; Zhu, X.; He, C.; Meng, Q.; Duan, C. *Dalton Trans.* **2009**, 2081.
(196) Wu, C.; Zhang, W.-J.; Zeng, X.; Mu, L.; Xue, S.-F.; Tao, Z.; Yamato, T. *J. Inclusion Phenom. Macrocyclic Chem.* **2010**, *66*, 125.
(197) Lou, X.; Qiang, L.; Qin, J.; Li, Z. *ACS Appl. Mater. Interfaces* **2009**, *1*, 2529.
(198) Mathews, C. P.; van Hold, K. E. *Biochemistry*, The Benjamin/Cummings Publishing Co., Inc.: Redwood City, CA, 1990.
(199) Ronaghi, M.; Karamohamed, S.; Pettersson, B.; Uhlen, M.; Nyren, P. *Anal. Biochem.* **1996**, *242*, 84.
(200) Xu, S.; He, M.; Yu, H.; Cai, X.; Tan, X.; Lu, B.; Shu, B. *Anal. Biochem.* **2001**, *299*, 188.
(201) Vance, D. H.; Czarnik, A. W. *J. Am. Chem. Soc.* **1994**, *116*, 9397.
(202) Mizukami, S.; Nagano, T.; Urano, Y.; Odani, A.; Kikuchi, K. *J. Am. Chem. Soc.* **2002**, *124*, 3920.
(203) Lee, J. H.; Park, J.; Lah, M. S.; Chin, J.; Hong, J. I. *Org. Lett.* **2007**, *9*, 3729.
(204) Lee, D. H.; Kim, S. Y.; Hong, J. I. *Angew. Chem., Int. Ed.* **2004**, *43*, 4777.
(205) Cho, H. K.; Lee, D. H.; Hong, J. I. *Chem. Commun.* **2005**, 1690.
(206) Fabbrizzi, L.; Marcotte, N.; Stomeo, F.; Taglietti, A. *Angew. Chem., Int. Ed.* **2002**, *41*, 3811.
(207) Lee, H. N.; Swamy, K. M. K.; Kim, S. K.; Kwon, J. Y.; Kim, Y.; Kim, S. J.; Yoon, Y. J.; Yoon, J. *Org. Lett.* **2007**, *9*, 243.
(208) Kim, S. Y.; Hong, J. I. *Tetrahedron Lett.* **2009**, *50*, 1951.
(209) Lee, H. N.; Xu, Z.; Kim, S. K.; Swamy, K. M. K.; Kim, Y.; Kim, S. J.; Yoon, J. *J. Am. Chem. Soc.* **2007**, *129*, 3828.
(210) Zhao, X.; Liu, Y.; Schanze, K. S. *Chem. Commun.* **2007**, 2914.
(211) Aldakov, D.; Anzenbacher, P., Jr. *J. Am. Chem. Soc.* **2004**, *126*, 4752.
(212) Kim, S. K.; Lee, D. H.; Hong, J. I.; Yoon, J. *Acc. Chem. Res.* **2009**, *42*, 23.
(213) Lee, D. H.; Im, J. H.; Son, S. U.; Chung, Y. K.; Hong, J. I. *J. Am. Chem. Soc.* **2003**, *125*, 7752.
(214) Lohani, C. R.; Kim, J.-M.; Chung, S.-Y.; Yoon, J.; Lee, K.-H. *Analyst* **2010**, *135*, 2079.
(215) Wu, J.-S.; Kim, H. J.; Lee, M. H.; Yoon, J. H.; Lee, J. H.; Kim, J. S. *Tetrahedron Lett.* **2007**, *48*, 3159.
(216) Kaewtong, C.; Noiseephum, J.; Uppa, Y.; Morakot, N.; Morakot, N.; Wanno, B.; Tuntulani, T.; Pulpoka, B. *New J. Chem.* **2010**, *34*, 1104.
(217) Hu, Z. Q.; Wang, X. M.; Feng, Y. C.; Ding, L.; Li, M.; Lin, C .S. *Chem. Commun.* **2011**, *47*, 1622.
(218) Martinez-Zaguilln, R.; Gillies, R. J. *Cell Physiol. Biochem.* **1996**, *6*, 169.
(219) Shimizu, Y.; Hunt, S. W. *Immunol. Today* **1996**, *17*, 565.
(220) Falke, J. J.; Bass, R. B.; Butler, S. L.; Chervitz, S. A.; Danielson, M. A. *Annu. Rev. Cell Dev. Biol.* **1997**, *13*, 457.
(221) Okamoto, C. T. *Adv. Drug Delivery Rev.* **1998**, *29*, 215.
(222) Satoh, H.; Hayashi, H.; Katoh, H.; Terada, H.; Kobayashi, A. *Am. J. Physiol.* **1995**, *268*, H1239.
(223) Kogot-Levin, A.; Zeigler, M.; Ornoy, A.; Bach, G. *Pediatr. Res.* **2009**, *65*, 686.
(224) Poschet, J.; Perkett, E.; Deretic, V. *Trends Mol. Med.* **2002**, *8*, 512.
(225) Zhang, W.; Tang, B.; Liu, X.; Liu, Y.; Xu, K.; Ma, J.; Tong, L.; Yang, G. *Analyst* **2009**, *134*, 367.
(226) Kang, S.; Kim, S.; Yang, Y.-K.; Bae, S.; Tae, J. *Tetrahedron Lett.* **2009**, *50*, 2010.
(227) Hasegawa, T.; Kondo, Y.; Koizumi, Y.; Sugiyama, T.; Takeda, A.; Ito, S.; Hamada, F. *Bioorg. Med. Chem.* **2009**, *17*, 6015.
(228) Best, Q. A.; Xu, R.; McCarroll, M. E.; Wang, L.; Dyer, D. J. *Org. Lett.* **2010**, *12*, 3219.
(229) Bojinov, V. B.; Venkova, A. I.; Georgiev, N. I. *Sens. Actuators, B* **2009**, *B143*, 42.
(230) Nathan, C. *J. Clin. Invest.* **2003**, *111*, 769.
(231) Yang, X.-F.; Guo, X.-Q.; Zhao, Y.-B. *Talanta* **2002**, *57*, 883.
(232) Rieth, T.; Sasamoto, K. *Anal. Commun.* **1998**, *35*, 195.
(233) Hampton, M. B.; Kettle, A. J.; Winterbourn, C. C. *Blood* **1998**, *92*, 3007.
(234) Winterbourn, C. C.; Hampton, M. B.; Livesey, J. H.; Kettle, A. J. *J. Biol. Chem.* **2006**, *281*, 39860.
(235) Andersen, J. K. *Nat. Med. (Suppl.)* **2004**, S18.
(236) Sugiyama, S.; Okada, Y.; Sukhova, G. K.; Virmani, R.; Heinecke, J. W.; Libby, P. *Am. J. Pathol.* **2001**, *158*, 879.
(237) Hazell, L. J.; Arnold, L.; Flowers, D.; Waeg, G.; Malle, E.; Stocker, R. *J. Clin. Invest.* **1996**, *97*, 1535.
(238) Pattison, D. I.; Davies, M. J. *Curr. Med. Chem.* **2006**, *13*, 3271.
(239) Winterbourn, C. C.; Kettle, A. J. *Free. Radical Biol. Med.* **2000**, *29*, 403.
(240) Lou, X.; Zhang, Y.; Li, Q.; Qin, J.; Li, Z. *Chem. Commun.* **2011**, *47*, 3189.
(241) Kenmoku, S.; Urano, Y.; Kojima, H.; Nagano, T. *J. Am. Chem. Soc.* **2007**, *129*, 7313.
(242) Yang, Y.-K.; Cho, H. J.; Lee, J.; Shin, I.; Tae, J. *Org. Lett.* **2009**, *11*, 859.
(243) Chen, X.; Lee, K.-A.; Ha, E.-M.; Lee, K. M.; Seo, Y. Y.; Choi, H. K.; Kim, H. N.; Kim, M. J.; Cho, C.-S.; Lee, S. Y.; Lee, W. J. *Chem. Commun.* **2011**, 4373.
(244) Chen, X.; Wang, X.; Wang, S.; Shi, W.; Wang, K.; Ma, H. *Chem.—Eur. J.* **2008**, *14*, 4719.
(245) Zheng, H.; Shang, G.-Q.; Yang, S.-Y.; Gao, X.; Xu, J.-G. *Org. Lett.* **2008**, *10*, 2357.
(246) Hyman, L. M.; Stephenson, C. J.; Dickens, M. G.; Shimizub, K. D.; Franz, K. J. *Dalton Trans.* **2010**, *39*, 568.
(247) Chang, M. C. Y.; Pralle, A.; Isacoff, E. Y.; Chang, C. J. *J. Am. Chem. Soc.* **2004**, *126*, 15392.
(248) He, F.; Tang, Y.; Yu, M.; Wang, S.; Li, Y.; Zhu, D. *Adv. Funct. Mater.* **2006**, *16*, 91.
(249) He, F.; Feng, F.; Wang, S.; Li, Y.; Zhu, D. *J. Mater. Chem.* **2007**, *17*, 3702.
(250) Sanchez, J. C.; Trogler, W. C. *J. Mater. Chem.* **2008**, *18*, 5134.
(251) Dickinson, B. C.; Huynh, C.; Chang, C. J. *J. Am. Chem. Soc.* **2010**, *132*, 5906.
(252) Albers, A. E.; Okreglak, V. S.; Chang, C. J. *J. Am. Chem. Soc.* **2006**, *128*, 9640.
(253) Maeda, H.; Yamamoto, K.; Nomura, Y.; Kohno, I.; Hafsi, L.; Ueda, N.; Yoshida, S.; Fukuda, M.; Fukuyasu, Y.; Yamauchi, Y.; Itoh, N. *J. Am. Chem. Soc.* **2005**, *127*, 68.
(254) Xu, K.; Liu, X.; Tang, B.; Yang, G.; Yang, Y.; An, L. *Chem.—Eur. J.* **2007**, *13*, 1411.
(255) Pacher, P.; Beckman, J. S.; Liaudet, L. *Physiol. Rev.* **2007**, *87*, 315.
(256) Yang, D.; Wang, H.-L.; Sun, Z.-N.; Chung, N.-W.; Shen, J.-G. *J. Am. Chem. Soc.* **2006**, *128*, 6004.
(257) Schulz, J. B.; Lindenau, J.; Seyfried, J.; Dichgans, J. *Eur. J. Biochem.* **2000**, *267*, 4904.
(258) Herzenberg, L. A.; De Rosa, S. C.; Dubs, J. G.; Roederer, M.; Anderson, M. T.; Ela, S. W.; Deresinski, S. C.; Herzenberg, L. A. *Proc. Natl. Acad. Sci. U.S.A.* **1997**, *94*, 1967.
(259) Yang, X.-F.; Liu, P.; Wang, L.; Zhao, M. *J. Fluoresc.* **2008**, *18*, 453.
(260) Yang, Y.-K.; Shim, S.; Tae, J. *Chem. Commun.* **2010**, *46*, 7766.

(261) Li, H.; Fan, J.; Wang, J.; Tian, M.; Du, J.; Sun, S.; Sun, P.; Peng, X. *Chem. Commun.* **2009**, 5904.
(262) Tang, B.; Xing, Y.; Wang, X.; Chen, Z.; Tong, L.; Xu, K. *Chem. Commun.* **2009**, 5293.
(263) Pires, M. M.; Chmielewski, J. *Org. Lett.* **2008**, *10*, 837.
(264) Shibata, A.; Furukawa, K.; Abe, H.; Tsuneda, S.; Ito, Y. *Bioorg. Med. Chem. Lett.* **2008**, *18*, 2246.
(265) Chen, X.; Ko, S.-K.; Kim, M. J.; Shin, I.; Yoon, J. *Chem. Commun.* **2010**, 2751.
(266) Heins, J.; Welker, P.; Schönlein, C.; Born, I.; Hartrodt, B.; Neubert, K.; Tsuru, D.; Barth, A. *Biochim. Biophys. Acta* **1988**, *954*, 161.
(267) Wrenger, S.; Hoffmann, T.; Faust, J.; Mrestani-Klaus, C.; Brandt, W.; Neubert, K.; Kraft, M.; Olek, S.; Frank, R.; Ansorge, S.; Reinhold, D. *J. Biol. Chem.* **1997**, *272*, 30283.
(268) Lorey, S.; Faust, J.; Mrestani-Klaus, C.; Kaehne, T.; Ansorge, S.; Neubert, K.; Buehling, F. *J. Biol. Chem.* **2002**, *277*, 33170.
(269) Thompson, C. B. *Science* **1995**, *267*, 1456.
(270) Song, Z.; Steller, H. *Trends Cell Biol.* **1999**, *9*, M49.
(271) Liu, J.; Bhalgat, M.; Zhang, C.; Diwu, Z.; Hoyland, B.; Klaubert, D. H. *Bioorg. Med. Chem. Lett.* **1999**, *9*, 3231.
(272) Wang, Z.-Q.; Liao, J.; Diwu, Z. *Bioorg. Med. Chem. Lett.* **2005**, *15*, 2335.
(273) Chandran, S. S.; Dickson, K. A.; Raines, R. T. *J. Am. Chem. Soc.* **2005**, *127*, 1652.
(274) Knox, R. J.; Friedlos, F.; Boland, M. P. *Cancer Metastasis Rev.* **1993**, *12*, 195.
(275) Hajo, A. K. D.; Winston, G. W. *J. Biochem. Toxicol.* **1991**, *6*, 277.
(276) Huang, M.-T.; Miwa, G. T.; Cronheim, N.; Lu, A. Y. *J. Biol. Chem.* **1976**, *254*, 11223.
(277) Hosoda, S.; Nakamura, W.; Hayashi, K. *J. Biol. Chem.* **1974**, *249*, 6416.
(278) Iyanagi, T. *Chem. Scr.* **1987**, *27*, 31.
(279) Huang, S.-T.; Lin, Y.-L. *Org. Lett.* **2006**, *8*, 265.
(280) Kataoka, K.; Harada, A.; Nagasaki, Y. *Adv. Drug Delivery Rev.* **2001**, *m47*, 113.
(281) Peppas, N. A.; Bures, P.; Leobandung, W.; Ichikawa, H. *Eur. J. Pharm. Biopharm.* **2000**, *50*, 27.
(282) Christie, R. J.; Grainger, D. W. *Adv. Drug Delivery Rev.* **2003**, *55*, 421.
(283) Murthy, N.; Xu, M.; Schuck, S.; Kunisawa, J.; Shastri, N.; Frechet, J. M. J. *Proc. Natl. Acad. Sci. U.S.A.* **2003**, *100*, 4995.
(284) Lutolf, M. P.; Hubbell, J. A. *Nat. Biotechnol.* **2005**, *23*, 47.
(285) Langer, R.; Tirrell, D. A. *Nature* **2004**, *428*, 487.
(286) Ratner, B. D.; Bryant, S. J. *Annu. Rev. Biomed. Eng.* **2004**, *6*, 41.
(287) Drury, J. L.; Mooney, D. J. *Biomaterials* **2003**, *24*, 4337.
(288) Kiick, K. L. *Science* **2007**, *317*, 1182.
(289) Duncan, R. *Nat. Rev. Drug Discovery* **2003**, *2*, 347.
(290) Lee, C. C.; MacKay, J. A.; Frechet, J. M.; Szoka, F. C. *Nat. Biotechnol.* **2005**, *23*, 1517.
(291) Boas, U.; Heegard, P. M. H. *Chem. Soc. Rev.* **2004**, *33*, 43.
(292) Haag, R.; Kratz, F. *Angew. Chem., Int. Ed.* **2006**, *45*, 1198.
(293) Mangold, S. L.; Carpenter, R. T.; Kiessling, L. L. *Org. Lett.* **2008**, *10*, 2997.
(294) Yatzeck, M. M.; Lavis, L. D.; Chao, T.-Y.; Chandran, S. S.; Raines, R. T. *Bioorg. Med. Chem. Lett.* **2008**, *18*, 5864.
(295) *Cytochrome P450: Structure, Mechanism, and Biochemistry*; Ortiz de Montellano, P. R., Ed.; Kluwer Academic/Plenum Publishers: New York, 2005.
(296) Liu, J.; Ericksen, S. S.; Besspiata, D.; Fisher, C. W.; Szklarz, G. D. *Drug Metab. Dispos.* **2003**, *31*, 412.
(297) Li, J.; Petrassi, H. M.; Tumanut, C.; Masick, B. T.; Trussell, C.; Harris, J. L. *Bioorg. Med. Chem.* **2009**, *17*, 1064.
(298) Lou, X.; Zhang, L.; Qin, J.; Li, Z. *Langmuir* **2010**, *26*, 1566.
(299) Shen, Y.; Yang, X.-F.; Wu, Y.; Li, C. *J. Fluoresc.* **2008**, *18*, 163.
(300) Franzini, R. M.; Kool, E. T. *Org. Lett.* **2008**, *10*, 2935.
(301) Sidell, F. R.; Borak, J. *Ann. Emerg. Med.* **1992**, *21*, 865.
(302) Han, S.; Xue, Z.; Wang, Z.; Wen, T. B. *Chem. Commun.* **2010**, 8413.
(303) Nagamura, T.; Tanaka, H.; Matsumoto, R. *Sens. Actuators, B* **2010**, *B146*, 253.
(304) Takahashi, K.; Tajima, M.; Matsunaga, K.; Miura, H. *Chem. Lett.* **2009**, *38*, 158.
(305) Khetan, S. K.; Collins, T. J. *Chem. Rev.* **2007**, *107*, 2319.
(306) Ager, D. J.; Prakash, I.; Schaad, D. R. *Chem. Rev.* **1996**, *96*, 835.
(307) Stephenson, C. J.; Shimizu, K. D. *Org. Biomol. Chem.* **2010**, *8*, 1027.
(308) Shiraishi, Y.; Miyamoto, R.; Zhang, X.; Hirai, T. *Org. Lett.* **2007**, *9*, 3921.
(309) Wu, L.; Dai, Y.; Marriott, G. *Org. Lett.* **2011**, *13*, 2018.
(310) Kou, S.; Lee, H. N.; van Noort, D.; Swamy, K. M. K.; Kim, S. H.; Soh, J. H.; Lee, K.-m.; Nam, S.-W.; Yoon, J.; Park, S. *Angew. Chem., Int. Ed.* **2008**, *47*, 872.